U.S. Department
of Transportation
**Federal Railroad
Administration**

Mechanics of Ballast Compaction

Volume 4: Laboratory Investigation of the Effects of Field Compaction Mechanisms

FRA/ORD-81/16.4
DOT-TSC-FRA-81-3, IV

Final Report
March 1982

C.M. Panuccio
D.R. McMahon
E.T. Selig

NOTICE

This document is disseminated under the sponsorship of the Department of Transportation in the interest of information exchange. The United States Government assumes no liability for its contents or use thereof.

NOTICE

The United States Government does not endorse products or manufacturers. Trade or manufacturers' names appear herein solely because they are considered essential to the object of this report.

Technical Report Documentation Page

1. Report No.	2. Government Accession No.	3. Recipient's Catalog No.
FRA/ORD-81/16.4		

4. Title and Subtitle	5. Report Date
MECHANICS OF BALLAST COMPACTION Volume 4: Laboratory Investigation of the Effects of Field Compaction Mechanisms	March 1982
	6. Performing Organization Code DTS-731
7. Author(s) C.M. Panuccio, D.R. McMahon and E.T. Selig	8. Performing Organization Report No. DOT-TSC-FRA-81-3,IV
9. Performing Organization Name and Address Department of Civil Engineering * State University of New York at Buffalo Parker Engineering Building Buffalo NY 14214	10. Work Unit No. (TRAIS) RR219/R2309
	11. Contract or Grant No. DOT-TSC-1115
12. Sponsoring Agency Name and Address U.S. Department of Transportation Federal Railroad Administration Office of Research and Development Washington DC 20590	13. Type of Report and Period Covered Final Report Jan 76-Sep 79
	14. Sponsoring Agency Code RRD-12

15. Supplementary Notes

*Under contract to: U.S. Department of Transportation
Research and Special Programs Administration
Transportation Systems Center
Cambridge MA 02142

16. Abstract

This report describes a preliminary series of laboratory tests which attempt to simulate some of the effects of maintenance procedures and traffic on the physical state of ballast as measured by the ballast density test, plate load test, and lateral tie push test. The first part of the report examines ballast compaction with a commercial vibratory plate. The second part considers manual tie tamping. The third part investigates the effect of cyclic loading of ballast with a surface plate, which represents plates on crib and shoulder compaction machines. Vibratory compaction and traffic were shown to be effective means of compacting ballast. However, more research is needed to quantify the effects of the controlling variables.

This report is Volume 4 of the Final Report on the subject contract.

17. Key Words	18. Distribution Statement
Ballast, compaction, density, bearing test, lateral tie push test, tamping, trackbed	DOCUMENT IS AVAILABLE TO THE U.S. PUBLIC THROUGH THE NATIONAL TECHNICAL INFORMATION SERVICE, SPRINGFIELD, VIRGINIA 22161

19. Security Classif. (of this report)	20. Security Classif. (of this page)	21. No. of Pages	22. Price
Unclassified	Unclassified	136	

Form DOT F 1700.7 (8-72) Reproduction of completed page authorized

PREFACE

This report describes a laboratory investigation of ballast physical state changes associated with simulated field compaction techniques. The work is part of a contract to evaluate ballast compaction and recommend guidelines for using compaction to improve track performance. This study was conducted by the Research Foundation of the State University of New York at Buffalo (SUNYAB) under contract to the U.S. Department of Transportation, Transportation Systems Center, in Cambridge, Massachusetts, sponsored by the U.S. Department of Transportation, Federal Railroad Administration, Office of Research. The contract number was DOT/TSC/1115. The technical monitor was Andrew Sluz.

Principal Investigator for the study was Ernest T. Selig, Professor of Civil Engineering at SUNYAB. Technical direction of the work described in this report was also provided by Carmen M. Panuccio, Research Engineer. The laboratory work was principally the responsibility of Donald R. McMahon, who was a Graduate Research Assistant at SUNYAB during this part of the research. Help in conducting the laboratory tests was provided by C. A. Thomas, Undergraduate Research Assistant, and H. E. Stewart, Graduate Research Assistant. Technical advice on instrumentation and measurement techniques was provided by B. C. Dorwart and J. I. Johnson, Graduate Research Assistants.

METRIC CONVERSION FACTORS

Approximate Conversions to Metric Measures

Symbol	When You Know	Multiply by	To Find	Symbol
	LENGTH			
in	inches	*2.5	centimeters	cm
ft	feet	30	centimeters	cm
yd	yards	0.9	meters	m
mi	miles	1.6	kilometers	km
	AREA			
in^2	square inches	6.5	square centimeters	cm^2
ft^2	square feet	0.09	square meters	m^2
yd^2	square yards	0.8	square meters	m^2
mi^2	square miles	2.6	square kilometers	km^2
	acres	0.4	hectares	ha
	MASS (weight)			
oz	ounces	28	grams	g
lb	pounds	0.45	kilograms	kg
	short tons (2000 lb)	0.9	tonnes	t
	VOLUME			
tsp	teaspoons	5	milliliters	ml
Tbsp	tablespoons	15	milliliters	ml
fl oz	fluid ounces	30	milliliters	ml
c	cups	0.24	liters	l
pt	pints	0.47	liters	l
qt	quarts	0.95	liters	l
gal	gallons	3.8	liters	l
ft^3	cubic feet	0.03	cubic meters	m^3
yd^3	cubic yards	0.76	cubic meters	m^3
	TEMPERATURE (exact)			
°F	Fahrenheit temperature	5/9 (after subtracting 32)	Celsius temperature	°C

*1 in = 2.54 (exactly). For other exact conversions and more detailed tables, see NBS Misc. Publ. 286, Units of Weights and Measures, Price $2.25, SD Catalog No. C13.10:286.

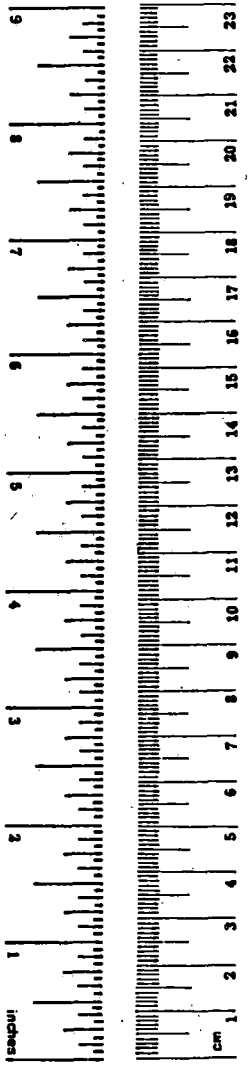

Approximate Conversions from Metric Measures

Symbol	When You Know	Multiply by	To Find	Symbol
	LENGTH			
mm	millimeters	0.04	inches	in
cm	centimeters	0.4	inches	in
m	meters	3.3	feet	ft
m	meters	1.1	yards	yd
km	kilometers	0.6	miles	mi
	AREA			
cm^2	square centimeters	0.16	square inches	in^2
m^2	square meters	1.2	square yards	yd^2
km^2	square kilometers	0.4	square miles	mi^2
ha	hectares (10,000 m^2)	2.5	acres	
	MASS (weight)			
g	grams	0.035	ounces	oz
kg	kilograms	2.2	pounds	lb
t	tonnes (1000 kg)	1.1	short tons	
	VOLUME			
ml	milliliters	0.03	fluid ounces	fl oz
l	liters	2.1	pints	pt
l	liters	1.06	quarts	qt
l	liters	0.26	gallons	gal
m^3	cubic meters	35	cubic feet	ft^3
m^3	cubic meters	1.3	cubic yards	yd^3
	TEMPERATURE (exact)			
°C	Celsius temperature	9/5 (then add 32)	Fahrenheit temperature	°F

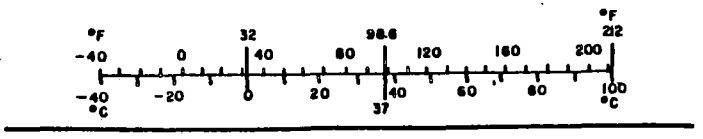

ADDITIONAL CONVERSION FACTORS

TO CONVERT

Units	Symbol	From	To	Multiply By	Symbol
length	in.	inches	millimeters	25.4	mm
	ft	feet	meters	0.305	m
area	sq in. ($in.^2$)	square inches	square centimeters	6.45	cm^2
	sq ft. (ft^2)	square feet	square meters	0.0929	m^2
force (weight)	lb	pounds	newtons	4.45	N
pressure	lb/sq in. (psi)	pounds per square inch	kilonewtons per square meter	6.89	kN/m^2
pressure/length	lb/cu in. (pci)	pounds per cubic inch	meganewtons per cubic meter	0.2716	MN/m^3
volume	cu ft (ft^3)	cubic feet	cubic meters	0.03	m^3
density	lb/ft^3 (pcf)	pounds per cubic foot	megagrams per cubic meter	0.016	Mg/m^3

TABLE OF CONTENTS

LIST OF ILLUSTRATIONS

LIST OF TABLES

LIST OF ABBREVIATIONS AND SYMBOLS

AASHTO = American Association of State Highway and Transportation Officials

BBI = Ballast Bearing Index, psi

BBI_K = Modified Ballast Bearing Index, pci

BDT = Ballast Density Test

CCD = Cumulative Cyclic Deformation, in.

CNR = Canadian National Railroad

DCDT = Direct Current Displacement Transducer

E_r = Elastic Recovery, %

f = frequency, Hz

FAST = Facility for Accelerated Service Testing; Pueblo, Colorado

ICG = Illinois Central Gulf Railroad

ISL = Initial Static Load or tie resistance at zero in. tie displacement, lb

LR = Load Ratio of cyclic load to static load

LTPT = Lateral Tie Push or Pull Test

LVDT = Linear Variable Differential Transducer

MGT = Million Gross Tons

MTS = Materials Testing System

PLT = Plate Load Test

SLR = Load Ratio of Static Load to 1490 lb (6631 N)

USCS = Unified Soil Classification System

x = Number of cycles

y = Cumulative cyclic deformation, in.

Δ_P = Total or peak displacement per cycle in inches

Δ_R = Rebould displacement per cycle after complete unloading in inches

ε_c = Cyclic strain, percent

γ_{xy} = correlation coefficient

EXECUTIVE SUMMARY

The first part of this report describes an investigation of tamping and compaction of ballast using laboratory-simulated field conditions. A track bed was constructed in the laboratory and tie tamping and compaction operations were performed in order to examine the effects on the resulting physical state of the ballast. The ballast physical state was measured using the three in-situ tests developed at SUNYAB. These were the plate load test (PLT), which measures vertical ballast stiffness, the ballast density test (BDT), and the lateral tie push test (LTPT), which measures the resistance offered by the ballast to an individual tie displaced laterally. In general, tamping machinery is used for track maintenance work, while ties are manually tamped only for spot work. However, all of the tie tamping in this project was performed manually, because mechanical tamping equipment could not be used in the laboratory.

Simulation of a railroad track ballast bed that has been conditioned by traffic, but which has not been recently subjected to maintenance operations, was attempted in the laboratory by filling a large test box with a 12-in.-(0.305-m-) thick layer of limestone ballast and compacting it with a vibratory plate compactor. An increase in ballast density of about 12 pcf from the loose state was observed after only 25 to 50 passes with the vibratory compactor. Most of the ballast bearing stiffness increase occurred within approximately 500 passes of the vibratory plate compactor. The laboratory ballast density and stiffness values after 1000 compactor passes compared favorably well with field test results for a track bed after long periods of traffic.

Several lateral tie push tests were performed when a standard railroad tie was placed on the compacted bed with no crib or shoulder, and the effects

of various weights placed on the tie were evaluated. Tests were also performed for a semi-filled crib, a full crib, and a full crib with a surcharge load. The ballast shoulder section was subsequently formed and lateral tie push tests were performed on a compacted base, as well as a loose base resulting from various amounts of tamping raises. These ballast physical state test results were also compared with previous reported data.

The lateral resistance of an individual tie after manual tie tamping was not affected by the height of the tamping raise for a full, loose ballast crib and shoulder condition. The lateral tie resistance increased nearly linearly as the amount of ballast in the cribs increased. Even when the cribs were over-filled, the tie resistance continued to increase in a similar fashion. Thus, the crib component of resistance is a significant contributor to the total lateral resistance of an unloaded tie. For ties of various weights placed on a compacted base with no crib or shoulder ballast, the lateral tie resistance was approximately equal to one-half of the tie weight.

The field lateral tie resistance forces from the LTPT were generally greater than the laboratory forces for the tamped-only condition by 50 to 150 lb (223 to 668 N). The laboratory PLT and BDT results, however, compared very favorably to the field test results for the tamped-only condition. Thus, representative field track conditions appear to have been reproduced in the laboratory.

The second part of the report describes an investigation of the factors influencing ballast compaction with surface vibrating plates. This series of tests with a single oscillating plate on the ballast surface was intended to simulate a typical compaction element from a crib and shoulder compactor. To accomplish this, a single, flat, steel plate having dimensions comparable

to those for ballast compactors was fabricated and attached to a cyclic load actuator. The plate was first loaded statically. Then an alternating load was applied at a low enough frequency to eliminate vibration. The load-displacement response was recorded for a loose, crushed limestone ballast in small test boxes under controlled loading conditions. The effects of the following factors on the compaction of ballast were investigated: 1) magnitude of static load, 2) magnitude of cyclic load, 3) ballast depth, 4) cycles of loading, 5) frequency, and 6) lateral boundary effects. In addition, BDT and PLT tests were performed on the compacted zone after the required number of loading cycles was achieved. These two physical state tests permit a comparison with field experience.

The cumulative cyclic deformation (settlement) of the plate increased as the ratio of cyclic to static load was increased for a given static load. The cumulative cyclic deformation also increased as the static load increased for a constant ratio of cyclic to static load. The ballast density increased by only about 3 pcf from the loose state after application of 300 load cycles. The final density state appeared to be independent of the loading conditions. The plate bearing stiffness value at a given deformation increased as the static load was increased for a given ratio of cyclic to static load. Similarly, as the ratio of cyclic to static load was increased for a given static load, the bearing stiffness increased. When the sample ballast depth was decreased, both the static deformation and the cumulative cyclic deformation decreased. When the lateral boundary constraints of the box were removed by using a larger box, the deformations increased for a given set of loading conditions, but the amount of compaction was essentially unchanged. Within the frequency range of 0.1 to 2 Hz, the ballast physical state resulting from compaction with the oscillating plate was essentially independent of frequency.

The physical state for the loose ballast condition in the lab prior to compaction with the oscillating plate was comparable to the observed physical state in the field under two conditions. These conditions were under the center of the tie after reballasting and in the crib near the rail after tamping. However, the ballast stiffness in the crib after crib compaction in the field was much greater than that achieved in any of the lab tests. The conclusion was drawn that the vibration effects from the high frequency used in the field contributed significantly to the amount of compaction achieved by an oscillating plate.

1. INTRODUCTION

The track system response is directly affected by the physical state of the ballast material within the track bed. Changes in the physical state, as well as track geometry, are primarily attributed to train traffic loading conditions, environmental influences (such as temperature and weather), and track maintenance operations. These features have a profound impact upon the ballast state with regard to vertical track stiffness and lateral track stability.

The first two factors are time dependent, and consequently an interactive effect is induced upon the ballast behavior, such that isolation and quantification of either variable is difficult to assess. However, track maintenance is a relatively short term condition, which easily provides for measurement of the changes in the ballast state with respect to different maintenance practices.

One such maintenance practice commonly used to rectify track geometry irregularities resulting from train loadings is an out-of-face surfacing and lining operation which utilizes a ballast tamping-leveling-lining machine. This operation generally requires raising the track [1 in. (25.4 mm) to 3 in. (76.2 mm)] and subsequently leaves the ballast in the cribs and under the ties in a rather loose and unstable state as compared to a dense state from traffic-induced compaction. Slow orders are usually initiated in order to minimize the possibility of lateral track buckling. Traffic can proceed at normal operating speeds once a sufficient amount of tonnage has passed and the track has achieved a stable condition.

However, while the lateral resistance to track buckling increases with traffic, a progressive deterioration of track geometry also simultaneously occurs. When track line, surface and change in cross level approach intolerable limits, then damage to the track system, components of the train, and to the transported goods results. Also, a reduction in train speed is required to prevent possible derailments. Thus, another out-of-face surfacing and lining operation is necessary, and the process is repeated.

The addition of ballast crib and shoulder compaction machines to normal track maintenance operations supposedly reduces the number of slow orders, lengthens cycle times for major track maintenance, and initially increases track stability. This machine follows the ballast tamping-leveling-lining machine and densifies the ballast in the crib zones near the rails and on the shoulder. Limited use of these compaction machines has been made in the United States and, thus, the implications on the long-term effects of extending the time for programmed track maintenance cycles and increased track stability are not well established.

In addition, different ballast compaction machines possess significantly different characteristics, which compound an evaluation of their effectiveness in compacting ballast. These characteristics include the size, shape and location of the crib and shoulder plates, the static down pressure, the generated force, and the application time.

The compacted state of the ballast in the cribs and under the tie is changed by three different processes: 1) tamping, 2) crib and shoulder compaction, and 3) train traffic. Only a limited amount of reliable field

data are available, and laboratory data are nonexistent to quantify the differences in ballast physical state caused by these compaction processes.

The objective of this current research is the laboratory simulation of the three field compaction processes previously mentioned. A simulated used track bed was constructed and tie tamping operations were performed upon a typical track structure in order to examine the resulting physical state of the ballast. In addition, the effects of crib compaction on the ballast state were also investigated. Where applicable, the changes in the ballast physical state were evaluated using three in-situ tests developed at SUNYAB, which have been described by Selig, et al. (Ref. 1). These tests are the plate load test (PLT) which measures vertical ballast stiffness, the ballast density test (BDT), and the lateral tie push test (LTPT) which measures the resistance offered by the ballast to an individual tie displaced laterally.

Since the ballast in an old track bed is compacted in the center of the track as well as in the area under the rails, it was decided that the entire track bed should be compacted. The simulated track bed for the present study was formed by running a vibratory plate compactor over a 12-in. (0.305-m) deep layer of limestone ballast in a large test box. At certain intervals during the compaction, ballast density tests and plate load tests were performed in an effort to determine the degree of compaction achieved. The results of these tests are analyzed in Section 3 and compared to related field test results in order to evaluate the effectiveness of this compaction technique.

In addition to creating a simulated track bed, the laboratory test

track section was also subjected to a tamping operation. In everyday practice of railroad maintenance operations, two methods are available by which ties can be tamped. One method is by mechanical means and the other is manual. A discussion of the specifications of different types of mechanical tampers and details of the tamping operation are provided by Selig, et al. (Ref. 2).

In general, tamping machinery is used for large scale track rehabilitation work, while ties are manually tamped only on small track work jobs. The major advantages in using a mechanical tamper over manual tamping are that mechanical tamping 1) is much faster, and 2) provides more uniform tamping from tie to tie. However, all of the tie tamping in this project was performed manually, since it is more easily adaptable to laboratory conditions. The effectiveness of this tamping procedure was evaluated by the LTPT, PLT, and BDT and compared to available field data in Section 4.

Since very little is known about the effectiveness of ballast compaction machines, an investigation of the factors influencing this method of ballast compaction was conducted. Vibrating compaction plates placed on the crib surface are the principal means in densifying the ballast. Thus, the simplest approach is a simulation of a single crib compaction plate on a volume of ballast equivalent to that which would be compacted in the crib by one plate.

A single flat steel plate having dimensions comparable to those in the reviewed specification sheets of ballast compactors (Ref. 2) was fabricated and attached to a structural cyclic load actuator. The load-displacement response was recorded for a loose crushed limestone ballast in small test boxes under controlled loading conditions. The effects of the following

factors on the compaction of ballast were investigated: 1) magnitude of static load, 2) magnitude of cyclic load, 3) ballast depth, 4) cycles of loading, 5) frequency, and 6) lateral boundary effects. In addition, BDT and PLT tests were performed on the compacted zone after the required number of loading cycles was achieved. These two physical state tests are the only available methods by which comparison can be made to field data and, thus, infer the reliability of this laboratory simulation. The results of this investigation are presented in Section 5.

2. COMPACTION CONSIDERATIONS

2.1 CURRENT METHODS OF MEASUREMENT

The key element affecting track system response is the changes in the physical state of the ballast material with respect to tamping, crib and shoulder compaction, and train traffic. The changes in ballast state are most commonly measured by single and panel section lateral tie pull or push tests (LTPT). This method is at best only an indirect indicator of the ballast state, since the resistance is a function of the amount of ballast-tie interaction. However, this test is directly relevant in determining the availability of lateral tie resistance to prevent track buckling.

For the LTPT on individual ties, the spikes, tie plates and rail anchors are removed from the tie. Then by using the rails as a reaction, the load required to move the tie a certain distance in a direction perpendicular to the rails is measured.

Panel section tests encompass the same basic testing technique. Instead, a short segment of track consisting of several ties spiked to the rails is detached from the main track. The rails are of equal length and usually cut in the same crib. A yoke is attached to one rail at the center of the panel section. The total force required to move the panel section is measured, and the resulting displacement of each tie is recorded. This method is favored over the single tie test because the rail-tie-ballast interaction is believed to more closely duplicate the actual lateral resistance of track to buckling.

SUNYAB has been actively involved with ballast physical state changes obtained from single lateral tie push tests. A laboratory evaluation of

the factors affecting lateral tie resistance was conducted by Ciolko (Ref. 3). Panuccio and Dorwart (Ref. 4) correlate field LTPT results with train traffic loading and track maintenance operations. In the latter case, the tamping and crib and shoulder compaction operations are emphasized.

The SUNYAB in-situ ballast density test (BDT) and the plate load test (PLT) methods are believed to be direct measures of the ballast physical state and presently the most effective and reliable means of evaluating the amount of ballast compaction. Laboratory evaluations were performed by Chen (Ref. 5) for the BDT and by Wayne (Ref. 6) for the PLT. Panuccio and Dorwart (Ref. 4) and Yoo (Ref. 7) correlate field test results for the PLT and BDT, respectively.

The in-situ ballast density test essentially measures the density of a small volume of material at specific locations in the crib or under the tie. This basic method involves excavating of a hole approximately 7 in. (178 mm) in diameter and 5 in. (127 mm) deep, lining with a flexible membrane, and measuring the volume of water required to fill the hole. The weight of the excavated ballast material is measured and the density computed. This technique has been referred to as the water replacement method and is a direct measure of the amount of compaction.

The plate load test is performed at the same test locations as the density test. This test involves the static loading of a 5-in. (127 mm)-diameter rigid plate and simultaneously measuring the deformation resulting from that loading. This method gives a relative measure of the ballast stiffness and of the effect of compaction on the ballast physical state.

The preceding discussion of SUNYAB's ballast physical state tests was presented in capsule form, however, further discussion will ensue in the following chapter. The details of the final test apparatus and test procedures for the lateral tie push test, the in-situ ballast density test, and the plate load test are described by Selig, et al. (Ref. 1).

2.2 OLD TRACKBED AND MANUAL TIE TAMPING

Immediately after track lining and surfacing, i.e., raising and tamping, the ballast in the cribs, on the shoulders and under the ties is in the loosest physical state that exists for field conditions. As traffic passes over a section of recently surfaced track, the track structure slowly settles. The track bed ballast, as well as the surrounding crib and shoulder ballast, densifies and obtains varying degrees of stiffness. In a relative sense, the ballast achieves its most stable condition immediately before the track is subjected to another out-of-face maintenance operation.

For the ballast located directly underneath the tie, i.e., the track bed, a smooth surface is formed at the tie-ballast interface. This smooth surface is the product of traffic loading, which causes a high degree of ballast particle interlocking and mechanical degradation of the ballast particles. Thus, if a tie was carefully removed from an old track structure, i.e., one that has been subjected to several million gross tons (MGT) of traffic since its last maintenance cycle, the ballast surface under the tie would be very smooth and the crib ballast would be compacted to such a state that it would almost remain in place.

From the previous discussion, the ballast at a given location in the track structure attains two distinctly different states of compaction. One

condition occurs with the tamping operation while another condition is achieved with the application of several MGT of train traffic. The ballast under the tie in the track bed will undoubtably demonstrate the greatest differences in stiffness and density for the two conditions.

Previous laboratory investigations in the areas of track bed simulation and tie tamping are limited. Peterson (Ref. 8) built a simulated track bed by compacting a 12-in. (0.305-m)-thick layer of initially loose ballast in two 6-in. (0.152-m) lifts with a vibratory plate compactor. The area under the tie ends, i.e., outer 34 in. (0.864 m) of the tie and 6 in. (0.152 m) of the shoulder extending beyond the tie ends, was compacted by making 5 passes with the compactor for each lift. The ballast under the center third of the tie was left uncompacted. A track section consisting of a three tie-rail system was placed on the track bed and full cribs and shoulder were formed. Manual tie tamping was performed on the track section with standard hand tamping irons however, the tamping procedure was not specifically stated. A 0.45 MGT equivalent train traffic loading was used to seat the track section prior to performing lateral tie pull tests.

Ciolko (Ref. 3) determined the effect on lateral tie resistance for simulated track beds prepared in loose and dense states. The ballast depth was approximately 12 in. (0.305 m) in both cases. The loose density condition was achieved by pouring ballast with a small free fall height from containers into a test box. The dense state was achieved by compacting a ballast area 10.5 ft (3.20 m) long by 2.87 ft (0.875 m) wide with 4000 uniformly distributed blows from a pneumatic plate tamper. A tie was placed on the track bed and, the cribs and shoulder were formed by placement of the ballast in

a loose state. No tie tamping per se was performed prior to testing.

These two previous laboratory investigations apparently attempted to achieve and evaluate only relatively different ballast physical state conditions both in the crib and under the tie, which were probably sufficient for their purposes. However, to more effectively simulate field conditions, such as the common tie tamping procedure performed on a highly trafficked or compacted track bed, the laboratory sample preparations must closely duplicate the resulting field ballast physical states for proper evaluation. It is these objectives that this current study will attempt to fulfill.

Ciolko's (Ref. 3) large test box, designed to represent a section of a typical track stucture, was available and the same crushed limestone ballast was used, provides the required laboratory apparatus and materials. In addition, a vibratory plate compactor was employed as a means to quickly and effectively achieve the compacted track bed condition. Manual tie tamping was accomplished with the standard track tools and the recommended field procedure. The BDT, the PLT, and the LTPT, were also available to evaluate the simulated field conditions.

2.3 CRIB COMPACTION APPARATUS

Characteristics of Field Equipment. Ballast compactors (Fig. 2.1), when used, are the final operation in programmed track maintenance after lining-leveling and tamping. Generally, a set of eight crib compaction plates compact the ballast in the same crib area as the tamping tools. The center of the plates both inside and outside the rails in the crib are located 9 in. (229 mm) to 11 in. (279 mm) from the rail centerline. Simultaneously, another longer pair of compaction plates, with or without an

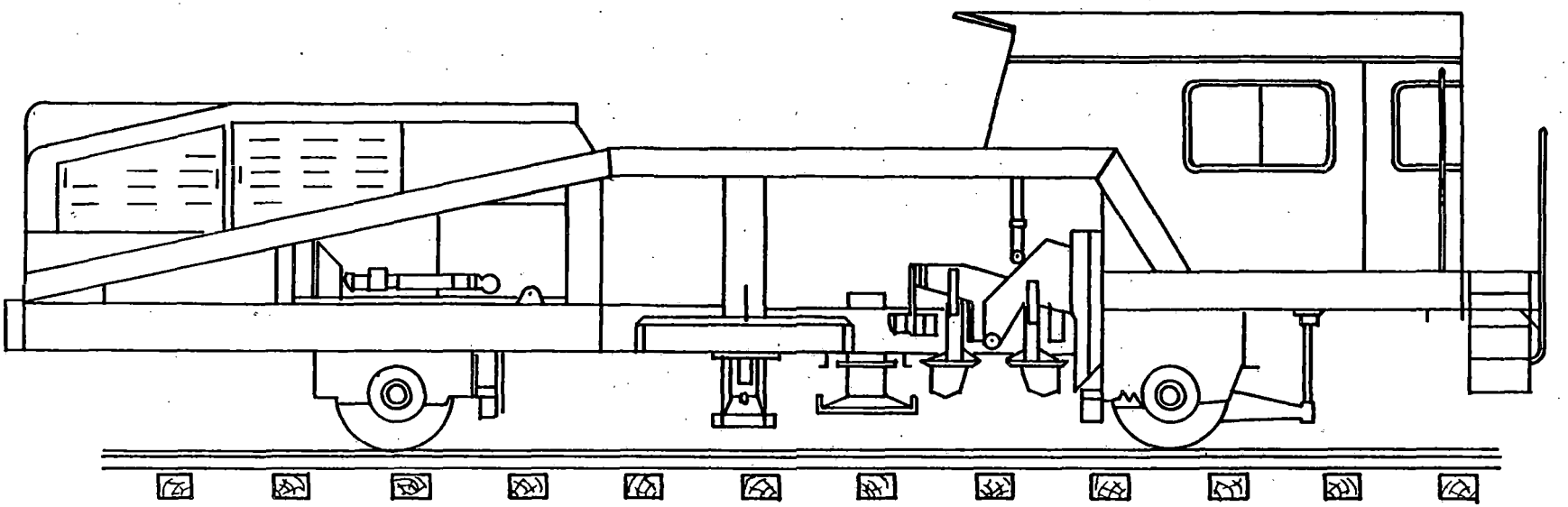

Figure 2.1. Typical Ballast Crib and Shoulder Compaction Machine (Ref. 9)

attached shoulder pressure plate, compacts the ballast at the tie end or on the shoulder (Fig. 2.2).

The compaction plates are initially set into vibration, hydraulically lowered onto the ballast until a predetermined static down pressure is achieved, vibrated for a preset application time, and then raised. The operator then positions the crib compaction plates over the next tie and the cycle is repeated automatically.

Each compaction plate generates two components of force to the ballast. The first is a hydraulically applied static load. The second is a cyclic load induced by the vibratory motors. Vibrating motors of the crib, shoulder, or tie end compaction plates are one of two types (Ref. 10):

1) a rotating eccentric mass producing a constant generated dynamic force at a given frequency, or

2) an eccentric shaft producing a constant amplitude of oscillation.

An adequate comparison of the two methods is prohibited, since reliable field measurements of the relative degree of ballast compaction are not available.

The available manufacturer's specifications on ballast crib and shoulder compaction equipment are shown in Table 2.1. Included are characteristics of the compacting plates, such as type, shape, and size, range of application or cycle time, frequency of vibration, as well as the rated static and dynamic forces. Major differences in equipment occur with the type and outputs of the vibratory motors. The reliability of the rated dynamic force is questionable, since this value depends upon the physical state of the ballast and the subsequent interaction with the compacting plates.

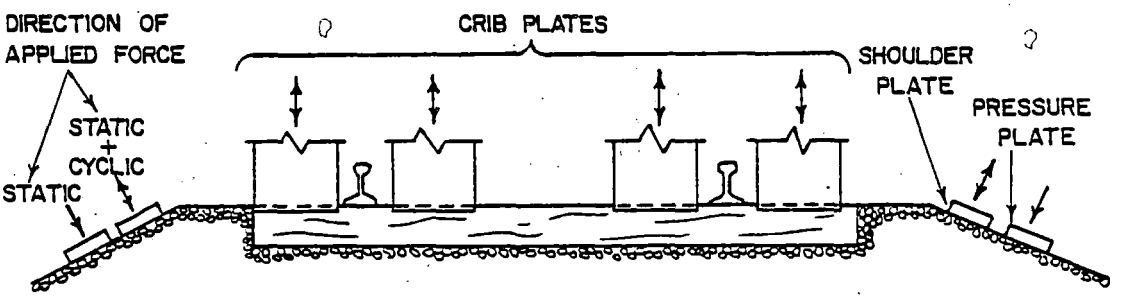

a) CROSS - SECTIONAL VIEW

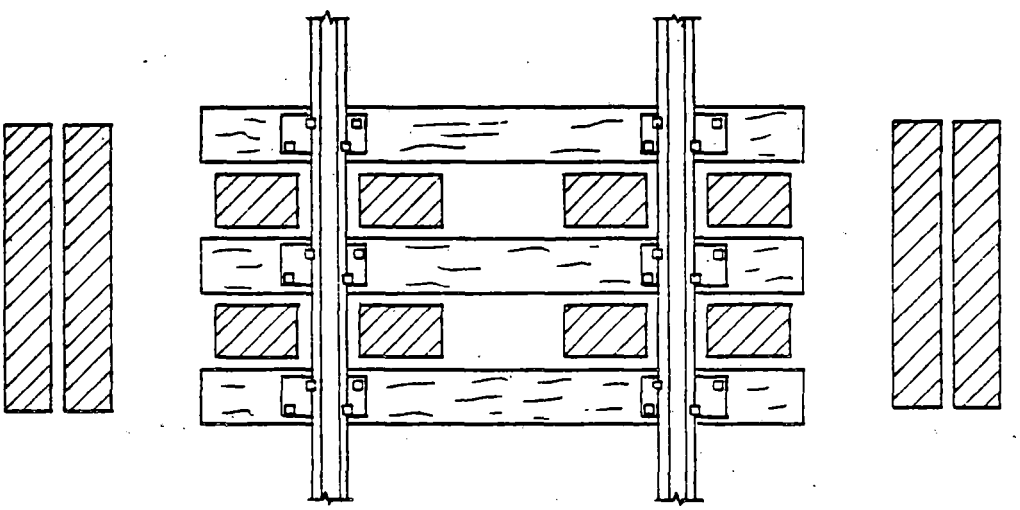

b) TOP VIEW

Figure 2.2. Schematic Diagram of the Location and Size of Ballast Crib and Shoulder Compaction Plates

Table 2.1. Characteristics of Ballast Crib and Shoulder Compaction Equipment

Reference	Manufacturer	Model Number	Application Time (Sec.)	Crib Compaction Plates			
				Frequency f(Hz)	Size	Rated Force (lb) Static	Dynamic
9	Plasser and Theurer	VDM800U	Variable 1-15	38.5	114.7 in^2	1729	1101
11	Plasser-American	VDM800R	Variable 1-20 Used 3	35-38	≈6 in. x 12 in.	--	--
12	Plasser	VDM800	Variable†	38.5†	9.8 in. x 8.5 in.	--	--
13	Plasser and Theurer	CPM800R	Variable†	38.5	≈10 in. Length	--	--
14	Plasser-American	CPM800R	Variable†	38.5	14 in. x 8-7/8 in.	--	--
15	Plasser-American	CPM800	Variable† 3 and 5 Used	38.8	14.5 in. x 5.5 in.	1250	1600
10	Plasser and Theurer	Mainliner Universal 06-16CTM	Variable†	38.5	≈10 in.† Length	--	--
13	Plasser and Theurer, Windhoff	903 SW	Used 3	-	-	--	--
10 & 12	Windhoff	BV 102	Variable† Used 4 - 8	48	10.25 in. x 9.4 in.	--	2203†
		BV 102S	Variable†	48	" " †	--	2203
		BV 103	Variable†	48	" " †	--	2203†
		FD 41	Variable 2 - 20	48	--	--	1542-3745
16	Tamper	CSC	Variable	--	--	--	--
11	Tamper	CSC	1 - 9 Used 3-4	≈33.3	≈12 in. x 7-1/2 in.	--	--
16	Matisa	D-912	Variable 0 - 10	50	--	--	0-5500
		D-912R, D-9	Variable† 0 - 10	50†	--	--	0-5500†
17	Matisa	--	3 - 20	46.7	8 in. x 10 in.	--	2200-3750
17	Penn Central w/Jackson Vibrators	--	Variable†	--	--	--	--
17	Jackson	--	2 - 20	60-75	3 in. x 12 in.	275	6900

- Assumed

Table 2.1. Characteristics of Ballast Crib and Shoulder Compaction Equipment (continued)

Reference	Model Number	Tie End or Shoulder Compaction Plates				
		Frequency f(Hz)	Size	Shape	Rated Force (lb) Static	Dynamic
9	VDM800U	35	52.8 in. x 9.8 in.	Flat	2203	2423
		35	51.2 in. x 7.9 in.	Flat	2203	1729
11	VDM800R	35-38	≈ 6 ft in. length	Flat	—	—
12	VDM800	35†	57.1 in. x 7.9 in.	Flat	—	—
13	CPM800R	35†	4.5 ft. x 8 in.	Flat	—	—
14	CPM800R	35†	4.5 ft x 8 in.	Flat	—	—
15	CPM800	24.5	85 in. x 8 in.	Flat	1500	1700
10	Mainliner Universal 06-16 CTM	35†	4.5 ft. x 8 in.	Flat	—	—
13	903 SW	—	—	—	—	—
10 & 12	BV102	48	53.2 in. x 12.6 in.	Flat	—	2203†
	BV102S	48	"	Flat	—	2203†
	BV103	48	"	Flat	—	2203†
	FD 41	—	—	—	—	—
16	CSC	—	—	—	—	—
11	CSC	≈53.3	≈5 ft. in length	Flat	—	—
16	D-912	50	—	Flat	—	0-6600
	D-912R, D-9	50†	—	Flat†	—	0-6600†
17	Matisa	46.7	—	Flat	—	3300-5500
17	Penn Central w/Jackson Vibrators	72	18 in. x 18 in.	—	—	—
17	Jackson	60-75	24 in. x 36.5 in.	—	—	—

* Tie End Acts on a Horizontal Shoulder Section, Shoulder Acts on the Sloped Shoulder Section

† Assumed

The manufacturer's literature on ballast compactors suggested the following major advantages for use of this machine in conjunction with normal track maintenance operations:

1. Increase in the lifetime of cross level, line, and surface, and thus maintenance intervals.

2. Reduction in the number of loose ties; which are a cause of track deterioration, increased rail end wear, and increased rail failures.

3. Reduction in the number of slow orders after compaction compared to after tamping only.

4. Compaction plates deliver uniform force to the ballast; therefore, uniform compaction, track resistance, and settlement.

5. Under the tie, compaction increases vertical track stiffness and provides a uniform bearing surface (pressure distribution) which is less likely to deteriorate than after tamping alone.

6. Increase in lateral and longitudinal track resistance and track stability, both immediately and long term.

7. Vibrating frequency is equal to frequency of ballast, thus obtaining optimum compaction, i.e., increase in ballast density.

However, Powell (Ref. 18) reports that crib and shoulder compaction is effective in increasing the lateral resistance after tamping, only if a sufficient amount of ballast is present in the crib, i.e., a full crib. Some of the other listed items also are questionable.

The benefits listed indicate that track structure will respond more favorably for the short and long term conditions with the use of crib and

shoulder compaction following tamping than with tamping only. These findings are primarily supported by European studies, which from available published literature apparently lack sufficient quantities of reliable experimental data. Also, the implication that the same benefits would be derived on American railroads is misleading, since existing axle loads, track structures and track maintenance practices are distinctly different from those in Europe.

Laboratory Representation. In the summary of available manufacturers' literature on ballast compaction machines in Table 2.1, emphasis was concentrated upon the characteristic features of the compaction plate equipment. The compiled data indicated the range of variables to be considered in designing the laboratory simulation of a single crib oscillating plate.

The first factors to be determined for the crib plate were representative cross-sectional dimensions and ballast surface contact shape. The plate shapes illustrated in Table 2.1 are composed of the three following types: 1) a V-shape with a large or small apex angle located either in the center or offset from the center of the plate, 2) a flat plate with flared ends, and 3) a spherical shape with a large or small radius of curvature. Experimental data regarding the effectiveness of plate shape on the compaction of ballast are nonexistent. Therefore, the conventional flat crib plate was selected for this study.

Since the crib plate shape was determined, the physical dimensions of the plate were taken into consideration next. From Table 2.1, the plate lengths varied from 10 to 14.5 in. (0.254 to 0.369 m), and the plate widths varied from 5.5 to 9.4 in. (140 mm to 239 mm). The plate areas ranged from 80 to 115 $in.^2$ (0.052 m^2 to 0.074 m^2). However, the plate widths and areas

are assumed to be cross-sectional features of the plate and probably smaller than the actual widths and areas which come into contact with the crib ballast. An evaluation of all available data produced a reasonable estimate of equivalent flat crib plate contact area to be 116 $in.^2$ (0.075 m^2). This value is close to the single crib compaction plate area of a Plasser and Theurer VDM 800 U. For this plate area, reasonable estimates of the plate length and width for use in this study were 14.5 in. (0.368 m) and 8 in. (0.203 m), respectively. These dimensions were also very close to those measured on the FRA ballast compactor at the FAST site in Pueblo, Colorado. That machine was a Plasser-American CPM 800 R with plate dimensions of 14 in. (0.356 m) by 8-7/8 in. (0.225 m)[Ref. 14].

The next factors taken into consideration were the magnitudes of the applied static and cyclic loads per crib compaction plate. The reported values from Table 2.1 were 275 to 1729 lb (1224 to 7694N) for static load and 1101 to 6900 lb (4899 to 30,705 N) for single amplitude cyclic load. However, an uncertainty exists as to the methods used to obtain these rated load values. Thus, the effect of these variables on the compaction of ballast must be thoroughly examined. The Plasser and Theurer VDM 800 U does appear to have reasonable values of static load, i.e., 1729 lb (7694 N), and cyclic load, i.e., 1101 lb (4899 N), when the weight of the machine is considered.

The final characteristics to be considered for the crib plate are the frequency and application time for the cyclic load. Operating frequencies of 38.5 to 75 Hz and application times of 3 to 5 seconds are common. For these conditions, the range of an equivalent number of loading cycles would

be from 116 to 375. Since the structural load actuator used in this study is capable of applying cyclic loads at low frequencies only, i.e., less than 2 Hz, field frequencies and application times will be simulated for an equivalent number of loading cycles, rather than frequency and time. For this study, 300 cycles was considered a realistic estimate. The assumption was also made that the cyclic load could reasonably be represented by a sine wave loading function.

Given the size of the crib compaction plate, the equivalent volume of ballast material affected by the crib plate must be determined. This condition is illustrated in Fig. 2.3 for a 22-in. (0.559-m) tie spacing and a full ballast crib. Both the lateral boundaries and depths for in the crib and under the tie have been assumed to be representative of field conditions. The ballast depth under the base of the tie was assumed equal to a depth which would be disturbed by insertion of the tamping tools. Thus, a likely choice for a ballast depth is 12 in. (0.305 m). Since the effective depth over which the compaction plate acts is not known, several tests will be performed with ballast depth as a variable.

The crib plate definitely affects the ballast within the crib zone and somewhat underneath the tie. Based on a 5-in. (0.13-m) depth under the tie, an equivalent surface area was obtained by proportioning the volumes of material within the crib zone and under the tie. The computed surface area was approximately 362 and 410 $in.^2$ (0.234 and 0.264 m^2) for tie spacings of 20 and 22 in. (0.508 and 0.559 m), respectively. Thus, a test chamber, which is 20 in. (0.508 m) square and 12 in. (0.305 m) deep, was considered representative of an equivalent volume of ballast affected by a single crib

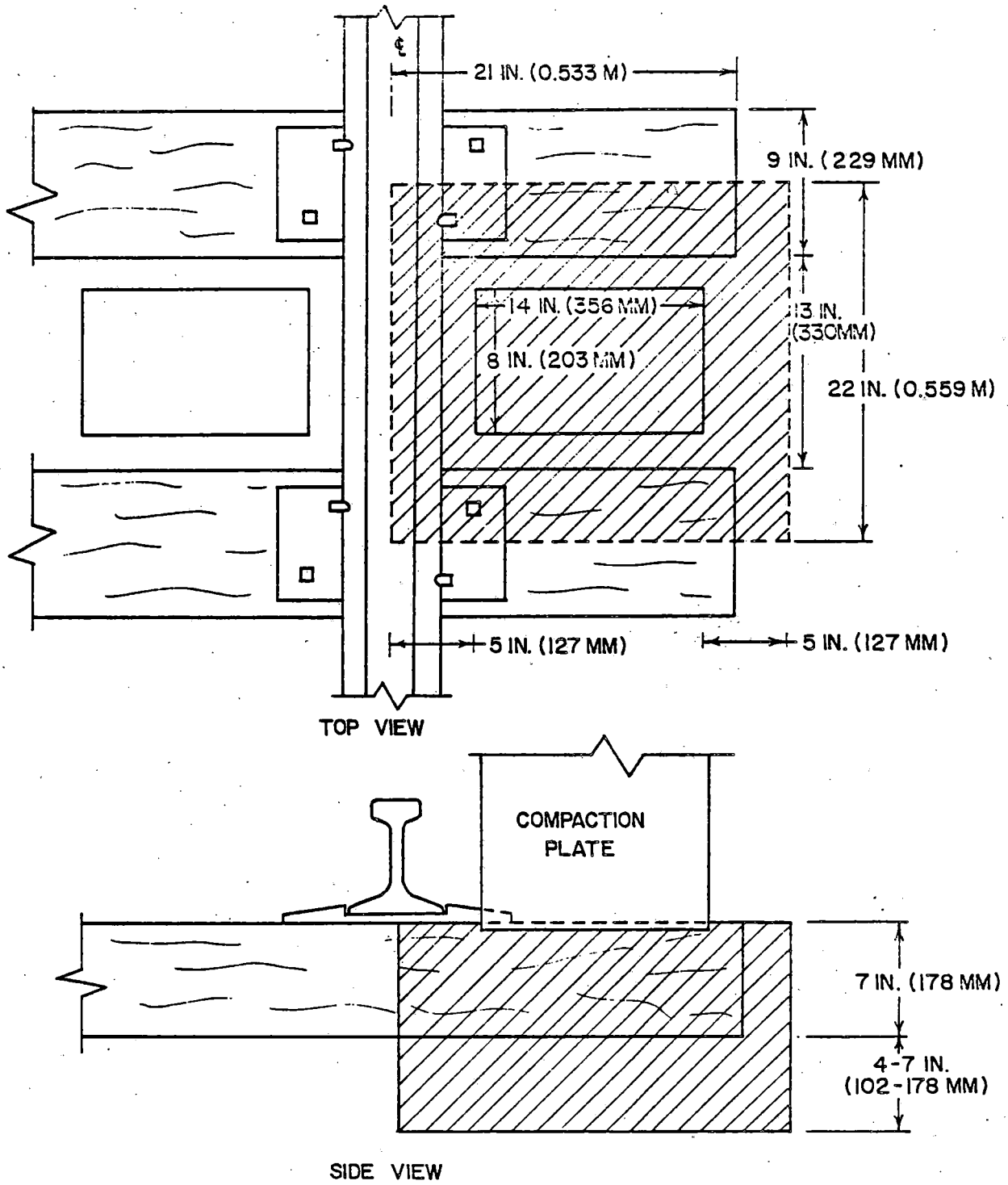

Figure 2.3. Ballast Area Influenced by Single Crib Compaction Plate

compaction plate. Since the 20-in. by 20-in. (0.508-m) box would have relatively rigid sides, testing in a larger box will be considered in order to identify the differences in lateral boundary conditions.

The ballast material selected for this study is a uniformly-graded, crushed limestone. This appears to be a common material used for railroad ballast on U.S. track. Also, since the tamping tools leave the crib ballast near the rails in a loose state, test specimens will be prepared initially at a loose density.

Each of the previously mentioned factors will have an effect on the amount of compaction the ballast material has achieved with the crib compaction plate. In order to identify the changes in physical state, the plate load and in-situ ballast density tests will be utilized.

3. INVESTIGATION OF SIMULATED TRACKBED

3.1 APPARATUS AND PROCEDURES

Test Box. A schematic diagram of the large test box used is the same as that reported by Ciolko (Ref. 3) and is shown in Fig. 3.1. The box is constructed of 3/4 in. (19.1 mm) and 1/2 in. (12.7 mm) plywood and is reinforced by 2 in. by 2 in. (50.8 by 50.8 mm) steel angle iron. Two steel A-frames are attached to each side of the test box and are located in such a position that placement of the two 6 ft (1.83 m)-long 132 RE rails will set the rails into proper track gage.

Ballast Materials Tested. The ballast material selected for testing was the same crushed limestone used by Ciolko (Ref. 3). The limestone, obtained from local quarries, was classified in the USCS system as GP, by AASHTO as A1, and by AREA as No. 4. The gradation curve is shown in Fig. 3.2, along with AREA specification limits on the No. 4 stone. The particle shape was angular with a specific gravity of 2.7 and absorption of 0.4%.

Sample Preparation Technique. In this study, the ballast was first prepared for the simulated track bed test series. The resulting ballast - physical state would provide a suitable track bed condition for the ensuing ballast preparation techniques used in the manual tie tamping series in Chapter IV. However, the sample preparation techniques for the two test series will be discussed separately.

Ballast was shovelled into the test box for a full 12-in. (305-mm) depth leaving it in a loose condition. The initial ballast physical state and its variability along the entire track bed was expected to primarily affect the initial rate of change of the physical state properties with the

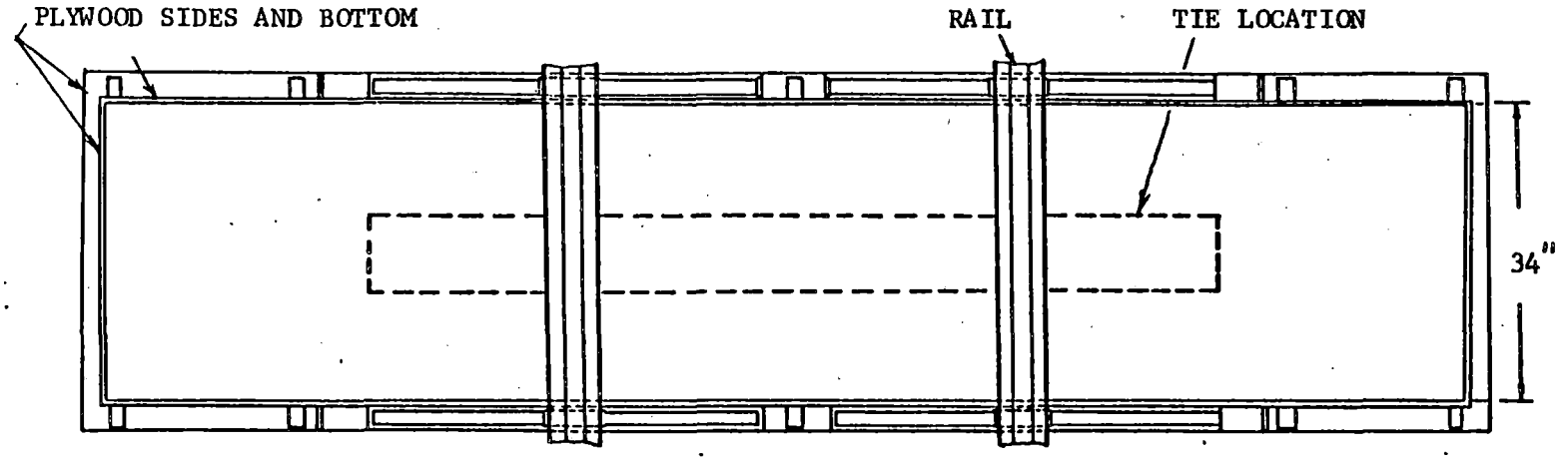

TOP VIEW

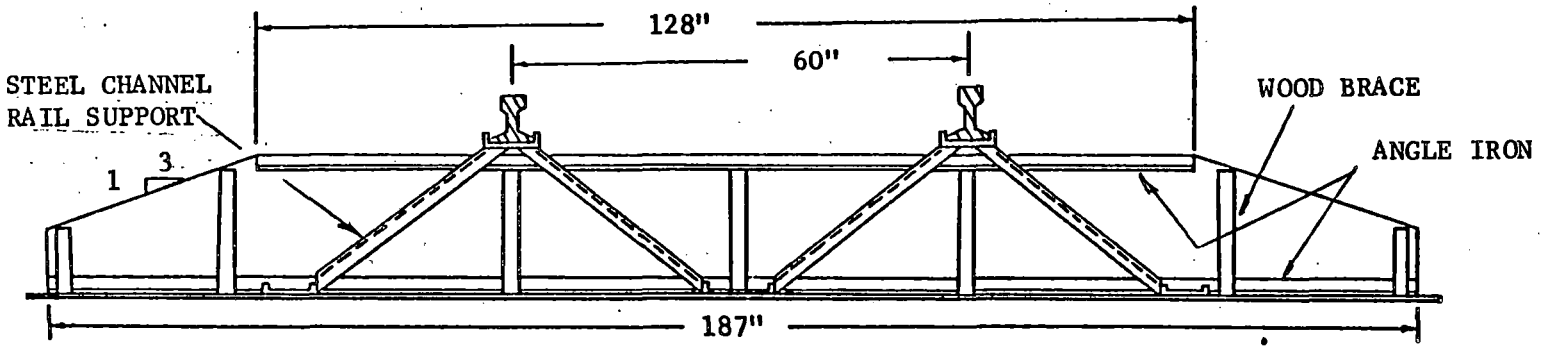

SIDE VIEW

Figure 3.1. Schematic Diagram of Large Test Box (Ref. 1)

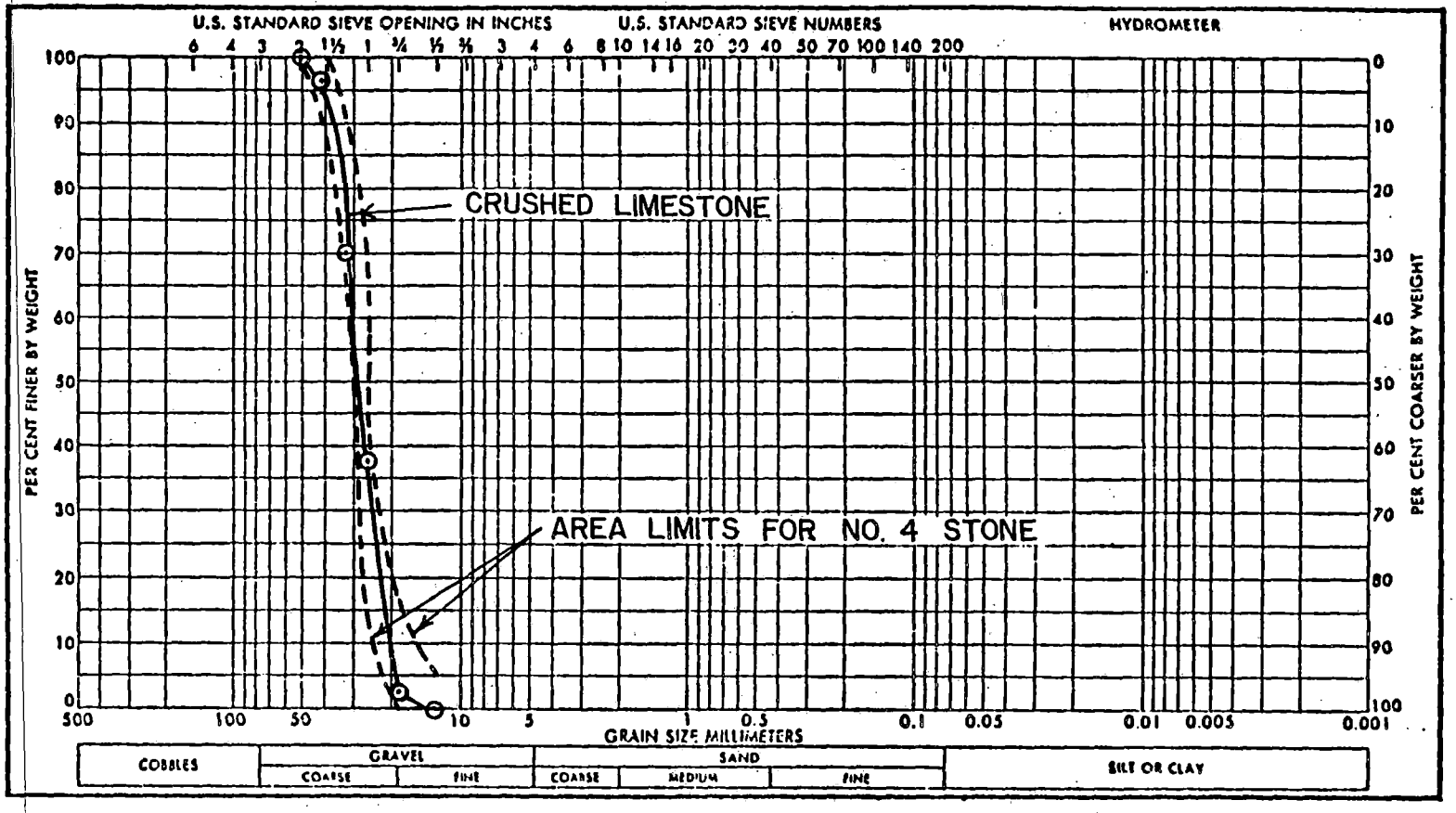

Figure 3.2. Gradation Curve for Crushed Limestone Ballast

amount of applied compaction effort, but not the final "stabilized" condition achieved after large amounts of compaction. Prior to compaction, rubber mats were placed on top of the ballast over the entire track bed. These rubber mats served: to prevent the ballast particles from "bouncing" out of the bed during vibratory compaction, and to prevent particle degradation. The simulated track bed was then created with 1000 passes from the vibratory plate compactor over the entire length of the test box.

Vibratory Plate Compactor. The mechanical compactor used to prepare the simulated track bed is a portable vibratory plate compactor, model S-50, manufactured by Stone Construction Equipment, Inc. (Ref. 19). The steel base plate dimensions are 3/8 in. (9.53 mm) thick by 24 in. (0.61 m) in. width and 21 in. (0.53 m) in length. At operating speed with the clutch engaged, the engine rotates an eccentric shaft which causes the base plate to vibrate. The rotation propels the machine forward, as well as imparting a compaction force to the ballast. The manufacturers' specifications (Ref. 19) rate the operating frequency at 83.3 Hz and the generated dynamic force at 5000 lb (22.3 kN).

Test Procedures and Program. After the ballast was initially prepared in a loose density state by the previously described technique, the vibratory plate compactor was used to compact the ballast. At certain intervals during the compaction process, ballast density tests and plate load tests were performed in order to monitor the changes in physical state of the ballast.

The individual locations of these tests were selected such that the following requirements were fulfilled: 1) all tests were performed in the center zone of the compacted track bed, 2) at a given number of passes, the

BDT's and PLT's were spaced at sufficient distances apart so as not to interfere with an adjacent test, and 3) after the completion of next successive series of compactor passes, BDT's and PLT's were performed at locations which would not have been influenced by previous testing. The plaster of paris used for the PLT and BDT was removed from the track bed at the completion of a test, and the resulting void was filled with fresh ballast.

The BDT apparatus (Fig. 3.3) consisted of a 7.5 in. (191 mm) inside diameter surface ring 6 in. (152 mm) high with top and bottom plates, a thin flexible rubber membrane, and a micrometer point gage. The circumference of the test hole is initially stabilized with a plaster of paris mixture to prevent the ballast particles from caving into the hole during excavation. A water volume measuring device (not shown) is used in conjunction with the point gage to measure the volume of water required to replace the volume of excavated ballast material. The head of water within the surface ring is sufficient to conform the membrane to the ballast surface in the sampling hole both before and after excavation. The ballast density is calculated by dividing the weight of the excavated ballast by the volume of the hole.

The primary components of the PLT loading system (Fig. 3.4) were a 20-ton (178 kN) capacity hydraulic load jack connected to a hand pump and an electronic load transducer. The latter was a four-arm bridge strain gage type load cell having a 10-ton (89-kN) capacity. The load cell is rigidly fixed and coaxially aligned with the moving head of the hydraulic load jack, and thus both provide direct measures of the applied load. The load cell output signal was connected to an X-Y recorder.

The deformation system is comprised of a direct current displacement transducer (DCDT) and a dial indicator which are also in coaxial arrangement.

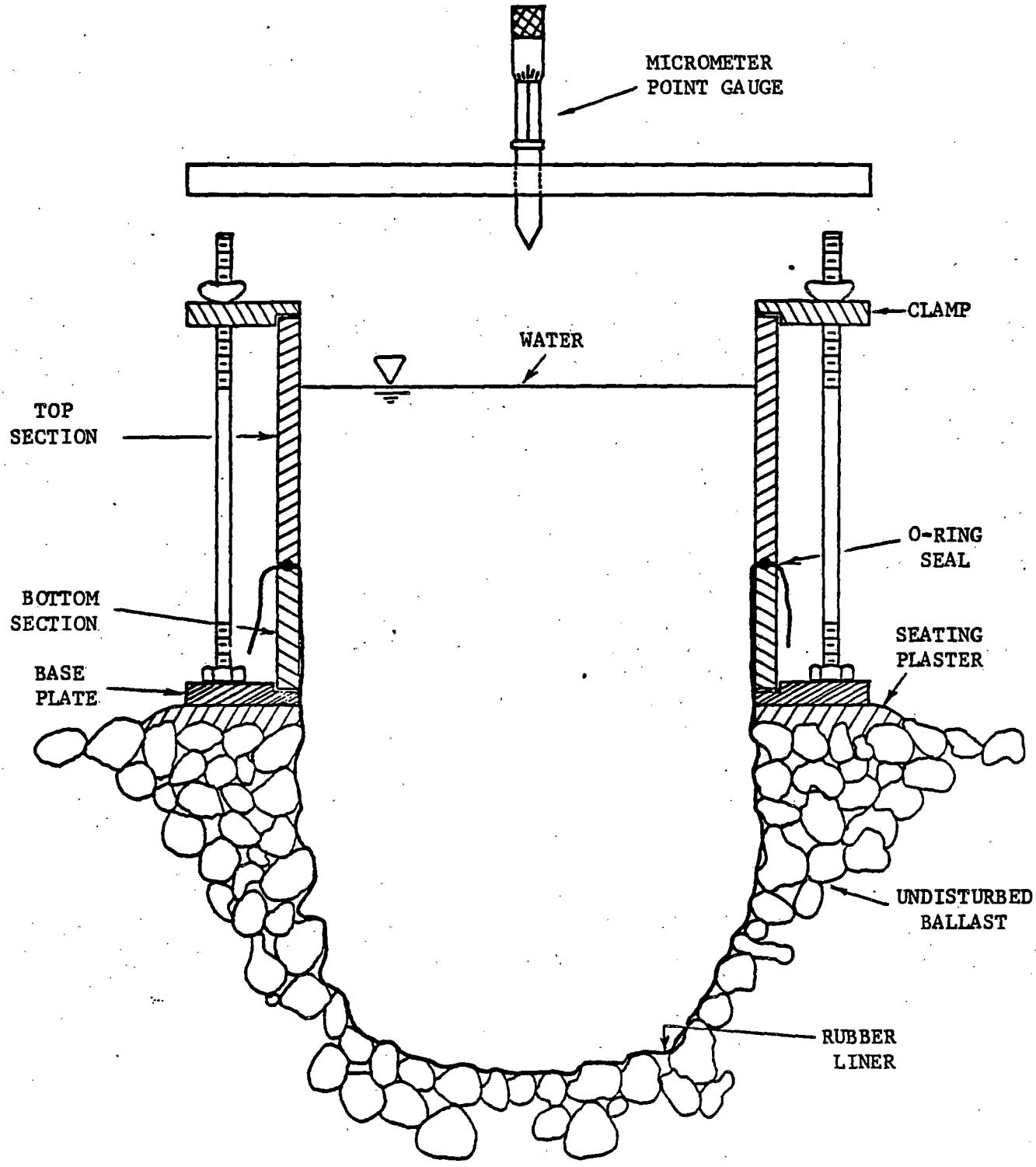

Figure 3.3. Illustration of Water Replacement Apparatus Set Up for Ballast Density Test (Ref. 1)

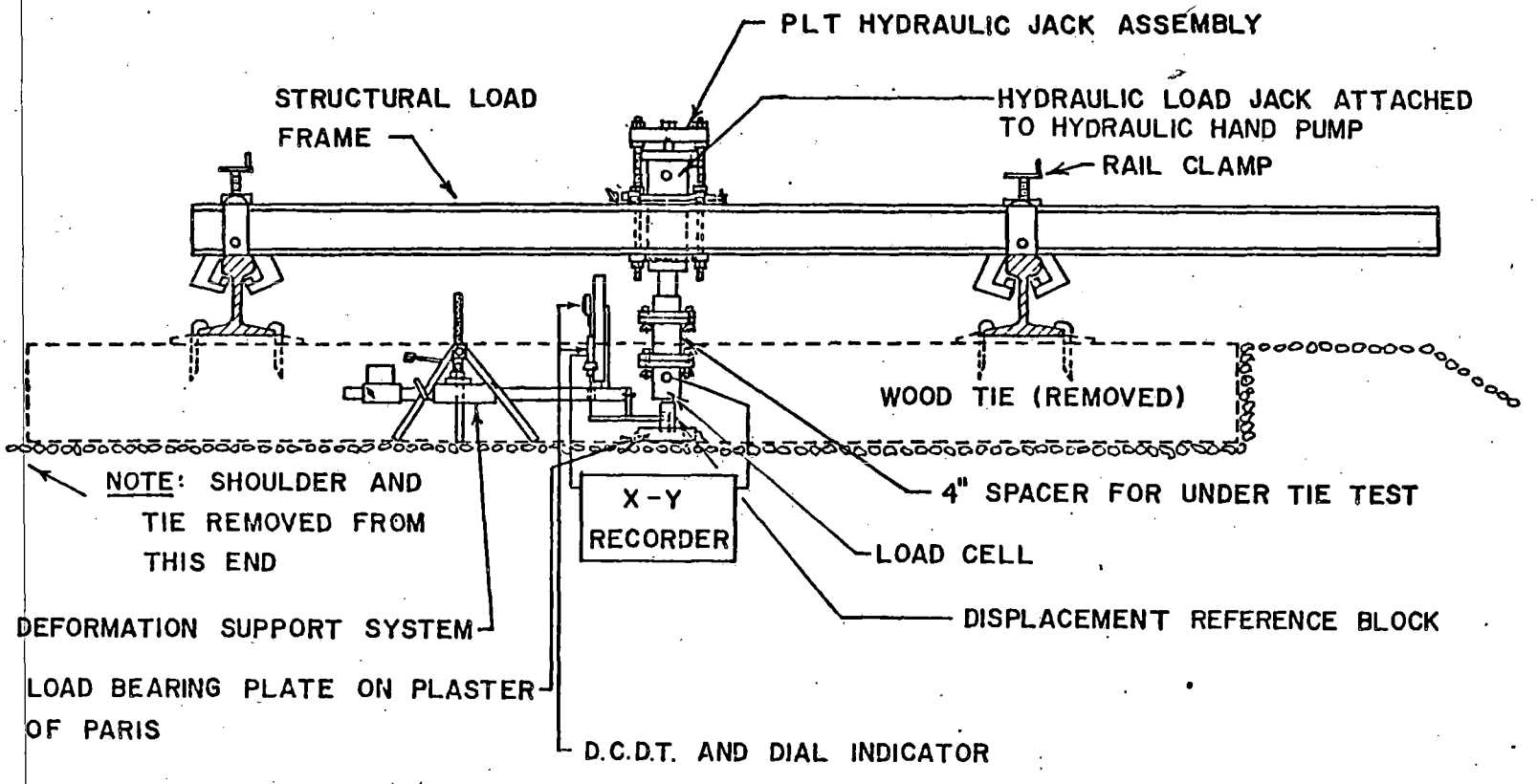

Figure 3.4. Assembled Plate Load Test Apparatus (Ref. 1)

The DCDT is powered by a 6 volt battery and is also connected to the X-Y recorder. The deformation system is mounted on a modified camera tripod equipped with a displacement lever arm. The lever arm is inserted into a slot in the deformation reference block, which is seated on the 5-in. (127-mm) diameter 1-in. (25.4-mm) thick steel bearing plate. The bearing plate is initially set in a level position on a thin layer of plaster of paris.

The hydraulic hand pump was used to displace the load jack piston and subsequently the plate such that the rate of deformation was about 0.25 in. (6.4 mm) per minute until a deformation of 0.3 in. (7.6 mm) was reached. At this point, the jack pressure was then released to unload the plate. This loading process was repeated a maximum of five times in the same manner except that the test was stopped at the peak load achieved during the first loading cycle rather than at 0.3 in. (7.6 mm) deformation.

From the recorded results for each plate test, the parameter Ballast Bearing Index (BBI) was determined. The BBI is equal to the plate load at 0.1, 0.2 or 0.3 in. (2.5, 5.1 or 7.6 mm) displacement divided by the plate area.

3.2 TEST RESULTS

At each test interval during the compaction of the track bed, i.e., after 2 passes, 5 passes, etc., a minimum of two plate load tests and one in-situ ballast density test were performed. These physical state tests would determine the number of passes required to achieve an old track bed condition using the vibratory plate compactor.

In-Situ Ballast Density Tests. Generally, the ballast density increased as the number of passes with the vibratory plate compactor increased

(Fig. 3.5). An apparently "stable" density condition is quickly produced with 25 to 50 passes. The density value achieved was approximately 110 pcf (1.76 Mg/m^3). After 50 passes, there was only a slight increase in density with additional passes from the compactor. This is particularly evident by noting that the final average ballast density at 1000 passes was 111 pcf (1.78 Mg/m^3).

There existed a large difference in the initial density values at zero passes (Fig. 3.5). This can quite possibly be attributed to the sample preparation technique, which may have produced a non-uniform density distribution along the length of the track bed. This technique could have also been responsible for some of the scatter in the density measurements with the higher number of compactor passes. The data scatter might also be influenced slightly by any nonuniformity of the compaction procedure and the associated ballast density test sampling locations. However, for the duplicate density tests performed at 50 and 200 passes, reasonably reproducible density measurements were obtained.

Plate Load Test. The BBI values obtained from plate load tests at each given number of passes were averagedat 0.1, 0.2 and 0.3 in. (2.5, 5.1 and 7.6 mm) deformation. These average values were plotted against the number of passes in Fig. 3.6. Examination of Fig. 3.6 reveals that the ballast stiffness continued to increase with the number of compactor passes until 500 passes was reached. At this point, the BBI values essentially stabilized at the three deformation levels.

The maximum average BBI value at 0.1 in. (2.5 mm) deformation was approximately 192 psi (634 kN/m^2), while at 0.2 in. (5.1 mm) this value was

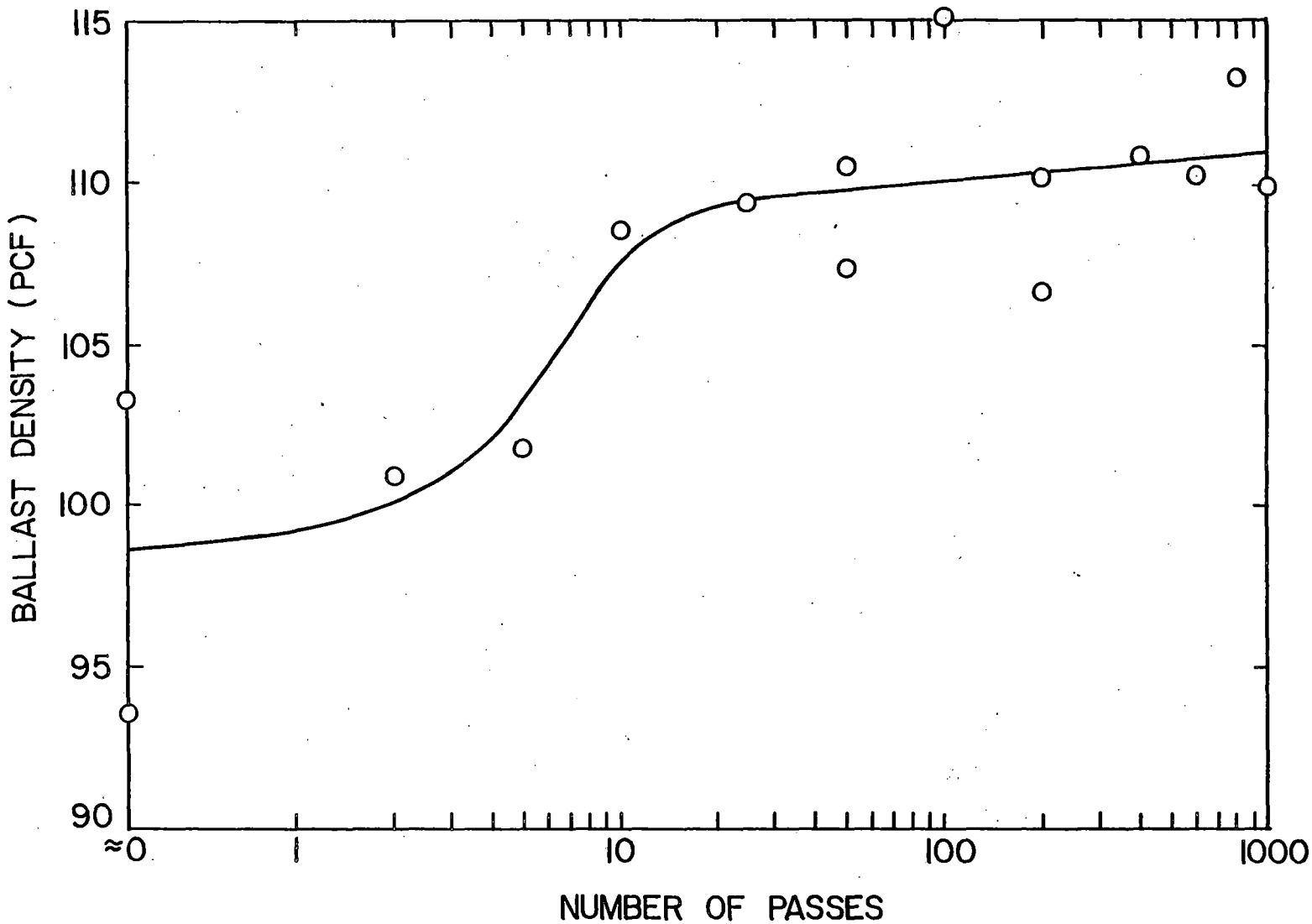

Figure 3.5. Relationship Between Ballast Density and Number of Compactor Passes for a Simulated Track Bed

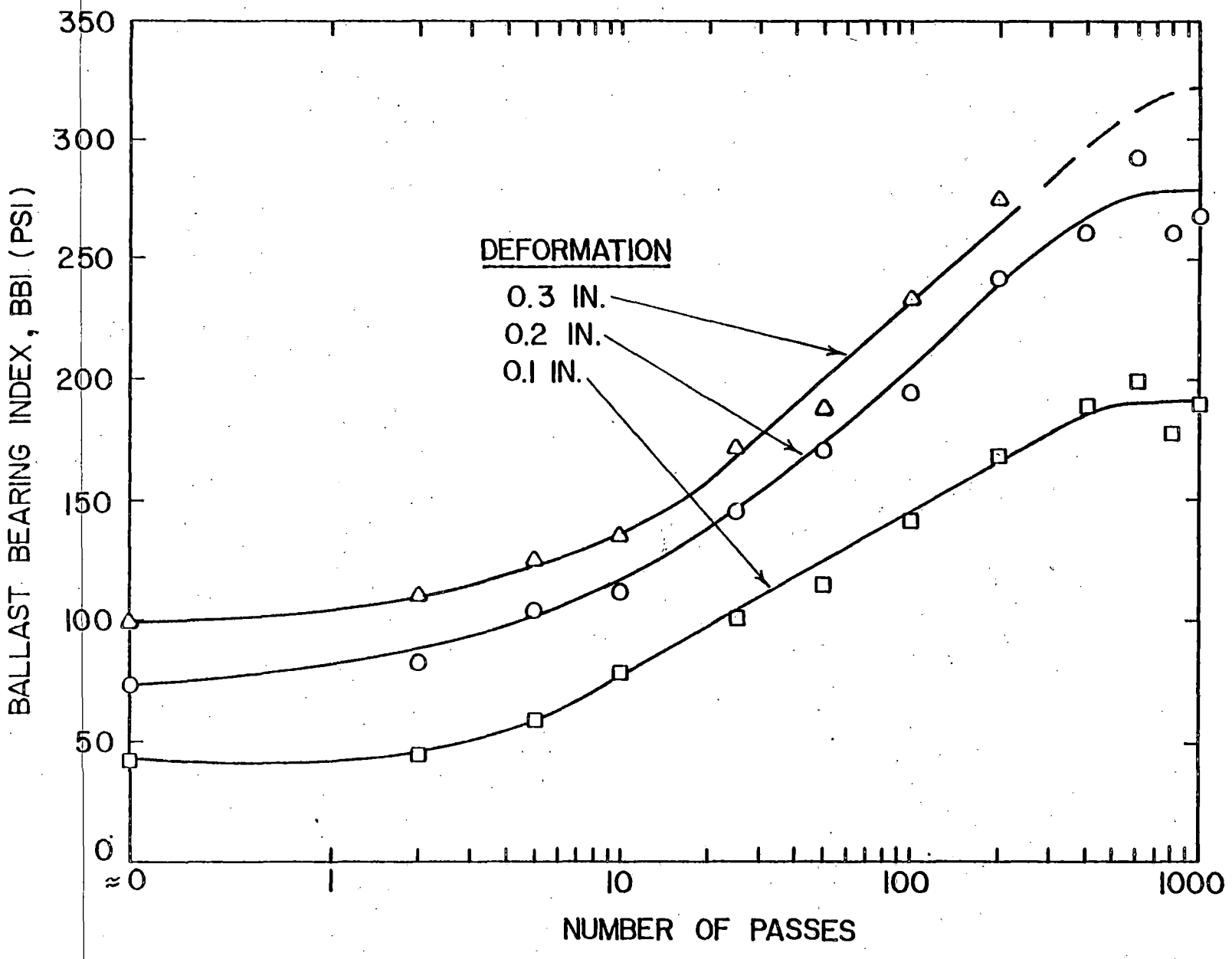

Figure 3.6. Relationship Between Strength and Number of Compactor Passes for a Simulated Track Bed

279 psi (1922 kN/m^2). The curve for 0.3 in. (7.6 mm) deformation was reasonably extrapolated after 200 passes because there are no test values to substantiate the curve. As the number of passes increased, the plate load resistance increased such that the test could no longer be carried out to 0.3 in. (7.6 mm) deformation without causing some damage to the large test box.

Unlike the ballast density test results, the plate load test results formed well defined trends with number of compactor passes and displayed reproducible test measurements. Once the BBI values stabilized, however, the scatter of the test results increased slightly. The reasons for this data scatter may, in part, be similar to those described for the in-situ ballast density test.

Correlation of PLT and BDT Results. For each given number of compactor passes, the average BBI values and the average ballast density measurements are plotted in Fig. 3.7. The resulting curves at 0.1 and 0.2 in. (2.5 and 5.1 mm) deformation produced a large scatter of data points but the general trends still appear. Initially, as the ballast density increased, then so did the BBI values. However, as the number of passes with plate compactor increase beyond approximately 25 passes, the ballast density leveled off very quickly (see Fig. 3.5). The BBI values did not level off until approximately 500 passes had been completed (Fig. 3.6). In other words, the BBI continued to increase with very little change in density. It is possible, therefore, to have two vastly different stiffness moduli values for the same density value. This fact suggests that plate load tests may be a better indicator of the physical state of the ballast.

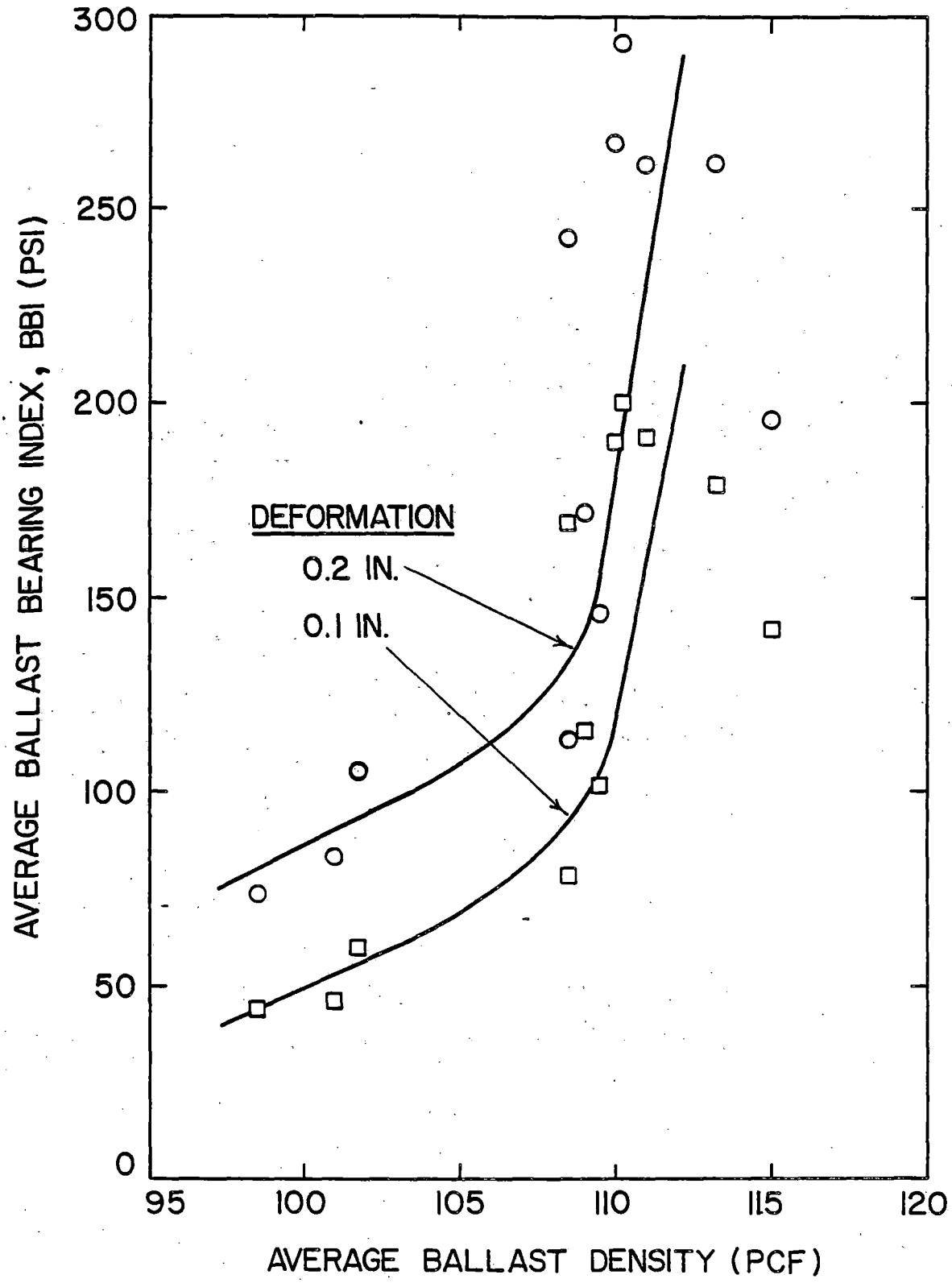

Figure 3.7. Strength-Density Relationship for the Simulated Track Bed

As indicated by Panuccio and Dorwart (Ref. 4), the plate load test is very sensitive to changes in the ballast physical state. However, the differences in the plate resistance and density trends with number of compactor passes may be accountable for other reasons. The BDT primarily samples the top 4 to 5 in. (0.10 to 0.13 m) of the ballast layer, whereas, the PLT effectively measures the ballast resistance to depths of 10 to 12 in. (0.25 to 0.31 m). With a few passes from the vibratory plate compactor, the ballast surface may quickly achieve a compacted state while the underlying ballast may still remain in a relatively loose state as compared to the surface. The PLT and BDT would thus measure two slightly different ballast physical state conditions. Additional passes from the compactor would subsequently produce higher degrees of compaction below the surface ballast. These changes would be more adequately reflected in the plate resistance measurements rather than in the ballast density.

3.3 COMPARISON WITH FIELD DATA

The plate load test and in-situ ballast density test results obtained from the simulated crushed limestone track bed are compared only to SUNYAB field data obtained with these devices. These field physical state test results are more thoroughly examined and compared with other available field data elsewhere (Refs. 4 and 7).

The field test sites were at both the Illinois Central Gulf Railroad (ICG) and at the Facility for Accelerated Service Testing (FAST). The ballast at ICG was a mixture of cleaned and screened in-situ limestone and steel slag. The ballast physical state tests were conducted at a traffic condition estimated at 5 MGT after the most recent tamping operation. At

FAST, these tests were conducted after 135 MGT of traffic on a crushed limestone ballast. The ballast gradations are similar in all cases.

The comparable field test location for the simulated track bed is in the center of the track and under the tie. For the plate load tests, the average BBI value at 0.2-in. (5.1-mm) deformation was 107 psi (737 kN/m^3) at ICG and 307 psi (2115 kN/m^3) at FAST. The simulated track bed at 1000 compactor passes produced a value of 279 psi (1922 kN/m^3) which is in fairly good agreement with the FAST data.

The in-situ ballast density test results at FAST yielded an average density of 109.7 pcf (1.76 Mg/m^3). At ICG, the corresponding average was 101.2 pcf (1.62 Mg/m^3), which is a value based upon an equivalent limestone density. An average density of 111.0 pcf (1.78 Mg/m^3) was obtained after 1000 passes from the simulated track bed, which again demonstrates good agreement with the FAST data.

In general, these comparisons indicate that a representative track bed was successfully constructed in the laboratory with the sample preparation techniques used.

4. INVESTIGATION OF MANUAL TIE TAMPING

4.1 APPARATUS AND PROCEDURES

Test Box. In addition to the features described in Section 3.1, the test box (Fig. 3.1) was designed such that the actual field track structure was also closely duplicated. The tie tested was 9 in. (229 mm) wide by 7 in. (178 mm) deep by 102 in. (2.59 m) long and weighed 208 lb (926 N). The depth of the box is 19 in. (483 mm) which allows for the tie to be used on top of a 12-in. (305-mm) layer of ballast. This depth of ballast beneath the tie, which was used for the simulated track bed, is a standard used by the railroad industry. The width of the test box is 35 in. (0.89 m). When the tie is placed in the center of the box, two 13-in. (0.330-m)-wide cribs are present on each side of the tie. This dimension yields an equivalent tie spacing of 22 in. (0.56 m), which also is a standard employed by several different railroads. The test box is long enough, i.e., 186 in. (4.73 m), to accommodate the testing of 12 in. (305 mm) or less flat shoulder width and variable shoulder slopes. In this study, the width was 12 in. (305 mm) and the slope was 3 horizontal to 1 vertical.

Tamping Equipment. The manual tie tamping was performed using two standard hand tools that are commonly used in railroad trackwork. One of these tools is a ballast fork, which is used for tie tamping and shovelling or "forking" ballast. The ballast fork is similar to a combined short handle shovel and farmer's pitchfork. The end of the ballast fork primarily consists of a series of ten parallel metal prongs. One advantage of using a ballast fork instead of a shovel to move ballast is that the fork enables the user to sift the fine grained materials out of the ballast.

The other hand tool used in the tie tamping test series is a lining bar. A lining bar is a round steel rod which is blunt on one end and wedge-shaped or pointed on the other. This bar serves an almost unlimited number of functions in everyday railroad trackwork.

Sample Preparation. Once the simulated track bed was prepared after 1000 passes from the vibratory plate compactor, the track section was ready for the tamping operation. The tie was positioned in the center of the test box such that both cribs were of equal width. The cribs were filled and shoulder section formed by shoveling the crushed limestone ballast (Fig. 2.2) into place in a relatively loose density state. Most of the particles in the crib that extended appreciable distances above the top of the tie were removed by running the ballast fork over the tie surface. The rails were set into position, thus leaving a space between the rails and the tie.

In order to tamp the ballast underneath the tie, the tie first had to be raised. This was accomplished by shoving the pointed end of the lining bar at approximately a 45° angle to the horizontal into the shoulder ballast and under the tie end. A spacer, having a thickness equivalent to a standard tie plate, was inserted between the rail and the tie. By utilizing the shoulder ballast as a fulcrum, a sufficient downward force was applied to the free end of the lining bar to move the tie and spacer upward until contact was securely made with the rail base. This process subsequently created a void under the tie. Using the ballast fork, the crib ballast outside the rail was cleared from the edge of the tie until this void was visible. Ballast was then shoved, with the fork, from the crib into the

void until the void was packed as tightly as possible. This process was repeated in the opposing crib outside of the rail and on both sides of the tie just inside the rail. The lining bar was withdrawn from the shoulder ballast and the tie remained in place. The spacer was then removed. This tamping sequence was also performed at the other end of the tie for the same four locations. Additional ballast was used to reform the cribs and shoulders. Thus, tamping was performed at a total of eight locations under the tie, the same eight locations that are tamped mechanically by a tamping machine.

Test Procedure and Program. The changes in the physical state of the ballast for the manual tie tamping test series were evaluated by the ballast density test (BDT), the plate load test (PLT), and the lateral tie push test (LTPT). The BDT and the PLT apparatus were previously described in Section 3.

The lateral tie push test apparatus is schematically illustrated in Fig. 4.1. The load and displacement measuring instrumentation are the same as those used for the plate load tests. The LTPT apparatus also utilizes the PLT structural load frame which, when clamped to the rails, provides the appropriate load reaction from the track structure. The load frame is modified for tie push testing by rigidly affixing the L-frame attachment to the end of the load frame. The load assembly is mounted within the L-frame attachment in a horizontal position such that the load system is coaxially aligned with the center line of the tie (Fig. 4.1). In order to insure good seating and uniform load distribution at the tie end, a serrated seating plate assembly is attached to the end of the load cell. This LTPT apparatus

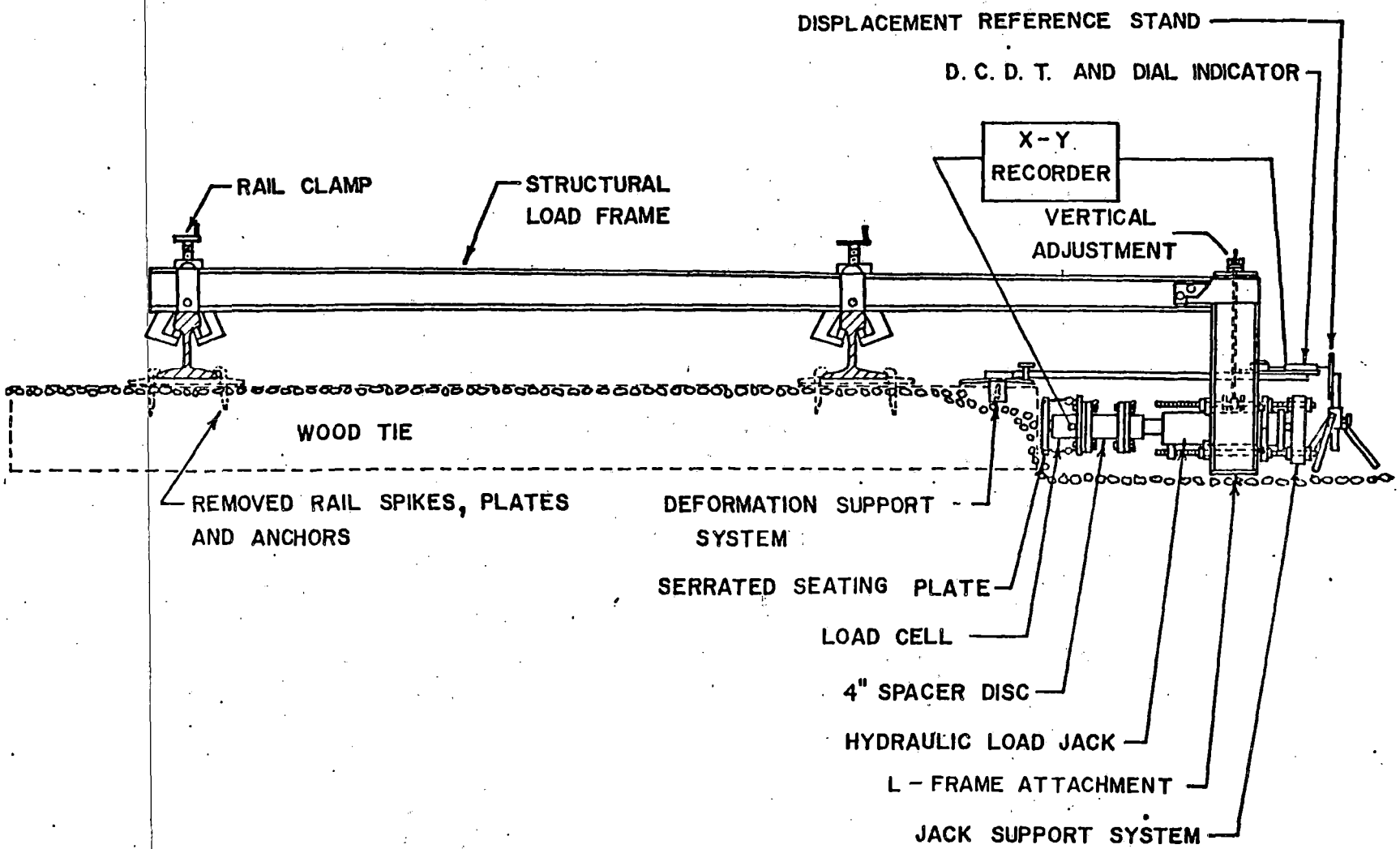

Figure 4.1. Assembled Lateral Tie Push Test Apparatus (Ref. 1)

provides the closest direct measurement of the ballast resisting forces acting upon a laterally displaced tie.

The tie displacement is measured by the DCDT and dial indicator connected in coaxial alignment and mounted horizontally on the deformation support frame. This frame is rigidly clamped to the same end of the tie that the load system acts upon. The end of the DCDT's moveable core is spring loaded against the reference plate of the displacement reference stand. The tripod-type reference stand is securely seated on the ballast shoulder and provides a reference datum point for the tie displacement measurements.

Using the hydraulic hand pump, load was applied to the tie end at a deformation rate of 0.25 in./min (6.35 mm/min) until a maximum displacement of 0.25 in. (6.35 mm) was reached. At this point, the maximum load and displacement were simultaneously recorded, and the jack pressure was released, which thus relieved the load on the tie. The permanent displacement was then recorded. The test procedure was then repeated for a second cycle.

The techniques used in the LTPT data reduction are very similar to those that are used for plate load test data reduction. For both cycles of the load-displacement plots, the corresponding loads or lateral tie resistance value at 0.039 (1), 0.079 (2), 0.157 (4) and 0.25 in. (6.35 mm) displacement levels were obtained. The initial static load (ISL) was determined by defining the load point where tie displacement began to occur. Also computed was the elastic recovery (E_r) of the tie, which is defined as

$$E_r = \frac{\Delta_p - \Delta_r}{\Delta_p} \times 100\%, \qquad (4\text{-}1)$$

in which Δ_p and Δ_r = peak and rebound displacements, respectively.

The test program for the manual tie tamping series is listed in Table 4.1. The effects on lateral tie resistance of the following factors were investigated: 1) different tie weights, 2) varying crib ballast depths with no shoulder, 3) overfilled cribs with no shoulder, and 4) height of and procedure used for the tamping raise. Several duplicate tests were incorporated into the test program for checks on reproducibility of results.

For each individual test series within the test program, the simulated track bed remained compacted until the tie tamping operation was performed. After completing all testing on the tamped tie, the crib and shoulder ballast was excavated, and the tie was removed. Approximately 2 to 3 in. (51 to 76 mm) of the remaining loose surface ballast was also removed such that the original track bed was exposed. In order to "smooth" out the surface of the simulated track bed which had been somewhat disturbed as a result of tamping operations, the rubber mats were placed over the ballast and the vibratory plate compactor with the added steel base plate was run over the track bed for 50 passes. The procedure for tie and ballast placement conditions was then repeated for the next tamping test series.

4.2 TEST RESULTS

Typical LTPT Load-Displacement Curves. Several of the lateral tie push test (LTPT) load-displacement curves on individual ties are shown in Fig. 4.2. Each curve is labeled with the appropriate test identification number, the ballast conditions that existed during testing, and the number of the applied loading cycles. These load-displacement curves are representative test results for most of the factors that were investigated.

Table 4.1. Test Program for Manual Tie Tamping in Crushed Limestone Ballast

LTPT Series No.	Density State	Test No.	Factors† Investigated	Total Height of Raise(in.)	Other Tests# Density	Other Tests# Plate Load
I	Compacted Base, Loose Crib & Shoulder	1	No Crib, No Shoulder	0	--	--
I		2	No Crib, No Shoulder	0	--	--
I		3	No Crib, No Shoulder, Wt. on Tie =191 lb	0	--	--
I		4	No Crib, No Shoulder, Wt. on Tie=191 lb	0	--	--
I		5	No Crib, No Shoulder, Wt. on Tie=402 lb.	0	--	--
I		6	1/2 Full Crib, No Shoulder	0	--	--
I		7	Full Crib, No Shoulder	0	Before LTPT I-7: I-1	--
I		8	Full Crib, Full 12 in. Shoulder	0	--	--
I		9	Full Crib, No Shoulder, Crib Load = 250 lb	0	--	--
I		10	Full Crib, No Shoulder, Crib Load = 500 lb	0	--	--
I		11	Full Crib, No Shoulder, Load Removed	0	--	--
I		12	Full Crib, No Shoulder, Loosened Crib	0	--	--
I		13	Full Crib, Full Shoulder, After Tamping	2	After LTPT I-13: I-2, I-3	After LTPT I-13: I-1, I-2, I-3, I-4, I-5, I-6

Table 4.1, Test Program for Manual Tie Tamping in Crushed Limestone Ballast (continued)

LTPT Series No.	Density State	Test No.	Factors† Investigated	Total Height of Raise (in.)	Other Tests#	
					Density	Plate Load
II	Compacted Base Loose Crib & Shoulder	1	No Crib, No Shoulder	0	--	--
II		2	Full Crib, No Shoulder	0	Before LTPT II-3+: II-1	Before LTPT II-3+: II-1
II		3	Full Crib, Full Shoulder, After Tamping	3	After LTPT II-3: II-2, II-3	After LTPT II-3: II-2, II-3, II-4, II-5, II-6, II-7
III	Compacted Base Loose Crib & Shoulder	1	Full Crib, Full Shoulder	0	Before LTPT III-1: III-1	Before LTPT III-1: III-1
III		2	Full Crib, Full Shoulder, After Tamping	0.5	--	--
III		3	Full Crib, Full Shoulder, After Tamping	0.5*	--	--
III		4	Full Crib, Full Shoulder, After Tamping	0.5*	--	--
III		5	Full Crib, Full Shoulder, After Tamping	0.5*	--	--

† All LTPT had 2 Cycles of Load

Performed on Conditions Established for the Given LTPT Test No. But Immediately Before or After That LTPT is Run.

\+ After Tamping and Before Filling Crib

* In Addition to Preceding Raise

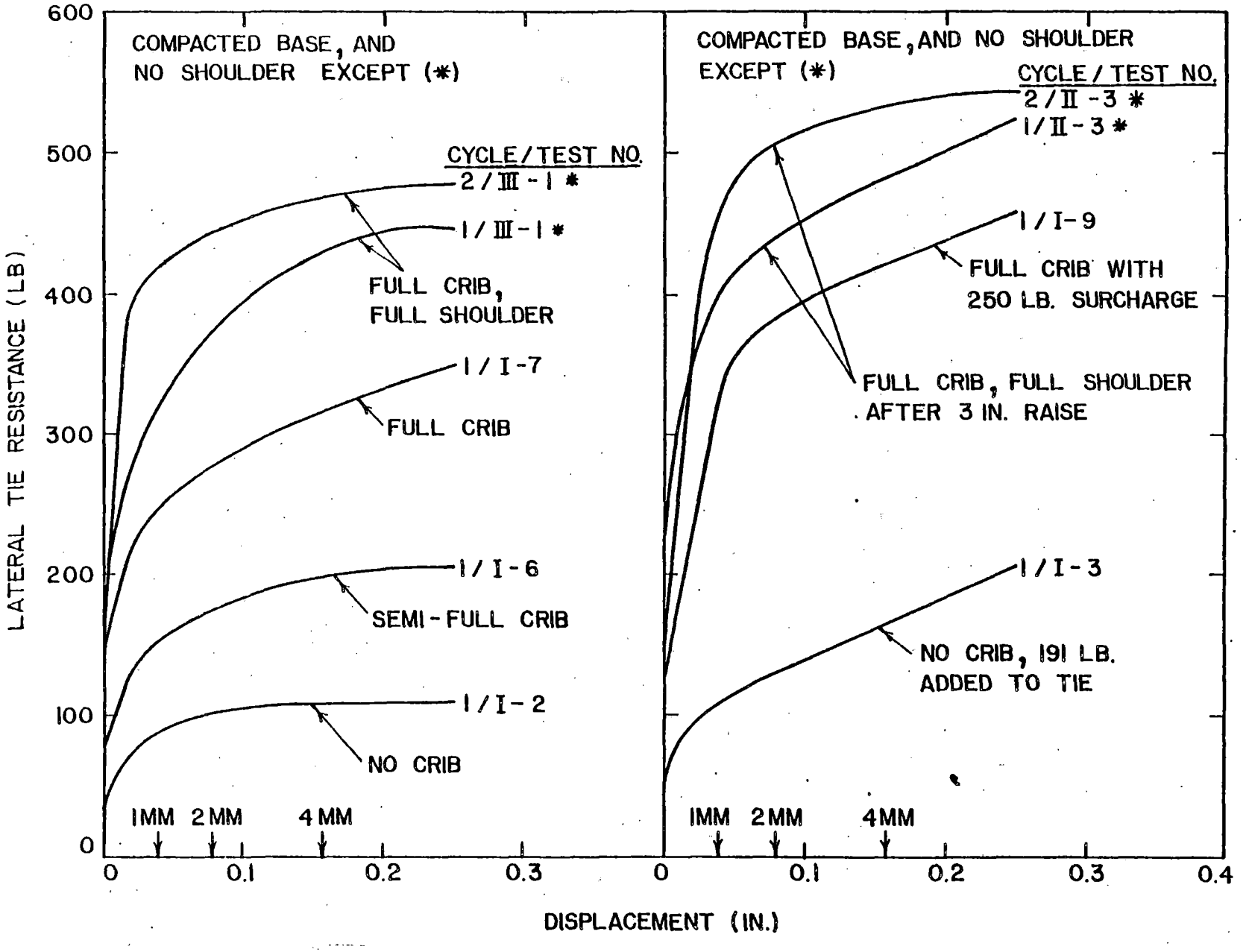

Figure 4.2. Typical LTPT Load-Displacement Curves

In general, the shapes of most LTPT load-displacement curves are fairly uniform although differing in the magnitudes of load. Initially, the rate of change of applied load with tie displacement is very large. However, as tie displacement continually increases, the slope of the curve decreases until the load is nearly constant. This response is typical and is confirmed from previous studies (Refs. 2, 3, and 4).

As one might expect from the curves in Fig. 4.2, the condition that offered the least lateral tie resistance was (Test No. I-2) for a tie resting on a compacted track bed with no crib or shoulder ballast. If the tie weight for the previous condition is nearly doubled (Test No. I-3), lateral tie resistance demonstrates a marked increase at all displacement levels. However, more important than increase tie weight, is the effect a semi-full crib (Test No. I-6) or a full crib (Test No. I-7) has upon increasing lateral resistance for a tie on a compacted base and no shoulder ballast.

Tests were also performed in which surcharge loads were applied to full crib ballast conditions in order to simulate overfilled cribs (Test No. I-9). From Fig. 4.2, for ties on a compacted base, the lateral tie resistance for a surcharged crib with no shoulder ballast slightly exceeds the tie resistance for a full crib and no shoulder condition (Test No. I-7) and yields comparable tie resistances values for a full crib and full shoulder condition (Test No. III-1). This comparison provides some indication as to the importance of crib ballast in the resistance to lateral tie movement.

The greatest lateral tie resistance occurred for the full crib and shoulder ballast conditions in the after tamping stage (Test No. II-3). This tie resistance is significantly higher than the tie resistance obtained

under similar conditions with the tie resting on a compacted base (Test No. III-1). This result is understandable and expected. Underneath the tie at the tie-ballast interface, a compacted base will have a smooth ballast surface while a freshly tamped base would exhibit a rougher surface. Thus, the differences in lateral tie resistance would be primarily attributed to the differences in the base component of resistance. From Fig. 4. 2, it is apparent that the second cycle of loading usually offers slightly greater lateral tie resistance than does the first cycle. This is most likely the result of a densified ballast shoulder condition due to load cycling.

The LTPT loads at several displacement levels and the percent elastic recovery (E_r) were determined for all tests performed. However, Panuccio and Dorwart (Ref. 4) have concluded that the E_r and the initial static load (ISL) values do not offer any potential as possible means of evaluating factors investigated by the LTPT. These values will, therefore, not be elaborated upon further. Also, LTPT series Number I-4 and I-12 will not be discussed since the actual test conditions existing during the time of testing are questionable.

The tie for each test condition (Table 4.1) generally received two cycles of loading. With the exception of tests performed with a full ballast shoulder, the lateral tie resistances from cycle one and cycle two will be averaged to present the general trends. In some of the cases with no shoulder, cycle number two produced slightly greater tie resistance load values than cycle number one. It is assumed that this difference is the result of a slightly changed ballast physical state condition occuring in the cribs or under the tie during cycle 1. This difference also may have

occurred with the individual sample preparation for each test condition. Thus, using the average lateral tie resistance at each displacement level appears acceptable. Also, as previously indicated, the variation of lateral tie resistance between both cycles is more pronounced for a full ballast shoulder condition and, therefore, the results for the two loading cycles will be analyzed separately.

Effect of Height of Raise. The test tie was raised by the sample preparation procedure described in section 4.1. In each case, the tie initially rested on the compacted base surrounded by full cribs and shoulder. This condition will represent a zero track raise. For test series I and II, the ties received full raises of 2 and 3 in. (51 and 76 mm), respectively. In test series III, the tie was raised and tamped in a series of four 0.5-in. (12.7-mm) increments until a full 2-in. (51-mm) raise was achieved. After a given increment, the cribs were refilled and the shoulders reformed prior to testing.

The lateral tie resistance as a function of the height of the tamping raise is shown in Fig. 4.3. Included in this figure are the first cycle loads at 0.0397 and 0.157 in. (1 and 4 mm) displacement levels and the second cycle loads at 0.157 (4 mm) displacement.

The first apparent result is that all tests conducted in the after tamping condition yielded significantly greater tie resistance values than the test conducted with a compacted base condition, i.e., zero tie raise. This trend is exhibited at all displacement levels and both cycles of loading (Ref. 20). The reason, which has been previously discussed, is believed to be the difference in the surface roughness of the ballast underneath the tie.

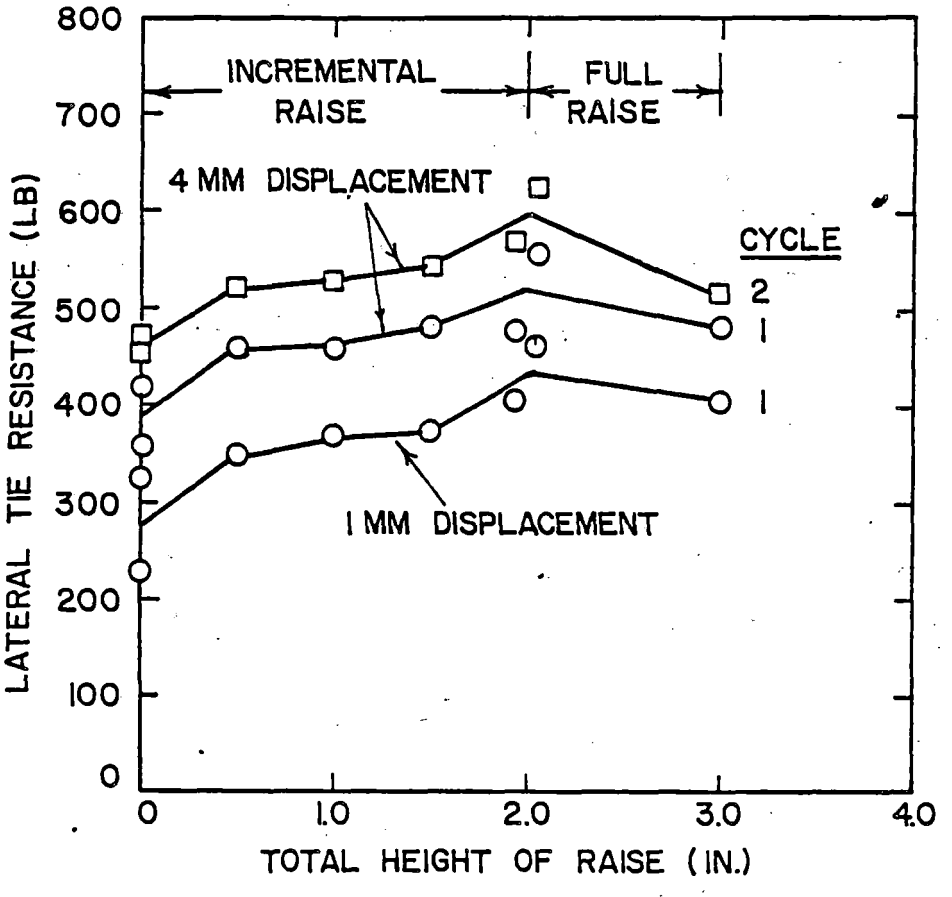

Figure 4.3. The Effect of the Height of a Tamping Raise on Lateral Tie Resistance

An examination of Fig. 4.3 reveals that for test series III, the incremental tamping raises produced fairly consistent lateral tie resistances at all displacement levels for both cycle 1 and 2 tie loadings. This result, in part, indicates uniformity of the manual tie tamping procedure and subsequent reproducibility of the test results. In a comparison to the results of the two tests performed with full 2-and 3 -in. (51 - and 76-mm) tamping raises, a 3-in. (76-mm) full raise produced results comparable to the incremental raise, while the 2-in. (51-mm) full raise yielded slightly greater tie resistance values. These findings appear to be consistent at all displacement levels and for both loading cycles (Ref. 20). An explanation for the different results obtained from the full 2 in. (51 mm) raise is not readily available, except for a possible association with normal testing variability. An overall assessment of the test results presented in Fig. 4.3 indicates that lateral tie resistance of a single tie does not appear to be a function of the height of the tamping raise nor of the method used to achieve the raise, i.e., full or in lifts.

For all tests receiving a tamping raise, the average second cycle lateral tie resistance of 551 lb (2452 N) was generally 64 lb (285 N) or 13 percent greater than the average first cycle tie resistance values at 0.157 in. (4 mm) displacement. This trend is consistent for the data sets shown in Fig. 4.3. Densification of the ballast shoulder during testing appears to be the most plausible explanation for these numerically small load increases.

Effect of Crib Depth. Several tests were performed in which the depth of the crib ballast was varied while all other conditions were kept constant. For all tests, the tie was placed upon the compacted track bed and no shoulder

ballast was formed. Crib ballast was generally prepared in a loose density state.

The three following crib ballast depth conditions were investigated: 1) zero or no crib, 2) 3.5 in. (89 mm) of ballast or semi-filled crib, and 3) a full 7 in. (178 mm) crib section. The importance of ballast crib depth on the lateral tie resistance is shown in Fig. 4.4. Note, that the first and second cycle loads were averaged for each test condition at each displacement level, and the loads from both cycles of loading generally yield similar results. This averaging will, therefore, not influence the data analysis.

As expected, tie resistance increases with the increasing amounts of crib ballast. For all displacement levels, the relationship between lateral tie resistance and crib depth appears to be nearly linear. A full crib offers three times more and a semi-filled crib offers approximately two times more lateral resistance than a no crib ballast condition. This trend is consistent at each displacement level (Ref. 20).

In conjunction with the first cycle lateral tie resistance for a zero track raise in Fig. 4.3, the contributions of three components of tie resistance can be determined with Fig. 4.4 for a loose crib and shoulder, and a compact base. At 0.157 in. (4 mm) displacement, shoulder resistance is 16 percent, crib resistance is 56 percent, and base resistance is 28 percent of the total resistance. The consistency in the test results is also demonstrated at all displacement levels and, more importantly, indicates that crib ballast is the main component of the total lateral tie resistance.

Effect of Overfill Height. In order to determine the effect of

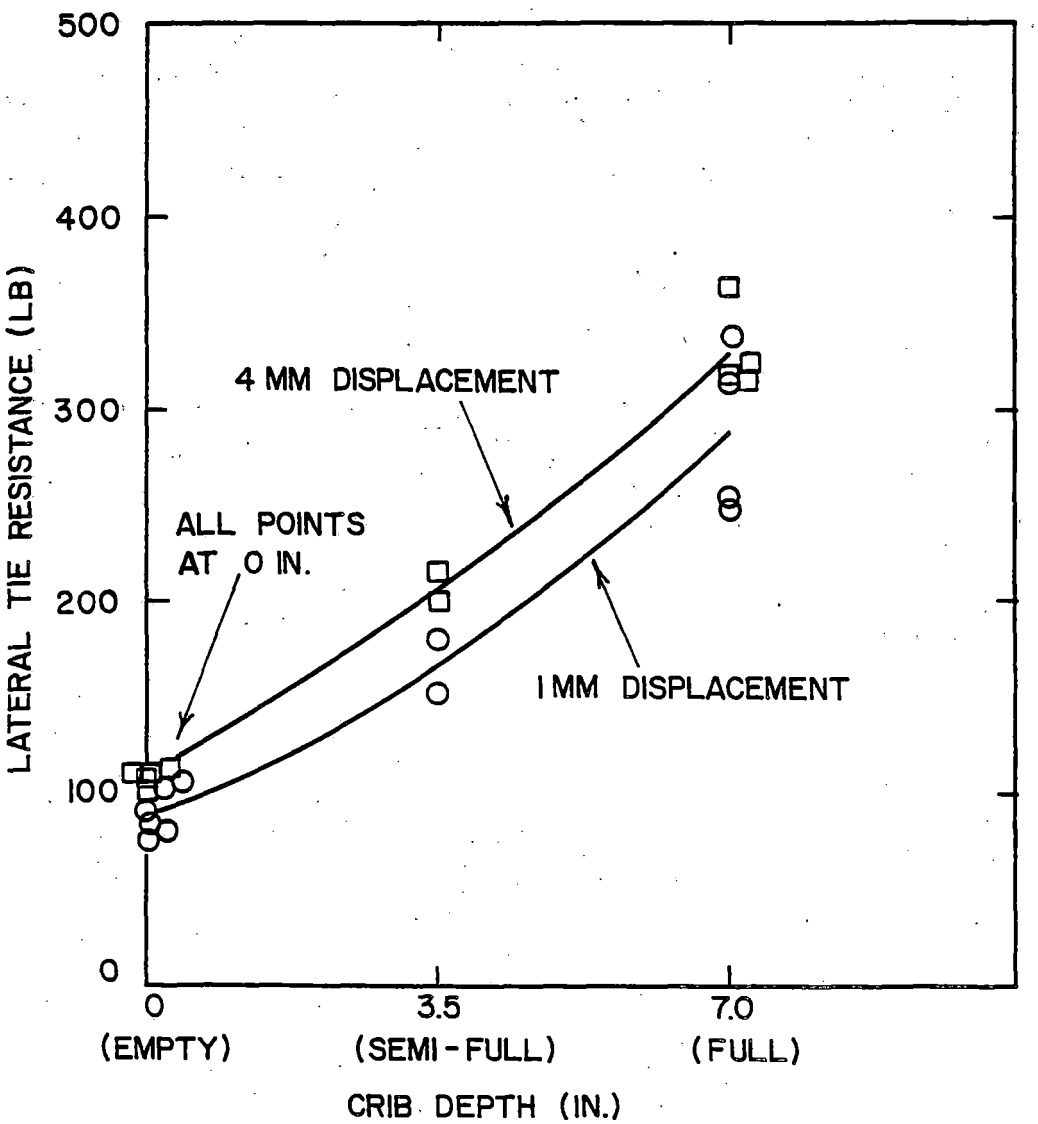

Figure 4.4. Relationship Between Lateral Tie Resistance on a Compacted Base with No Shoulder Ballast and Crib Depth

overfilling a railroad track crib with ballast, two tests were performed in which a surcharge load provided by concrete cylinders was uniformly distributed within each crib along the entire length of the tie. The first test was conducted with a surcharge load of 250 lb (1113 N) added to each crib while the second test used a 500 lb (2225 N) load. The lateral tie push tests were performed with the tie resting on a compacted base. No shoulder ballast was used and the cribs were full with loosely placed ballast.

The surcharge loads were converted to a volume of ballast in order to determine the crib ballast overfill height that each surcharge load represented. Generally, the ballast in the crib is in a loose state and has a ballast density of approximately 100 pcf (1.6 Mg/m^3). When this density is divided by the surface area of the crib, from end of tie to end of tie, the surcharge loads of 250 lb (1113 N) and 500 lb (2225 N) yielded equivalent overfill heights of 3.1 in. (79 mm) and 6.2 in. (158 mm), respectively. Thus, the average lateral tie resistance for both the first and second loading cycles can now be more conveniently illustrated as a function of crib ballast height (Fig. 4.5). The left side of Fig. 4.5 is the same as Fig. 4.4, while the right side shows the equivalent overfill heights. In general for each displacement level, the relationship between two parameters approaches linearity.

Weight of Tie. Several tests were performed with the tie resting on the compacted base with no crib or shoulder ballast and different uniformly distributed dead loads were applied to the top of the tie. Lateral tie resistance was determined for 1) an unloaded tie weighing 208 lb (926 N), 2) 191 lb (850 N) added to the unloaded tie, and 3) 402 lb (1789 N) added to the unloaded tie.

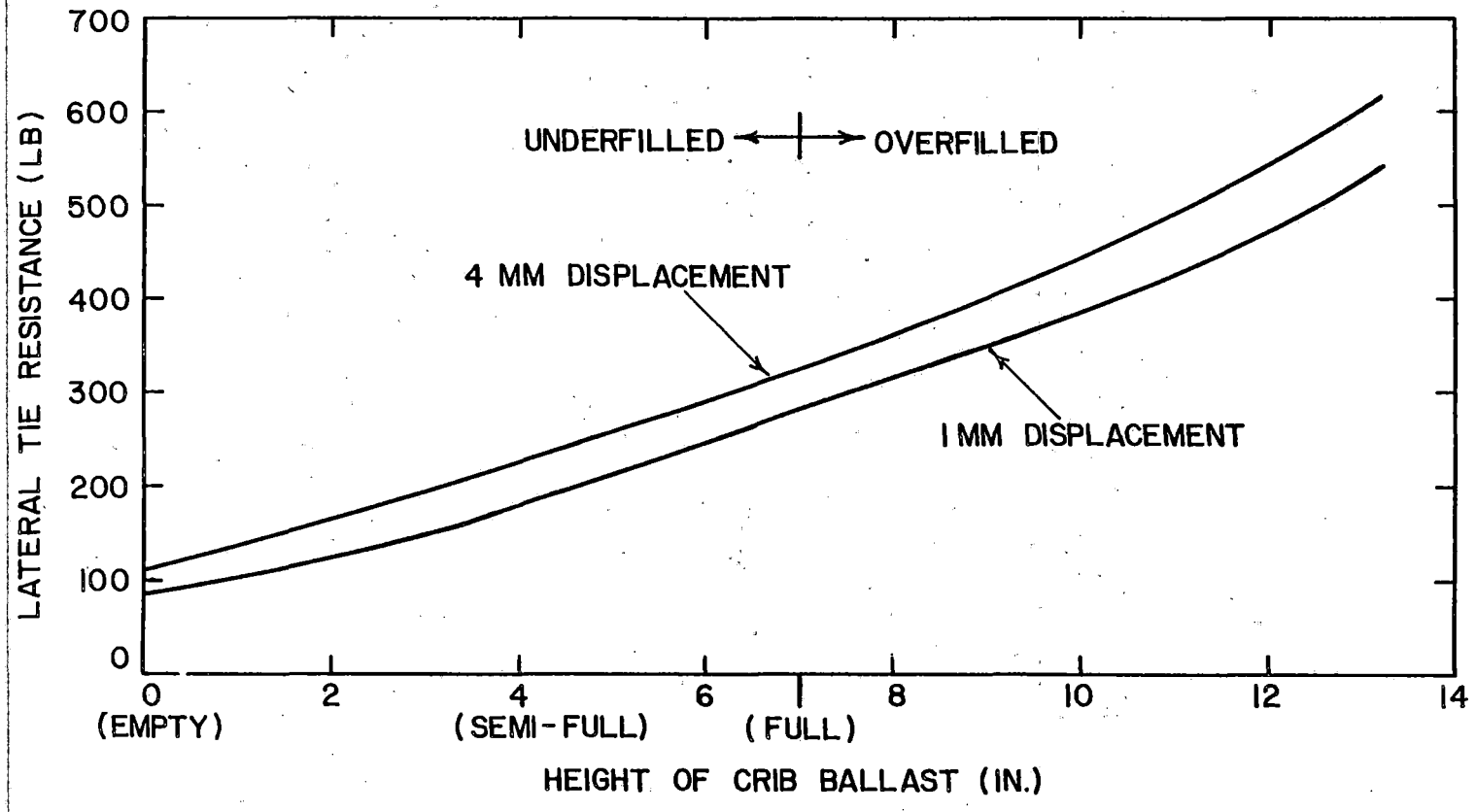

Figure 4.5. The Effect of an Overfilled Crib on Lateral Tie Resistance for a Compacted Base and No Shoulder

The relationship of lateral tie resistance as a function of tie weight is shown graphically in Fig. 4.6. Generally, the lateral tie resistance increases linearly with increasing tie weight.

For these tests, the smooth ballast surface underneath the tie is the only component of resistance, so cyclic loading of the tie is expected to yield fairly reproducible results. The differences that exist are primarily attributed to the nonuniformity of the compacted track bed condition along the length of the tie. Nevertheless, load values for both cycles of loading at each displacement level were averaged since the lateral tie resistances for this condition are considered as part of the normal data scatter.

The linear relationships shown in Fig. 4.6 also pass through the origin, which is reasonable considering the fundamental law of sliding frictional resistance. The lateral tie resistance under these conditions is equal to half of the tie weight at 0.157 in. (4 mm) displacement. This value of 0.5 is a fairly reliable average because the range is 0.43 to 0.54 for 0.0394 to 0.25 in. (1 to 6.35 mm) displacement levels, respectively (Ref. 20).

Density and Plate Load Tests. For comparative purposes, the average ballast density (Fig. 3.6) and the average BBI values (Fig. 3.7) at 0 and at 1000 passes from the simulated track bed tests were used as reference states for the BDT's and PLT's performed during the manual tie tamping series.

The in-situ ballast density test results from the manual tie tamping series are shown graphically in Fig. 4.7 for each specific test location. In the center of the track, the ballast densities in the crib and under the tie are comparable to the average densities obtained from the simulated track bed after 0 and 1000 passes, respectively. The test results are 112.8 pcf

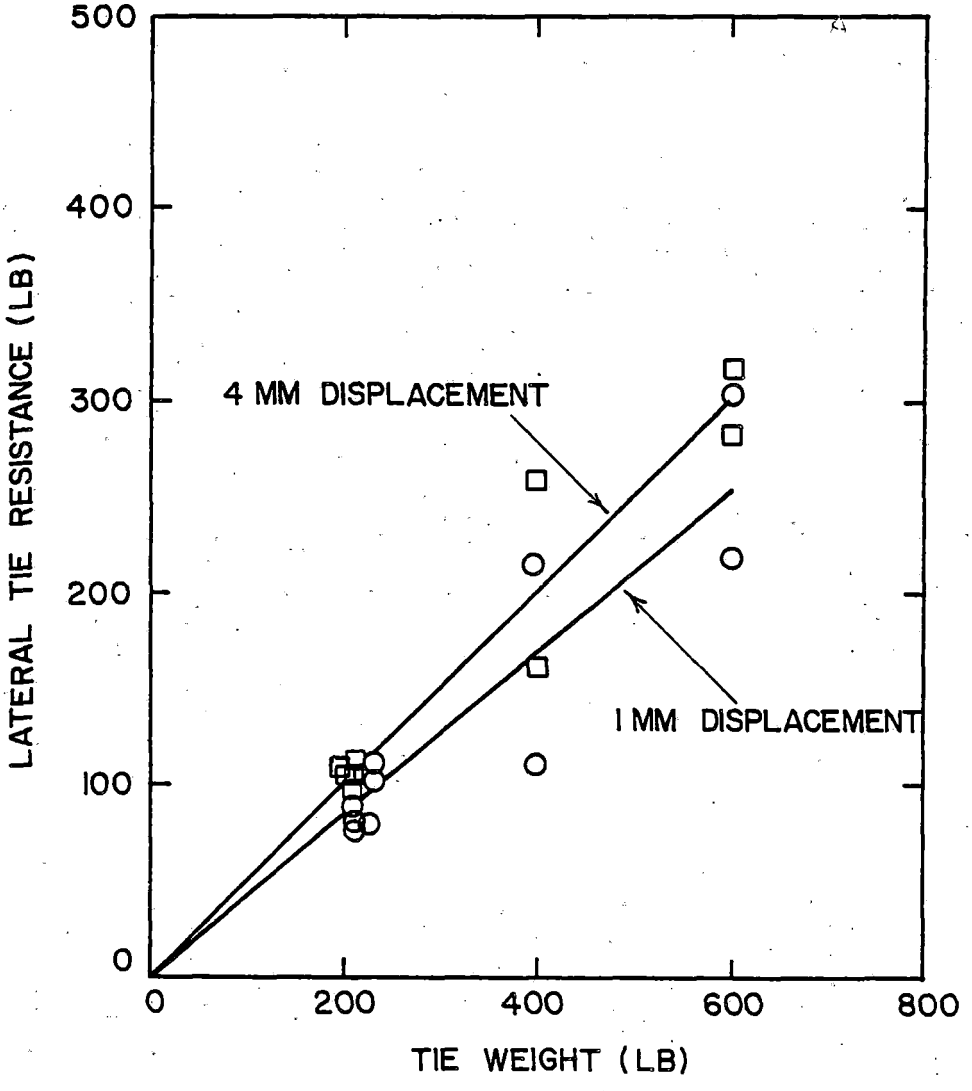

Figure 4.6. Relationship Between Lateral Tie Resistance on a Compacted Base with No Crib or Shoulder Ballast and Tie Weight

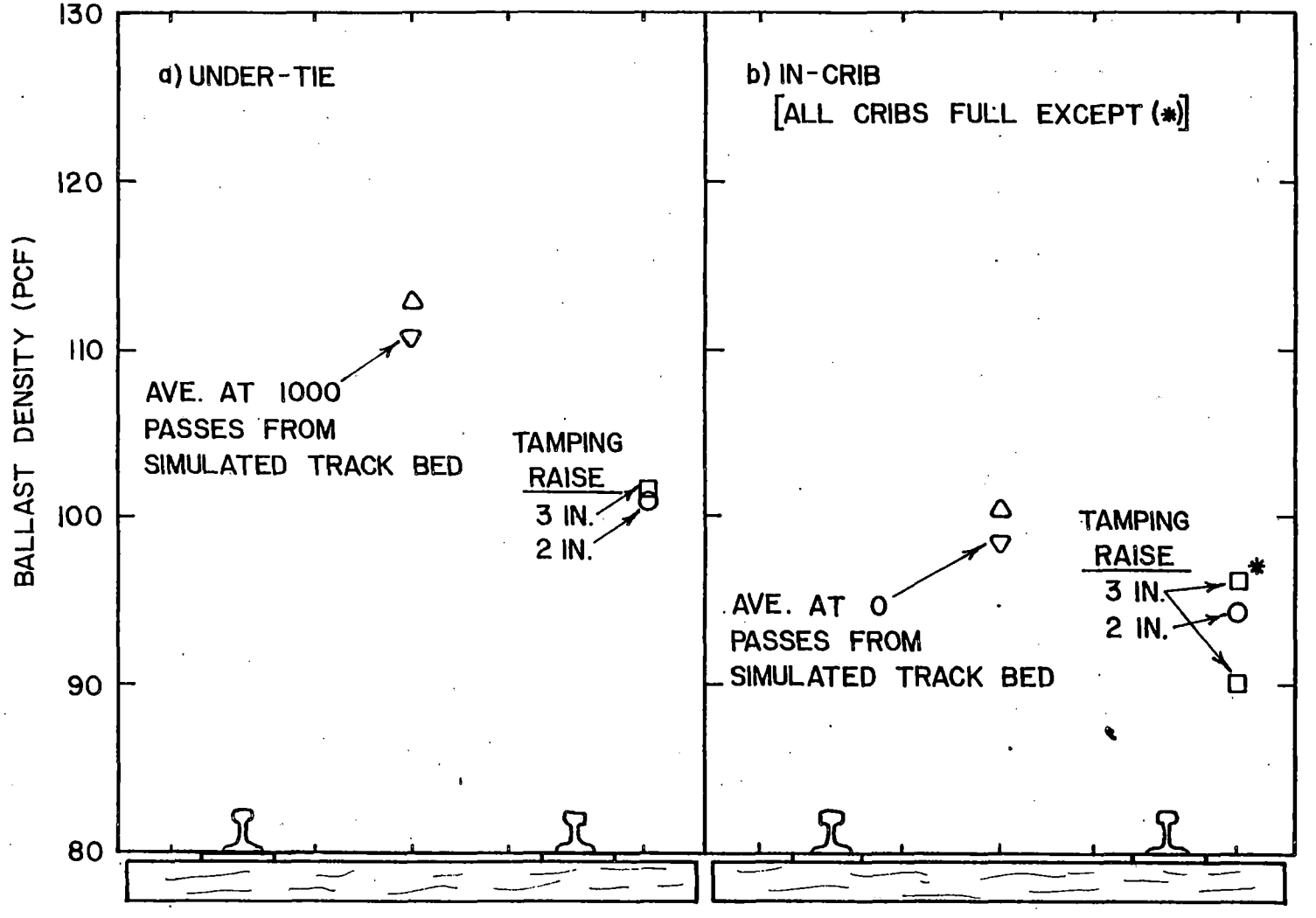

Figure 4.7. Ballast Density for Different Tamping Raises and Ballast Placement Conditions

(1.8 Mg/m^3) under the tie and 100.3 pcf (1.6 Mg/m^3) in the crib. The under-tie density is expected to be similar since the center of the track is not directly affected by the manual tamping process. The ballast density in the crib, in part, reflects the reproducibility of the loose state ballast placement conditions.

For tests performed near the rails in the zones of tamping, two notable features illustrated in Fig. 4.7 for the under-tie and in-crib tests are: 1) ballast densities are significantly lower than the respective center of track values, and 2) similar results are produced for the two different tamping raises. Note for the tests in the crib after a 3-in. (76-mm) raise, the two ballast densities differed somewhat. But the density for a partially full crib is representative of the loose crib ballast and not the compacted track bed. Therefore, the individual ballast densities and the resulting average of 93.0 pcf (1.49 Mg/m^3) for the 3-in. (76-mm) raise are, thus, comparable to the 94.3 pcf (1.51 Mg/m^3) density achieved for the 2-in. (51-mm) raise.

Although the densities in the crib near the rails are lower than the center of track density and the average density at 0 passes from the simulated track bed, it is uncertain if the tamping process solely produced a looser density state. This result may have been the product of the rebal-lasting technique used or simply associated with the normal amount of data scatter. The latter is based upon the fact that a density of 93.7 pcf (1.5 Mg/m^3) was achieved from one test at 0 passes for the simulated track bed tests (see Fig. 3.6). The range of 90 to 96 pcf (1.44 to 1.54 Mg/m^3) would, however, be typical of a loose density state condition.

The ballast densities under the tie in the zones of tamping were approximately equal and have an average of 101.3 pcf (1.62 Mg/m^3). This value is significantly greater than the crib ballast density in the tamped zone, but comparable to the center-of-track density in the crib. Density sampling into the top surface of the compacted track bed is not a major influencing factor. This ballast is inevitably disturbed by the tamping process to a depth of appriximately 1-1/2 in. (38 mm) below the compacted track bed surface. This, in addition to the height of the tie raises, would yield typical sampling depths for the ballast density test. In general, these test results tend to indicate that the manual tie tamping process exercised in this study left the ballast under the tie in a looser state than that which existed before tamping.

The plate load test results that were obtained from the manual tie tamping series are presented for the BBI values at 0.2 in. (5.1 mm) deformation as strength profiles in Fig. 4.8 since these values best represent the general trends.

The results of the plate load tests performed under the tie in the center of the track are very high because very little ballast migrated under the center of tie during the tamping process. In essence, the center of track plate tests were performed on the compacted track bed. The scatter of data points in the center of track is also on the same order of magnitude as the data in Fig. 3.7 after about 500 passes for the simulated track bed. From Fig. 4.8, the range of the BBI values at 0.2 in. (5.1 mm) deformation is from 236 psi (1262kN/m^2) to 318 psi (2191 kN/m^2). The average value of 264 psi (1819 kN/m^2) is consistent with the 279 psi (1922 kN/m^2) average obtained

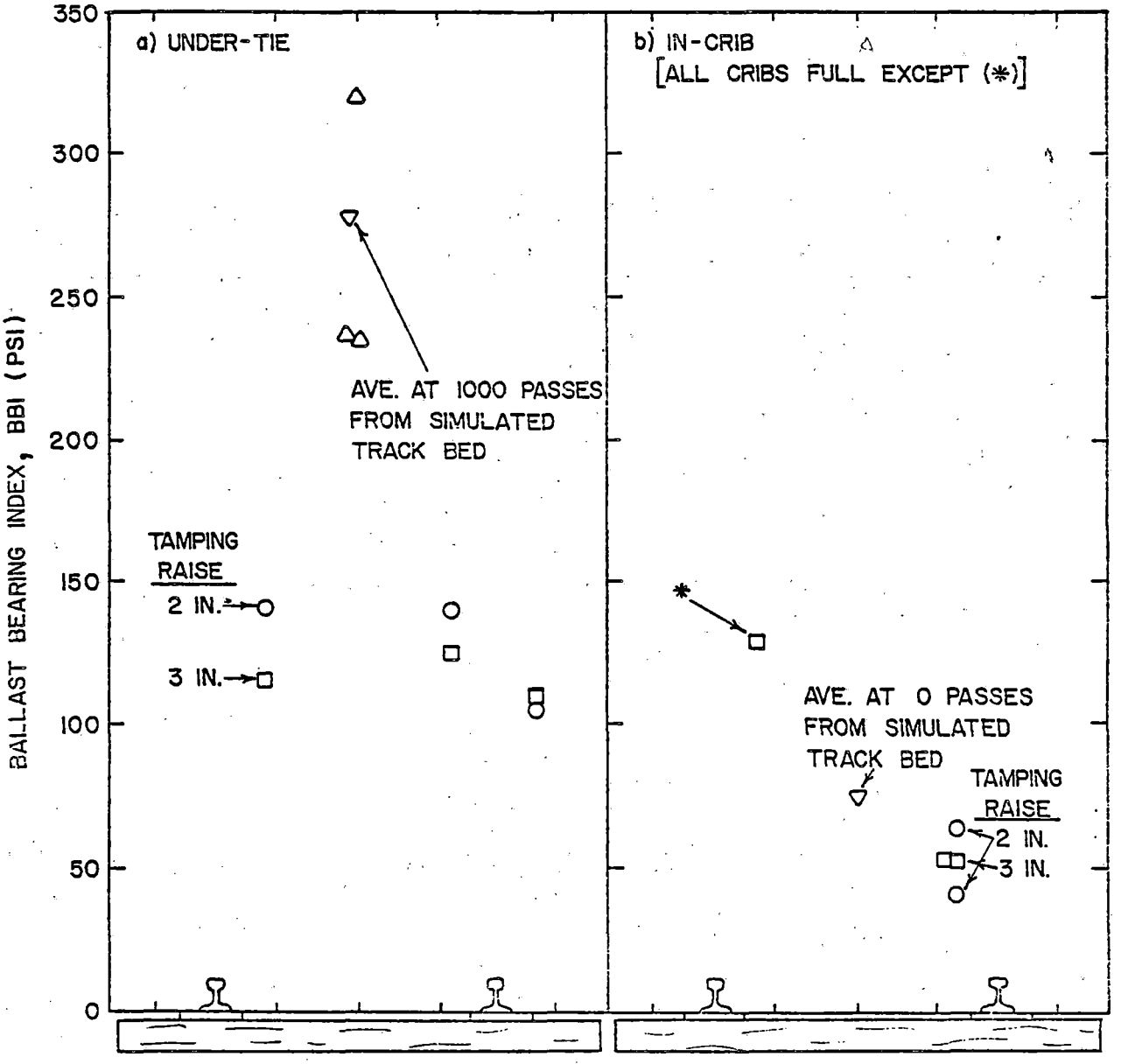

Figure 4.8. Ballast Bearing Index at 0.2 in. (5.1 mm) Deformation for Different Tamping Raises and Ballast Placement Conditions

after 1000 passes for the simulated track bed.

Generally, the plate load test results were fairly consistent for each different amount of tamping raise under the tie-under the rails, i.e., the area most affected by the tamping process. The BBI values after a 2 in. (51 mm) raise were slightly greater than those obtained after a 3 in. (76 mm) raise. The average BBI at 0.2 in. (5.1 mm) deformation after a 2 in. (51 mm) raise was approximately 128 psi (882 kN/m^2) but for a 3 in. (76 mm) raise it was approximately 116 psi (800 kN/m^2). This result appears logical because, after a 2-in. (51-mm) raise, there is a thinner layer of loose ballast between the bottom of the tie and the compacted track bed than there is after a 3-in. (76-mm) raise. However for both cases, the close proximity of the compacted track bed is expected to slightly influence the resulting ballast stiffness. The manual tamping process did reduce the average ballast stiffness under the rails to 46 percent of the center of the track ballast stiffness. The results of these plate load tests confirms the general trend stated for the ballast density tests (Fig. 4.7a).

For plate load tests performed in the crib under the rails, the average BBI at 0.2 in. (5.1 mm) deformation in Fig. 4.8b is approximately 52 psi (385 kN/m^2). This is approximatley 43 percent of the respective under-tie values. There is very little scatter among the test results in the cribs and the two tamping raises yielded nearly identical results for the full crib ballast conditions. The plate resistance after tamping is lower than the BBI value of 74 psi (510 kN/m^2) at zero passes on the simulated track bed. This also follows the same trend exhibited for the ballast density tests in the tamped zones of the crib (Fig. 4.7b). Although the results of these two

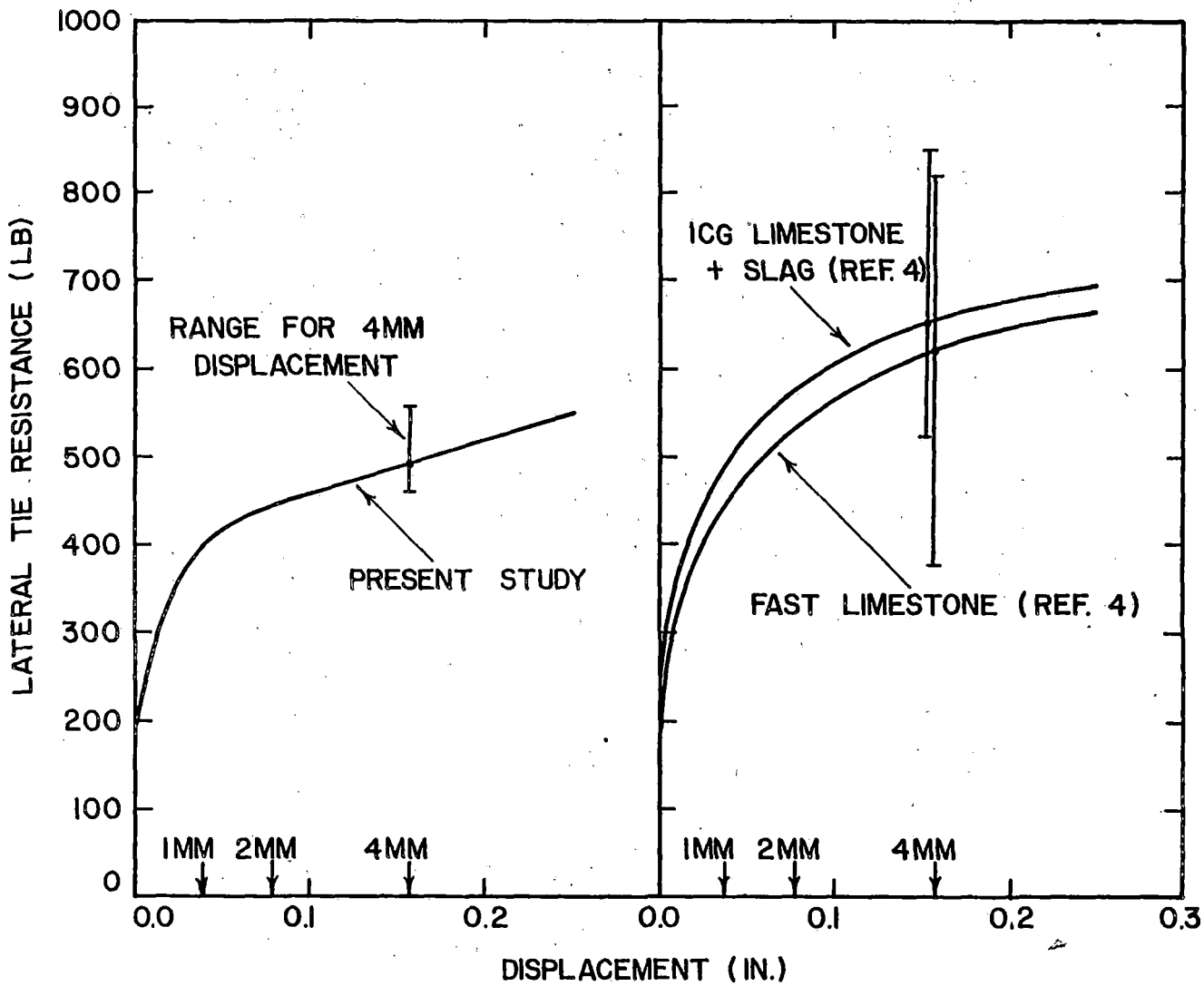

Figure 4.9. Comparison of LTPT Data After Tamping

ballast physical state tests are consistent, it is still inconclusive to state that the tamping process solely produced a looser crib ballast condition.

One plate load test, i.e., PLT II-5, was performed in the tamped zone of the crib prior to reballasting. Fig. 4.8 shows that the BBI value of 129 psi (889 kN/m^2) at 0.2 in. (5.1 mm) deformation is significantly greater than the BBI values in the crib, but it is approximately equal to the under-tie values. This result is expected because the ballast test conditions are similar for both this test and those under the tie. In each case, approximately 4 in. (0.102 m) of loose ballast overlies the compacted track bed, therefore, the plate resistances are comparable.

A correlation of the plate load and ballast density tests results for the manual tie tamping series follow the same trends established for the simulated track bed (see Fig. 3.8).

4.3 COMPARISON WITH FIELD DATA

The ballast physical state test results obtained from available field investigations were compared to those obtained in this study to provide an indication of the reliability of the laboratory test procedures used here. Pertinent lateral tie push test results are graphically compared in Fig. 4.9, while plate load test and in-situ ballast density test results are provided in Table 4.2. For convenience, the ballast bearing index at 0.2-in. (5.1-mm) deformation for the PLT and lateral tie resistance at 0.157-in. (4-mm) displacement for the LTPT were considered representative for comparative purposes.

A comparison of data from SUNYAB field testing at both Illinois Central Gulf Railroad (ICG) and at FAST was done by Panuccio and Dorwart (Ref. 4) and

Table 4.2. Comparison of Ballast Physical State Data

	Test Condition†	Plate Load Test BBI (psi) at 0.2 in.		In-Situ Ballast Density Test (pcf)	
		In-Crib	Under-Tie	In-Crib	Under-Tie
a) Loose State					
Present Study	a) 0 Passes, Track Bed	--	74	—	98.5
	b) Center of Track	--	--	100.3	--
	c) Under Rails After Tamping	52	122	93.4	101.3
Panuccio & Dorwart (Ref. 4) and Yoo (Ref. 7)	a) Under Rails After Tamping				
	1. ICG	60	119	92.1[x]	102.5[x]
	2. FAST	72	155	96.6	114.1
	b) Center of Track-ICG	47	35	96.2[x]	84.9[x]
b) Dense State					
Present Study	a) 1000 Passes, Track Bed	--	279	--	111.0
	b) Center of Track	--	264	--	112.8
Panuccio & Dorwart (Ref. 4) and Yoo (Ref. 7)	a) Under Rails				
	1. ICG-5 MGT	—	373	--	110.8[x]
	2. FAST-135 MGT	--	568	--	114.4
	b) Center of Track				
	1. ICG-5 MGT	--	107	--	101.2[x]
	2. FAST-135 MGT	--	307	--	109.7

† All Ballast is Limestone Except ICG Which is a Limestone and Steel Slag Mixture. All Ballasts Have Similar Gradations.

x - Converted to an Equivalent Limestone Density.

Yoo (Ref. 7). The former report includes both PLT and LTPT data, while the latter includes the BDT measurements.

The ballast at ICG was a mixture of steel slag and limestone. At ICG, the ballast physical state tests were performed in three different track conditions: 1) tamped only, 2) tamped and compacted, and 3) tamped plus 5 million gross tons of traffic. A limestone ballast was tested at FAST for the tamped only, 0.1 MGT, and 135 MGT conditions. The track structures i.e., tie weights and, ballast crib and shoulder conditions, were similar for both the laboratory and field tests.

A comparison of the average first cycle LTPT load-displacement curves after tamping for this project (Fig. 4.9a) and the field curves (Fig. 4.9b) indicates the laboratory values of lateral tie resistance range from 50 to 159 lb (223 to 668 N) lower than the field results. The reason for this difference is not readily apparent, because both the test apparatus and the test procedure were the same. However, an examination of the ranges of the lateral tie resistance values at 0.157 in. (4 mm) displacement indicates more favorable agreement.

At both field sites, plate load tests were performed at various locations within the track structure (Table 4.2). After the tamping operation at ICG, the average BBI at 0.2 in. (5.1 mm) deformation under the tie and under the rail was 119 psi (820 kN/m^2). The same test conditions at FAST yielded a value of 155 psi (1068 kN/m^2). The laboratory tests produced a comparable average BBI of 122 psi (841 kN/m^2).

Plate load tests were also performed in the crib area under the rails which is where the tamping tools operate, i.e., approximately 6 in. (0.153 m)

from the base of the rail. The BBI value at 0.2-in. (5.1-mm) deformation was 60 psi (413 kN/m^2) at ICG and 70 psi (482 kN/m^2) at FAST. The average BBI of 53 psi (365 kN/m^2) in the laboratory gave a comparable result. For this particular test condition, the BBI values from the laboratory manual tie tamping operation showed very good agreement with the results obtained after mechanical tie tamping from both field sites.

The in-situ ballast density test results demonstrate the same consistency as the plate load tests under the rails for the after tamping condition (Table 4.2). In the crib, the ballast density for this project was 93.4 pcf (1.49 Mg/m^3) which is comparable to the 92.1 pcf (1.47 Mg/m^3) for ICG and the 96.6 pcf (1.55 Mg/m^3) for FAST. Under the tie, this project yielded a density of 101.3 pcf (1.62 Mg/m^3) which is reasonably close to the 102.5 pcf (1.64 Mg/m^3) obtained at ICG but significantly less than the 114.1 pcf (1.83 Mg/m^3) obtained at FAST. The reasons for the FAST result being greater may be attributed to the track loading history and other factors at FAST which are adequately discussed by Yoo (Ref. 7). In general, the manual tie tamping operation satisfactorily duplicates the field ballast density conditions.

Plate load tests were also conducted under the tie in the center of the track, i.e., centered between the rails. For this test location, a similar discussion was previously focused in Chapter 3 upon the end results obtained from the simulated old track bed conditions. After 5 MGT of traffic at ICG, the average BBI at 0.2 in. (5.1 mm) deformation was 107 psi (737 kN/m^2), and the density was 101.2 pcf (1.62 Mg/m^3). After 135 MGT of traffic at FAST, the BBI was 307 psi (2115 kN/m^2), and the density was 109.7

pcf (1.76 Mg/m^3). In the laboratory, the corresponding average BBI value was 264 psi (1819 kN/m^2), and the ballast density was 112.8 pcf (1.80 Mg/m^3) which are comparable to the FAST results at 135 MGT. Note, however, that the laboratory center of track BBI values are low compared to those obtained under the rails for 5 MGT at ICG and 135 MGT at FAST (Table 4.2).

Generally, the plate load test and in-situ ballast density test data obtained in this project were in fairly good agreement with all of the field test data. The LTPT data from this project followed the same general trend in that the lateral tie resistance obtained in the laboratory was comparable, but somewhat less than the resistances obtained in the field.

5. INVESTIGATION OF CRIB COMPACTION PLATE

5.1 APPARATUS AND PROCEDURES

Test Boxes. The ballast test samples were prepared in 12-in. (305-mm) deep small and large test boxes, which were 20 in. (0.508 m) and 36 in. (0.914 m) square, respectively. The walls of each test box are constructed of 3/4-in. (19-mm) plywood and reinforced with 2-in. (51-mm) steel angle iron. The angle iron provided the additional lateral stiffness to ensure the container was rigid. The bottom of the test boxes are also 3/4 in. (19-mm) plywood and all bolt holes are counter sunk such that the connectors were flush with the plywood surface. This latter feature in conjunction with the stiffness of the base prevents the test box deformation from influencing the test results.

For the tests with the 9 in. (229 mm) and 6 in. (152 mm) ballast depths, 18-3/4 in. (0.48 m) diameter concrete spacer disks were fabricated and placed inside the test box prior to filling with ballast. These were the same disks that Wayne (Ref. 6) used.

Crib Compaction Plate. The crib plate is constructed of 7/16 in. (11 mm) thick steel plate having an 8-in. (203-mm) width and 14-1/2-in. (368-mm) length. The plate was reinforced against bending by welding 3-in. (76-mm) channel sections in a rectangular array on the plate. Two narrow steel plates were welded on the opposite flange of the channels to provide a compatible attachment to the bottom loading head of the MTS actuator (Fig. 5.1).

Two 18-in. (0.457-m) long aluminum S6 I-beam sections were placed vertically to act as structural fillers between the bottom of the actuator and the top of the compaction plate. The height and clearance between the I-

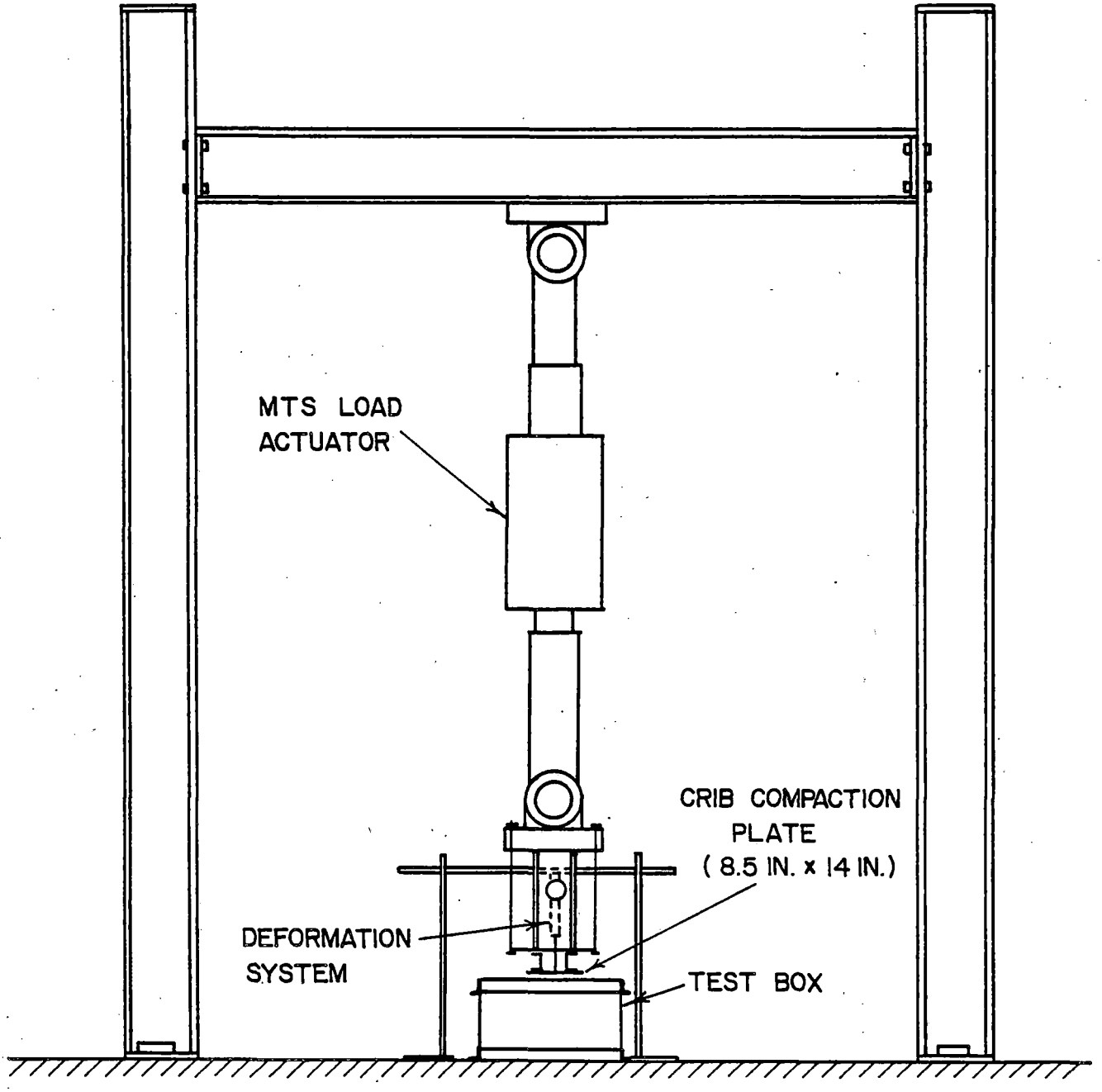

Figure 5.1. Schematic Diagram of the Test Setup

beams was sufficient for placement of the deformation measuring system. The crib compaction plate and the I-beam could easily be attached as a rigid unit to the MTS actuator by four threaded rods.

Load and Deformation Systems. The load applying and measuring system were provided for by the Structural and Materials Testing System, Model 902.-38 (Ref. 21). The three basic components of the system used are the structural actuator, the electronic control panel and the hydraulic power supply. The loads are programmed through the control panel and are hydraulically applied through the structural actuator. The control panel is capable of operating on either load control or stroke (displacement) control. The maximum load capability of the actuator is 250 kips (1,112 kN) static force and $\pm$ 250 kip (1,112 kN) dynamic force. The maximum stroke capacity is $\pm$ 4 inches (102 mm). Also located on the control panel is the function generator which controls the type of cyclic waveform applied, i.e., sine wave, and the applied frequency. Located on the structural actuator is a load cell transducer for recording the applied loads and a linear variable differential transformer (LVDT), which measures the displacement. The MTS operates on the "Closed Loop Control" concept. This entails constantly making an adjustment to either the load or the stroke based on the feedback signal.

The MTS actuator was suspended from an H-frame constructed of heavy structural steel sections (Fig. 5.1). Ample space is provided for the crib compaction plate apparatus and the test boxes.

The load input was recorded by wiring the Y-axis of the X-Y recorder into the MTS load transducer conditioner module. This module converts an AC current to DC current which drives the recorder pen on the load axis.

Originally, the plan was to use the LVDT located on the structural actuator to measure the ballast deformation under the applied static and cyclic loading conditions. However, deformations in the compaction plate attachments and the structural H-frame proved to be significant with respect to the measured ballast deformations. Thus, a new system was devised with an independent displacement transducer, i.e., DCDT, to eliminate this error.

The DCDT is connected in a series arrangement with a mechanical dial indicator having 1 in. (25.4 mm) travel. The displacement gages are rigidly fixed and aligned on a support track such that their pistons move freely. This is also the same deformation measuring system that is used for the plate load test.

The deformation system is located between the I-beams of the assembled crib compaction plate apparatus (Fig. 5.1). A seating hole is located at the center of the plate, such that the DCDT records the average plate displacement and is not influenced by plate rotation. The simplicity of this systems provides for easy assembly and alignment.

The DCDT was powered with a DC current provided by a standard 6-volt lantern battery. The voltage generated from the DCDT core movement powered the pen along the X-axis on the X-Y recorder.

Sample Preparation. The technique used satisfied two requirements: 1) the ballast sample would have a reproducible initial box density, and 2) the sample had to be in a loose density state. The same crushed limestone (see Fig. 3.2) was used for these tests.

A large metal scoop was filled with ballast and was held with the open

end of the scoop rested on the base of the test box. The scoop was gradually tilted such that the ballast was gently deposited uniformly across the area of the box. This procedure was continued until the ballast was level with the sides of the test box. The sample was leveled even with sides of the box by running a straight edge across the top. Any ballast particles that extended above the bottom of the straight edge were removed. Any large voids created by this process were filled such that the ballast was entirely below the straight edge. This process resulted in a very flat, even ballast surface.

This technique was successful in fulfilling the two major objectives. The overall average initial box density of 26 tests is 82.1 pcf (1.312 Mg/m^3) and the standard deviation is 0.992 pcf (0.016 Mg/m^3). The standard deviation is very low which means that reproducibility of the sample preparation technique is good. Also, the ballast was prepared in a loose state, when compared to loose state ballast densities of other published laboratory reports (Refs. 3, 5, and 6).

The 6-in. (152-mm) and 9-in. (229-mm) layer depth samples were prepared in a similar fashion to that of the 12-in. (305-mm) deep samples previously described. The difference was that the concrete spacer disks were placed in the bottom of the test box prior to filling with ballast. The technique used to prepare the large 3-ft (0.915-m) square test box samples was exactly the same as the small test box preparation technique. However, the initial box densities were not recorded for the large test box series.

Leveling of the ballast surface was an important step to insure proper operation of the MTS structural actuator. The actuator offers only axial

resistance or applies only an axial load. An uneven ballast surface would have created a bending moment in the actuator as the load was applied. An applied bending moment of significant magnitude thus has the capability of damaging the actuator.

Test Procedure and Program. After the ballast was prepared, the sample was subjected to static and cyclic loading utilizing the single crib compaction plate. The procedure for a typical test is as follows:

1. With the MTS structural actuator in fully retracted position, the ballast test box containing the prepared test sample was carefully centered under the crib compaction plate apparatus.

2. The DCDT was connected to the X-axis and the MTS load transducer conditioner module was wired into the Y-axis of the X-Y recorder. The MTS digital display was set to read the applied load.

3. Calibrate the displacement input by moving the brass rod an equal distance, usually 0.4 in. (10.1 mm), into and out of the DCDT housing several times.

4. Axes were inscribed on the load-displacement curve, and the plot was labeled with the date, test series number, recorder voltage range settings, and test conditions.

5. The MTS was switched to load control, and a small seating load, approximately 100 lb (445 N), was applied by the compaction plate to the ballast sample.

6. The deformation system was positioned and the DCDT was set so that it was fully retracted.

7. At this point, the dial gage reading on the deformation system and

the MTS digital display reading were recorded. These readings represented the initial point of the static loading portion of the load-deformation curve.

8. On the MTS control panel, the frequency and the type of waveform (sine) desired were programmed through the function generator. The cyclic load was programmed through the Span I control on the command input module and the load transducer conditioner module. The number of cycles was also specified.

9. The load on the ballast was increased gradually until the programmed initial static load was achieved.

10. The deformation dial gage reading and the digital display reading on the MTS control panel were recorded after the deformation ceased at the static load level.

11. The programmed cyclic load was applied. The recorder pen remained in the down position for 15 to 20 cycles, or until the permanent deformation for each cycle became very small. The pen was then lifted and placed down on a regular interval basis, usually every 25 cycles.

12. When the given number of loading cycles was reached, the program was stopped and both the dial gage reading and the MTS digital display reading were recorded.

13. The static load was gradually reduced to approximately 100 lb (445 N), wherein the final digital display and dial gage readings were recorded.

14. The deformation system was removed, and the small load on the ballast was removed.

In order to evaluate the changes in the physical state of ballast with

the crib compaction plate, the plate load test (PLT) and the in-situ ballast density test (BDT) were employed. Complete descriptions of the test apparatus and test procedures have been provided in Section 3.

However, the PLT loading system (Fig. 5.2) was adapted to the loading head of the MTS structural actuator, which primarily provided the dead weight reaction. The height of this system was approximately equal to that of the assembled crib compaction plate apparatus. Thus, the two systems were easily interchangeable and no modification was required to the remaining test equipment. The stroke of the MTS actuator was sufficient to properly position either apparatus with respect to the test specimen height.

The test program was designed in such a manner so that the effects of variations on the static and cyclic loads could be examined. Other effects that were tested were the influence of the layer depth and the effect of lateral boundary conditions. A summary of the tests performed with the variables for each test are shown in Table 5.1. Also listed is the physical state test that was performed following each compaction test.

5.2 TEST RESULTS

Load-Displacement Curves. A typical load-displacement curve illustrated in Fig. 5.3 shows that the ballast was first loaded statically to a predetermined level and then cycled about that level with a predetermined cyclic load for a given number of cycles. The MTS normally required several cycles before it actually reached the full programmed cyclic load. Following cycling, the ballast was unloaded. Examination of these curves (Ref. 22) revealed two important points: 1) the programmed cyclic load was rarely achieved, and 2) the mean static load ($F_{\text{static mean}}$), i.e., the mid-point

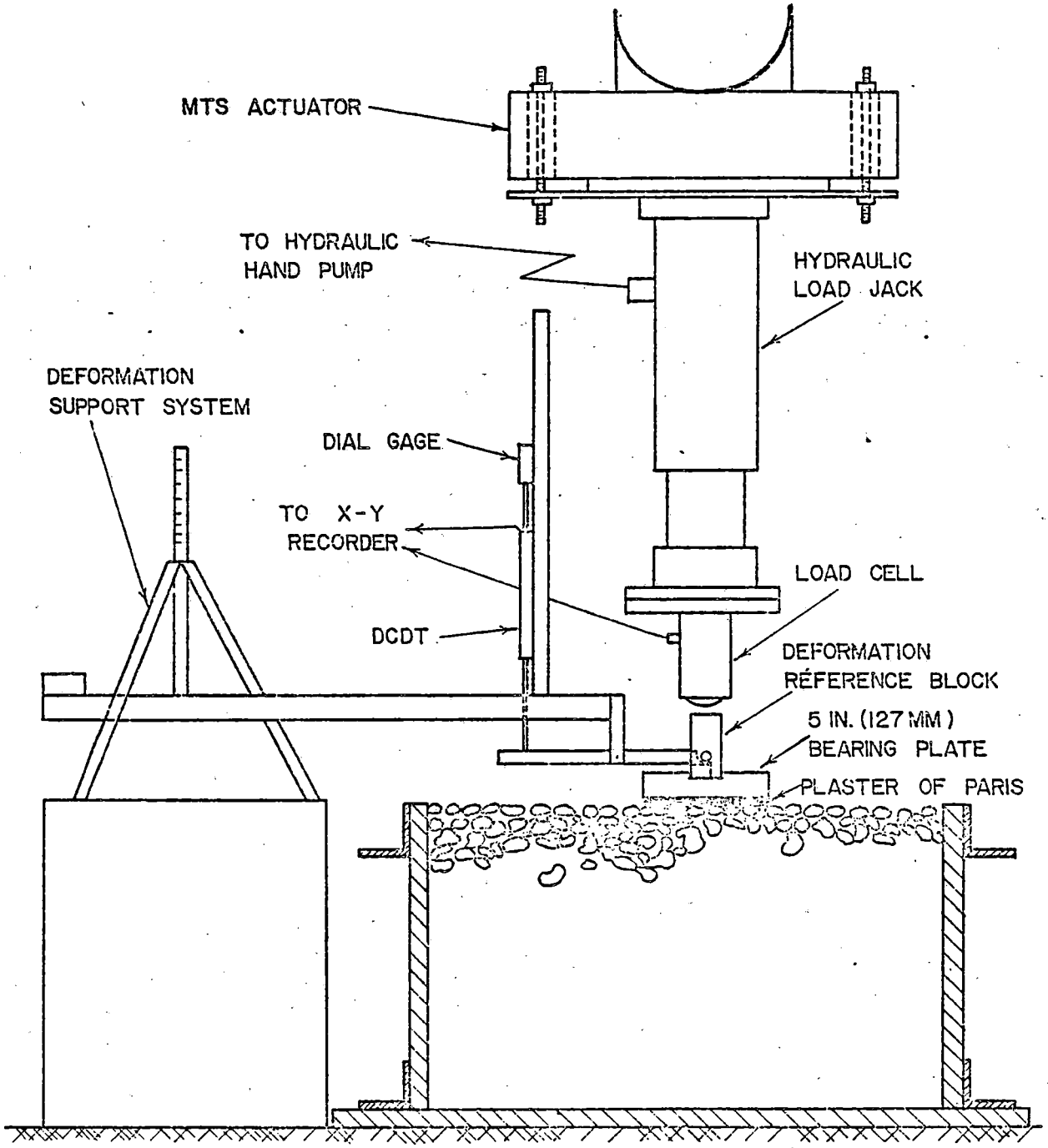

Figure 5.2. Schematic Diagram of Plate Load Test (PLT) Apparatus Setup

Table 5.1. Low Frequency Tests for Single Oscillating Plate on Limestone Ballast

Test No.	Frequency f (Hz)	Mean Static Load (lb)	Cyclic Load (lb)	Load Ratio (Cyclic/Static)	No. of Cycles	Ballast Depth (in.)	Test Box† Size	Other Tests
1A	1/2	1496	804	0.537	300	12	Small	PLT
1C	1/2	1544	813	0.527	300	12	Small	PLT
2A	1/2	1458	808	0.554	1500	12	Small	PLT
3A	1/2	2107*	914	0.434	300	12	Small	PLT
3B	1/2	3176	1844	0.581	300	12	Small	PLT
3C	1/2	3130	1817	0.581	300	12	Small	PLT
4A	1/2	6197	3728	0.602	300	12	Small	PLT
5A	1/2	1479	694	0.469	300	12	Small	BDT
6A	1/2	1497	688	0.460	1500	12	Small	BDT
7A	1/2	3155	1768	0.560	300	12	Small	BDT
8A	1/2	1518	774	0.510	150	12	Small	BDT
9A	4.0	1482	354	0.239	300	12	Small	PLT
10A	2.0	1532	644	0.420	300	12	Small	BDT
11A	1/2	1499	1258	0.839	300	12	Small	PLT
12A	1/2	3000	2700	0.900	300	12	Small	PLT
12B	1/2	2939	2729	0.929	300	12	Small	BDT
12C	1/2	3156	2591	0.821	300	12	Small	PLT
13A	1/2	1511	1262	0.835	300	12	Small	BDT
14A	1/10	1506	1190	0.790	300	12	Small	PLT
15A	1/2	1511	758	0.502	300	9	Small	PLT
15B	1/2	1482	847	0.572	300	9	Small	PLT

† Small Box = 20 in. x 20 in. x 12 in., Large Box = 36 in. x 36 in. x 12 in. An Initial Level Box Density Obtained for Each Sample

* 1/2 Sine Wave Used, All Other Tests are Full Sine Wave

Table 5.1. Low Frequency Tests for Single Oscillating Plate on Limestone Ballast (continued)

Test No.	Frequency f (Hz.)	Mean Static Load (lb)	Cyclic Load (lb)	Load Ratio (Cyclic/Static)	No. of Cycles	Ballast Depth (in.)	Test Box† Size	Other Tests
15C	1/2	1480	816	0.551	300	9	Small	PLT
16A	1/2	1455	829	0.570	300	6	Small	PLT
16B	1/2	1496	768	0.513	300	6	Small	PLT
17A	1/2	1426	771	0.541	300	12	Large	PLT
17B	1/2	1453	781	0.538	300	12	Large	PLT

† Small Box = 20 in. x 20 in. x 12 in., Large Box = 36 in. x 36 in. x 12 in.
An Initial Level Box Density Obtained for Each Sample

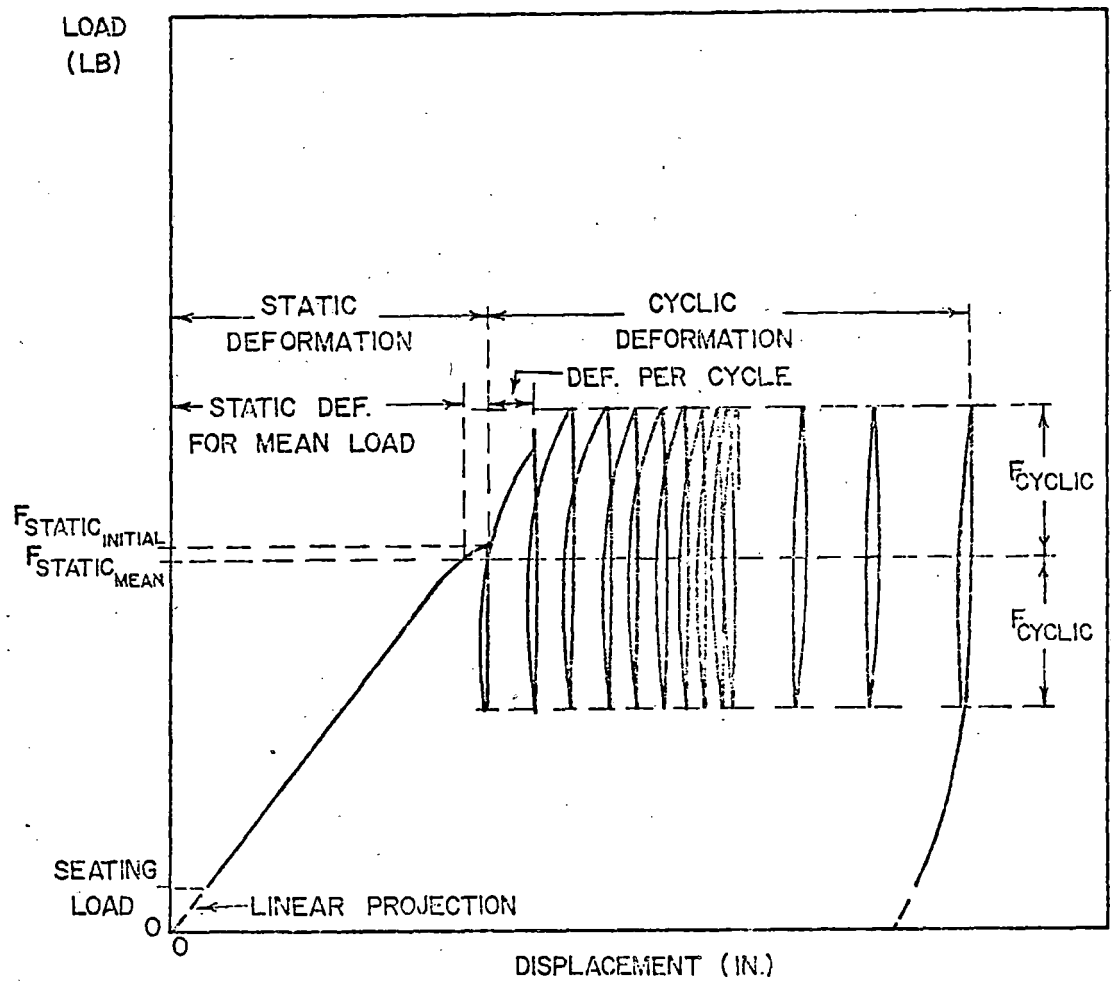

Figure 5.3. Typical Load-Displacement Curve for Crib Compaction Plate with Definition of Terms

between the lower and upper cyclic peak, did not coincide with the initial static load ($F_{static\ initial}$). However, these features do not pose a significant problem, and have been taken into consideration during the data reduction process (Ref. 22).

From Fig. 5.3, the intercept of the load-displacement curve was easily defined by a linear extrapolation of the static loading portion of the curve, and proportioning the recorded static load outputs for zero lb load, which subsequently defined zero displacement. The average cyclic load was obtained as one-half the total cyclic load output (peak to peak). As previously stated, this would subsequently define the mean static load during cycling and the associated mean static deformation could then be determined. The cumulative cyclic deformation (CCD) was determined as the deformation from the beginning of the first cycle to the unloading side of the cycle in question at the mean static load.

Static Load. For all of the test performed in the small test box with a 12 in. (305 mm) ballast depth, the mean static deformation increased as the mean static load was increased (Fig. 5.4). The shape of the overall average curve is concave upwards. The expected shape of this curve is concave downwards. The reason for the departure from the expected behavior is that the static deformation for the 6197 lb (27,577 N) load is low. This may have been caused by the limited depth of the test box. In other words, the effect of the bottom boundary influenced this test.

The average curves for the 3090 lb (13, 751 N) and the 1519 lb (6760 N) tests are also shown in Fig. 5.4. These load values represent the average for each particular load level. To compute the 3090 lb (13, 751 N) average

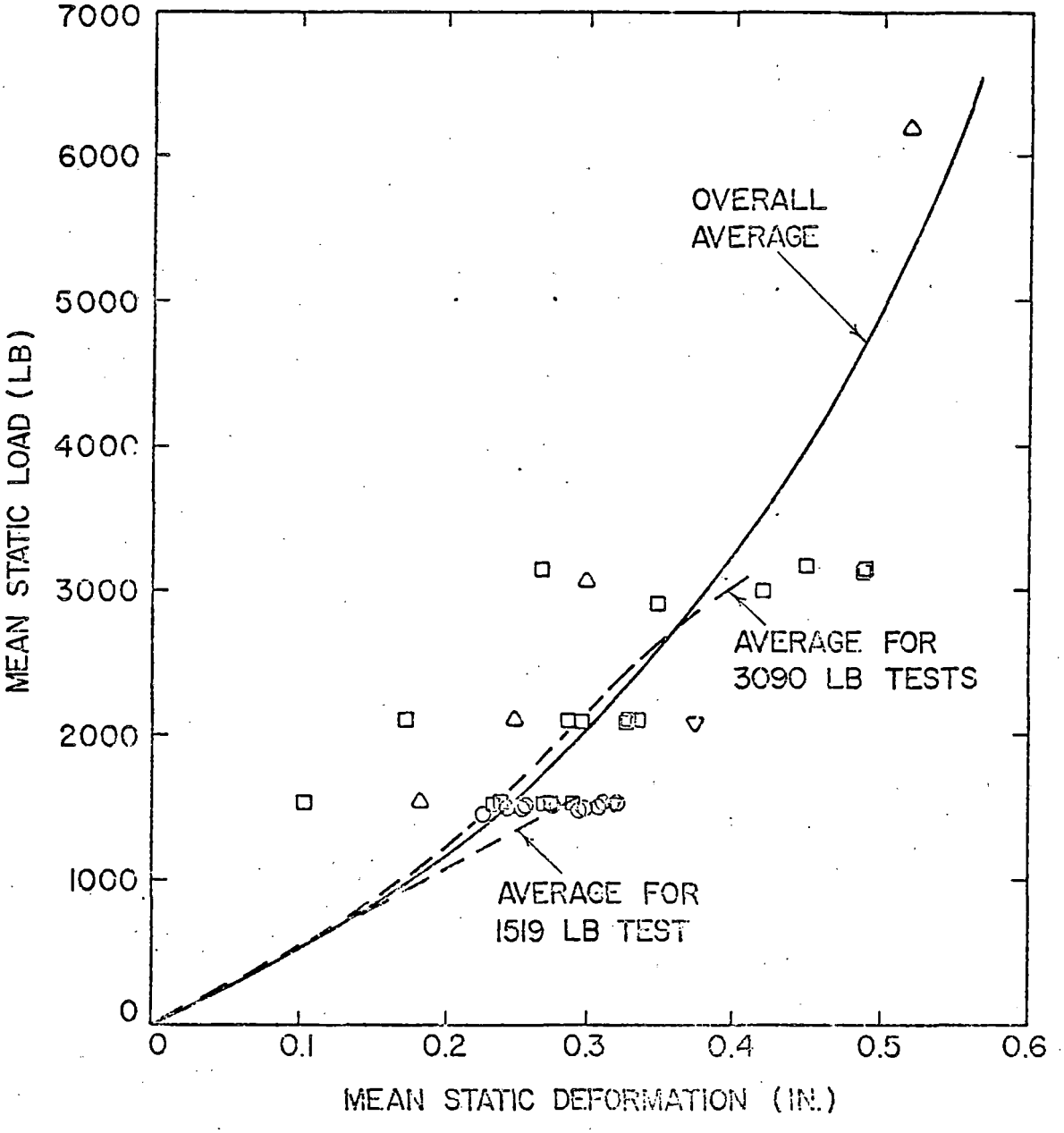

Figure 5.4. Relationship Between Mean Static Load and Static Deformation in the Small Test Box

curve, the average deformations at 1519 lb (6760 N), 2107 lb (9376 N) and 3090 lb (13, 751 N) were plotted. This latter curve is nearly linear, but has lower static deformations at 1519 lb (6760 N) average curve. This difference cannot be explained by the average initial box density, which for the 1519 lb (6760 N) tests was 81.9 pcf (1.312 Mg/m^3) and for the 3090 lb (13,751 N) tests was 82.1 pcf (1.315 Mg/m^3). However, note the results from one of the 3090 lb (13,751 N) tests produced extremely low static deformations, which when not considered, yields much better agreement between the two average curves.

The relationship between the mean static deformation and initial box density for different mean static loads is shown in Fig. 5.5. The general trend is for the static deformation to increase as the initial box density decreases for a given mean static load. The static deformation increases with an increasing mean static load at a given initial box density. These are both expected trends. However, the range of the initial densities from 81.0 pcf (1.298 Mg/m^3) to 83.5 pcf (1.338 Mg/m^3) is considered acceptable for the loose state, and, thus, the static deformations can be combined for the respective mean static loads.

The tests conducted with a mean static load of 1519 lb (6760 N) have a low particle contact stress and, therefore, the effect of the bottom box boundary would be insignificant in comparison to the effect on the test with a mean static load of 6197 lb (27,577 N). If the bottom boundary affected the 1519 lb (7770 N) test it would also influence the 3090 lb (13, 751 N) tests. This could be a partial explanation for the average 3090 lb (13,751 N) test curve in Fig. 5.4 not being co-linear with the average 1519 lb (6760 N)

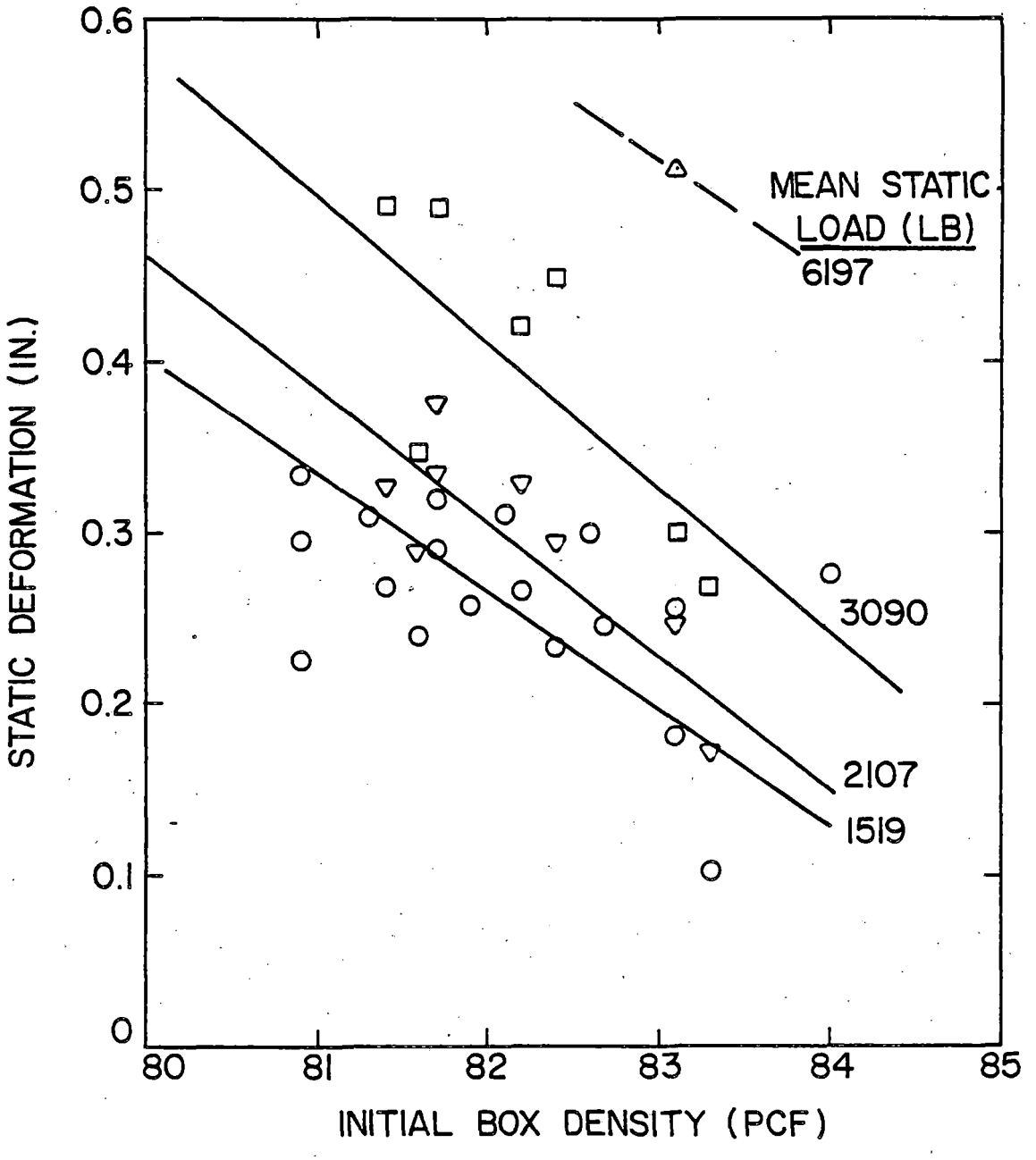

Figure 5.5. Static Deformation as a Function of Initial Box Density for 12-in. Layer Depth in Small Test Box

test curve. The effects of ballast depth will be discussed in more detail in the section on layer depth.

Cyclic Load. The cumulative cyclic deformation (CCD) occuring with the number of loading cycles are plotted in Fig. 5.6 for several individual tests conducted at a frequency of 1/2 Hz in the small test box. These tests represent different static and cyclic loading conditions, and are also divided according to different load ratios. The load ratio (LR) for a test is defined as the single amplitude cyclic load divided by the mean static load, i.e.

$$LR = \frac{F_{cyclic}}{F_{mean\ static}} \qquad (5\text{-}1)$$

The load ratios for each individual test are also listed in Table 5.1.

The solid lines in Fig. 5.6 are linear regression equations for log-log plots, which are compiled in Table 5.2 together with the correlation coefficients. These coefficients show that there is very good correlation between the cumulative cyclic deformation and the number of cycles on a log-log plot. The curves on these plots are, also, somewhat parallel.

The comparison of the cumulative cyclic deformation for various load ratios and mean static loads is more clearly illustrated in Figs. 5.7 for 300 cycles. The relationships for 10 and 100 cycles were shown to be similar (Ref. 22). These plots are based upon a dimensionless quantity called the static load ratio (SLR), which is defined as,

$$SLR = \frac{F_{mean\ static}}{1490} \qquad (5\text{-}2)$$

The load of 1490 lb (6631 N) is the average of the lowest mean static loads used during testing.

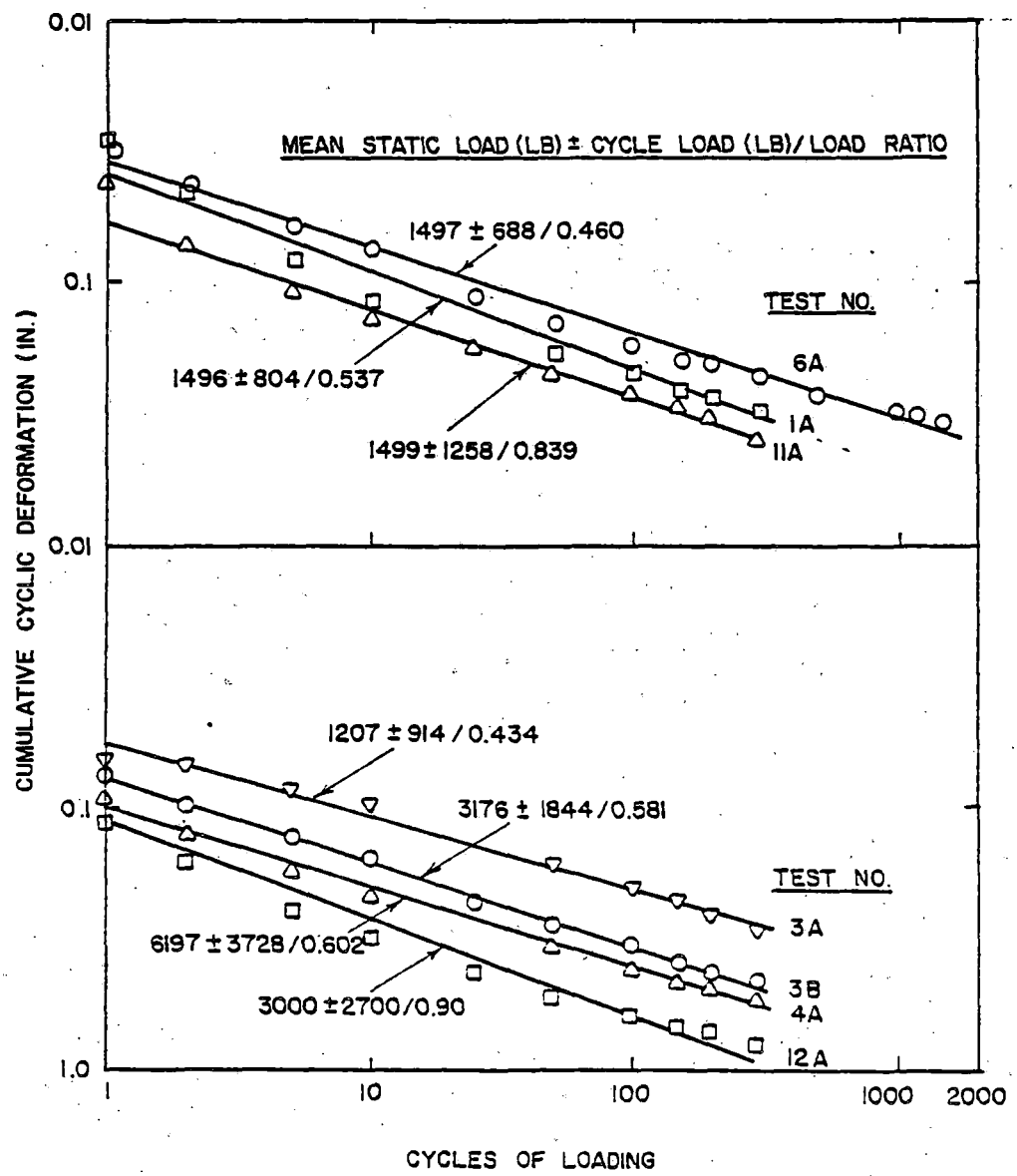

Figure 5.6. Typical Cumulative Cyclic Deformation-Cycles of Loading Relationships at Frequency = 1/2 Hz in Small Test Box for 12-in. (0.305-m) Ballast Depth

Table 5.2. Best Fitting Equations for Cumulative Cyclic Deformation vs. Cycles of Loading

Standard Conditions: 1490 lb $\pm$ 790 lb, LR = 0.53, f = 1/2 Hz, 300 Cycles, 12-in. Depth, Small Test Box

Test No.	Primary Variable(s)	Equation	Correlation Coefficient, γ_{xy}
8A	Cycles = 150	$y = 0.04\,x^{0.296}$	0.996
1A	" = 300	$y = 0.037x^{0.386}$	0.954
1C	" = 300	$y = 0.039x^{0.372}$	0.971
5A	" = 300	$y = 0.034x^{0.353}$	0.982
2A	" = 1500	$y = 0.056x^{0.339}$	0.992
6A	" = 1500	$y = 0.036x^{0.324}$	0.989
11A	Cyclic Load = ± 1260 lb	$y = 0.053x^{0.356}$	0.974
13A	"	$y = 0.065x^{0.371}$	0.975
3A	Static Load = 2107 lb	$y = 0.058x^{0.275}$	0.986
14A	f = 0.1Hz, Cyclic Load=±1190 lb	$y = 0.085x^{0.329}$	0.982
10A	f = 2.0Hz, " = ±644 lb	$y = 0.015x^{0.343}$	0.987
9A	f = 4.0Hz, " =±354 lb	$y = 0.008x^{0.441}$	0.993
15A	Depth = 9 in.	$y = 0.041x^{0.306}$	0.964
15B	" = 9 in.	$y = 0.028x^{0.384}$	0.998
15C	" = 9 in.	$y = 0.029x^{0.349}$	0.994
16A	" = 6 in.	$y = 0.018x^{0.35}$	0.992
16B	" = 6 in.	$y = 0.011x^{0.44}$	0.997
17A	Box Size = 3 ft x 3 ft	$y = 0.069x^{0.337}$	0.900
17B	Box Size = 3 ft x 3 ft	$y = 0.041x^{0.406}$	0.976
3B	Static Load = 3176 lb	$y = 0.077x^{0.32}$	0.997
3C	" = 3130 lb	$y = 0.053x^{0.366}$	0.997
7A	" = 3155 lb	$y = 0.056x^{0.317}$	0.987

Table 5.2. Best Fitting Equations for Cumulative Cyclic Deformation vs. Cycles of Loading (continued)

Standard Conditions: 1490 lb ± 790 lb, LR = 0.53, f = 1/2 Hz, 300 Cycles, 12 in. Depth, Small Test Box

Test No.	Primary Variable(s)	Equation	Correlation Coefficient, γ_{xy}
L2C	Cyclic Load = ±2591 lb	$y = 0.117x^{0.37}$	0.990
12A	" = ±2700 lb	$y = 0.133x^{0.336}$	0.985
12B	" = ±2729 lb	$y = 0.101x^{0.379}$	0.993
4A	Static Load = 6197 lb	$y = 0.101x^{0.302}$	0.992

where

x = Number of Cycles

y = Cumulative Cyclic Deformation (in.)

(A Log - Log Scale)

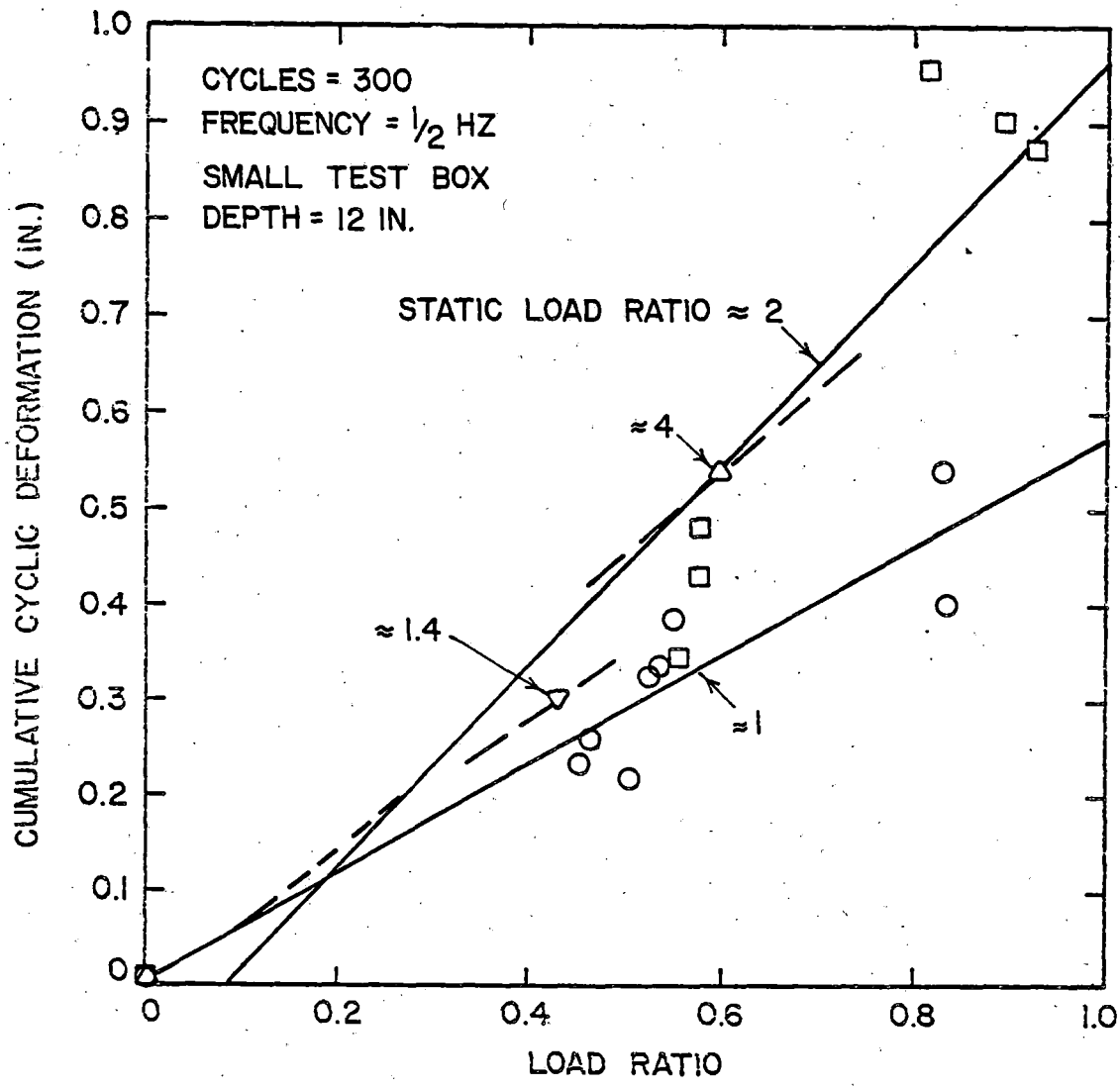

Figure 5.7. The Effect of Various Static and Cyclic Loading Conditions on Cumulative Cyclic Deformation

The general trend from Fig. 5.6 shows that the cumulative cyclic deformation increases as the static load ratio increases for a given load ratio. For a given static load ratio, the cumulative cyclic deformation increases with the load ratio. These trends are what is expected. The one exception to this trend occurred at 300 cycles for an SLR $\simeq$ 4, in which the cumulative cyclic deformation was less than the curve for an SLR $\simeq$ 2. However, the SLR $\simeq$ 4 represents only one data point, whereas the SLR $\simeq$ 1 and SLR $\simeq$ 2 represent several data points each.

The curves in Fig. 5.7 recognized as valid the origin on the graph by using (0,0) as another data point. The assumption was made that no cyclic deformation could occur at a load ratio of zero. Therefore, including (0, 0) as an actual data point for each set of curves appeared logical. For the data points of an SLR $\simeq$ 1, the regression analysis yielded a straight line through the origin for all cycles. However, for an SLR $\simeq$ 2, the line was slightly curved concave upward at low load ratios. For the straight line portion of the SLR $\simeq$ 2 curves and the SLR $\simeq$ 1 curves, the correlation coefficients are good (Ref. 22). For an SLR $\simeq$ 1.4 and 4, there is only one data point to represent each of the two conditions. A linear relationship was assumed for these two cases and a partial line was drawn to show the trend.

In order to quantitatively analyze the changes in the physical state of the ballast after compaction, either plate load tests or in-situ ballast density tests were performed.

The in-situ ballast density test was performed on the ballast in a loose, uncompacted state which provided a reference point for the other

tests. Ballast density tests were also conducted after compacting the ballast with a static load of 1479 lb (6582 N) and a cyclic load of 694 lb (3088 N) for 150, 300 and 1500 cycles. The resulting ballast density is plotted with the number of loading cycles in Fig. 5.8. A linear relationship exists between the ballast density and the cycles of loading. However, after 300 cycles of loading [load = 1479 $\pm$ 694 lb (6582 $\pm$ 3088 N)], the ballast density has increased by only 3 pcf (0.048 Mg/m^3) which is a rather small increment. For other loading conditions shown in Fig. 5.8, there was very little difference in the ballast density after 300 cycles, with one exception to this trend. This was a test with a static load of 3155 lb (14,040 N) and a cyclic load of 1768 lb (7868 N) for 300 cycles. The ballast density test gave a result that is significantly greater than the others and does not follow the trend set by the other tests. The initial box density was somewhat higher for this test but that really doesn't offer a valid explanation for the exceptionally high value. At this point, it is uncertain as to why this test yielded such a high density.

As was done with the ballast density test, ballast in the loose uncompacted state was subjected to a plate load test. The effect of the change in ballast stiffness with loading conditions would, thus, be shown in relation to the loose state test.

The loading condition of 1490 lb (6631 N) static load and 790 lb (3516 N) cyclic load was performed twice with 300 cycles and once with 1500 cycles. The relationship of the BBI at 0.2 in. (5.1 mm) deformation with the log of cycles of loading appears to be linear (Fig. 5.9). Because of this relationship, the BBI and log of cycles of loading is assumed to have

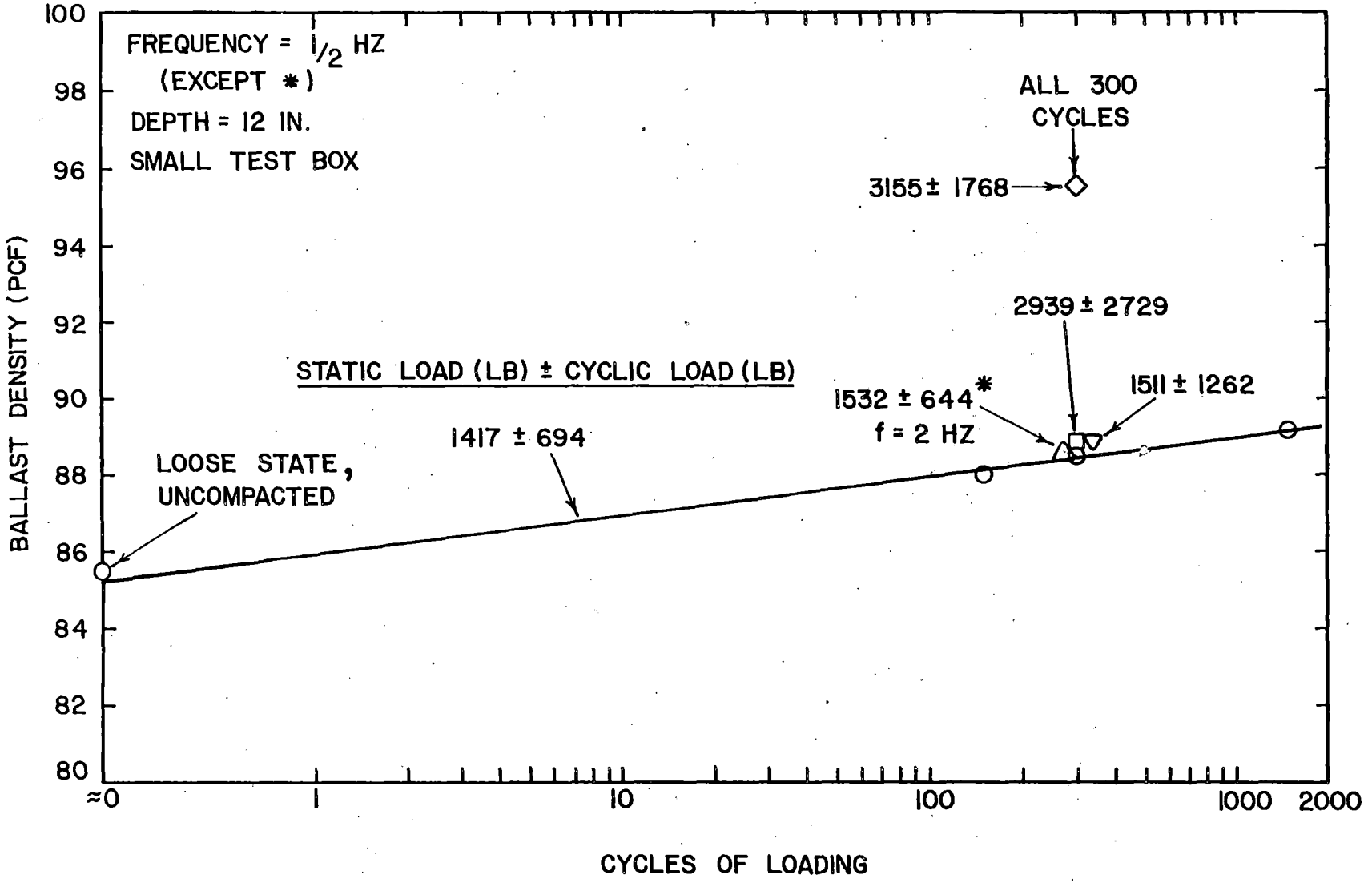

Figure 5.8. The Effect of Various Loading Conditions and Cycles of Loading on Ballast Density

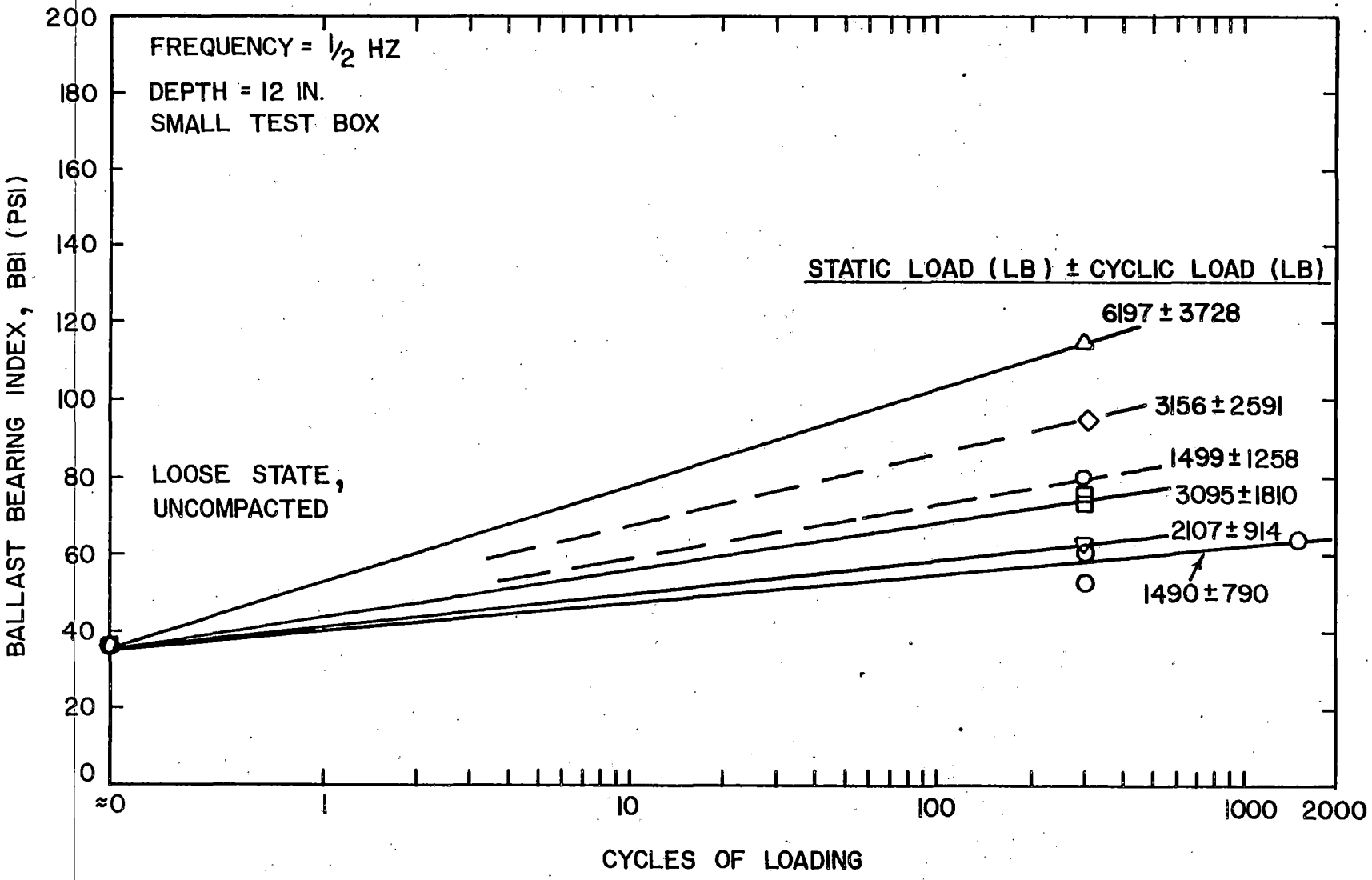

Figure 5.9. The Effect of Various Loading Conditions and Cycles of Loading on the Ballast Bearing Index at 0.2 in. (5.1 mm) Deformation

a linear relationship for all deformation levels and all other loading conditions.

One particularly interesting feature is that the BBI for the test with a static load of 1499 lb (6671 N) and a cyclic load of 1258 lb (5598 N) is greater than the tests with an average mean static load of 3095 lb (13,773 N) and an average cyclic load of 1810 lb (8055 N). This implies that the load ratio has a greater influence on the stiffness of the ballast than does the static load ratio. This result is more clearly illustrated in Fig. 5.10.

Ballast Depth. Experiments were performed testing the effect of various ballast depths in order to simulate the field condition in which loose, disturbed ballast is compacted on a dense compacted track bed. After tamping, the cribs may be filled or partially filled to various depths with loose, uncompacted ballast. It was this condition that these experiments were designed to simulate.

The average initial box densities and the applied static loads each are nearly equal for the various layer depth tests (Ref. 22), thus, a comparison of static deformations can be made. The average static deformation for 12 in. (305 mm) layer depth for the 1519 lb (6760 N) tests is 0.275 in. (6.99 mm), but the overall average at 1519 lb (6760 N) is 0.26 in. (6.6 mm) based on Fig. 5.4. The average static deformation for the 9 in. (229 mm) layer depth tests is 0.185 in. (4.7 mm) and for the 6 in. (152 mm) layer depth test is 0.132 in. (3.4 mm). The general trend for static deformations is that as the ballast layer depth decreases, so does the static deformation for a given static load.

Wayne (Ref. 6) found that a stress redistribution in the ballast occurred

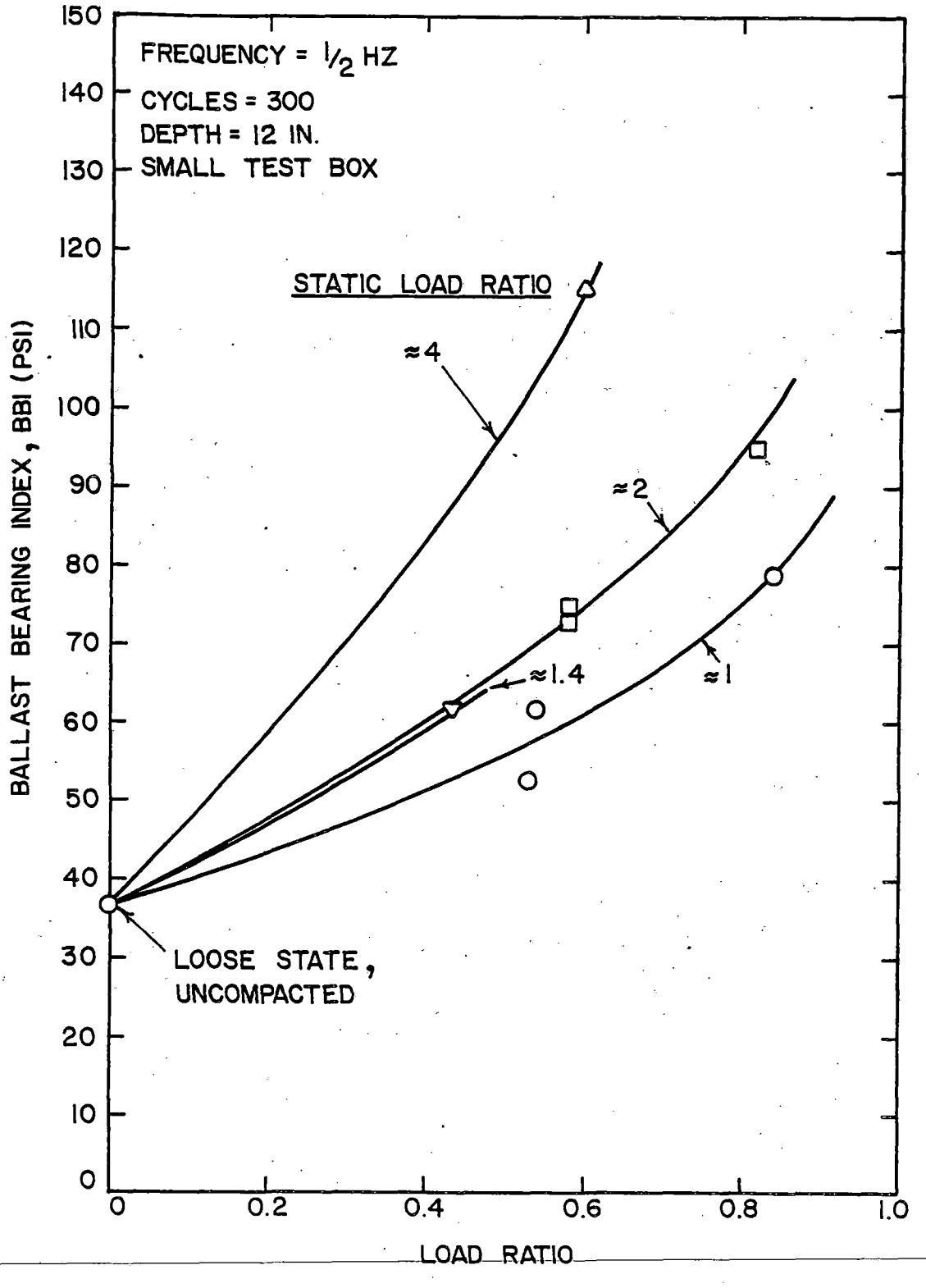

Figure 5.10. The Relationship Between Ballast Bearing Index at 0.2 in. (5.1 mm) Deformation and Load Ratio for Various Static Load Ratios

at a depth of 12 in. (305 mm) as well as at the lesser depths and the depth at which no bottom boundary effect takes place is definitely greater than 12 in. (305 mm). This is reasonable considering that the ratio of plate size to ballast depth is approximately equal to 1.0 for a 12 in. (305 mm) ballast depth.

The regression equations for cumulative cyclic deformation as a function of the cycles of loading for 9 in. (229 mm) and 6 in. (152 mm) ballast depths are listed in Table 5.2 along with the corresponding correlation coefficients. The coefficients in Table 5.2 show that there is a good correlation between the cumulative cyclic deformation and the cycles of loading on a log-log scale for each of the individual tests.

In Fig. 5.11, the cumulative cyclic deformation-load ratio relationship for the three different ballast depths are plotted at 10, and 300 cycles. The trends are assumed to be linear and passing through the origin. The complete lines in Fig. 5.11 represent the 12 in. (305 mm) layer depth of which the line for 300 cycles is the same as that appearing in Fig. 5.7 for an SLR of approximately 1.0. Fig. 5.11 demonstrates that the same trend appears for cyclic deformation as appears for static deformation, i.e., that deformation decreases as ballast depth decreases.

This trend is more clearly illustrated in Fig. 5.12, in which cumulative cyclic deformation is plotted as a function of ballast depth for a load ratio = 0.54. From this figure, it appears that the amount of compaction decreases with decreasing ballast depth. Also plotted in Fig. 5.12 is the cyclic compaction strain (ε_c) which is defined as,

$$\varepsilon_c = \frac{\text{CCD}}{\text{Ballast depth}} \times 100\% \quad . \qquad (5\text{-}3)$$

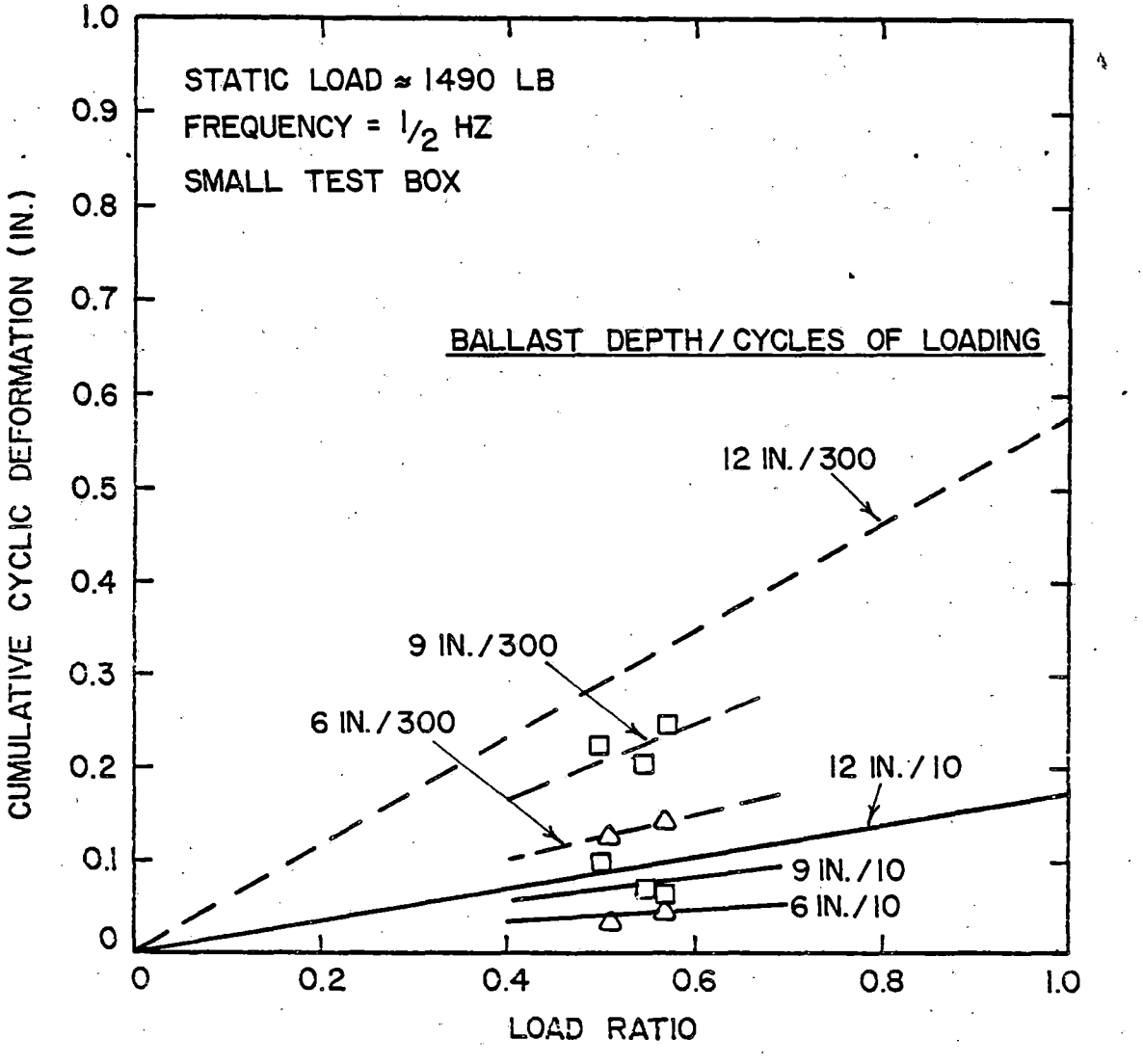

Figure 5.11. The Relationship Between Cumulative Cyclic Deformation and Load Ratio for Different Ballast Depths

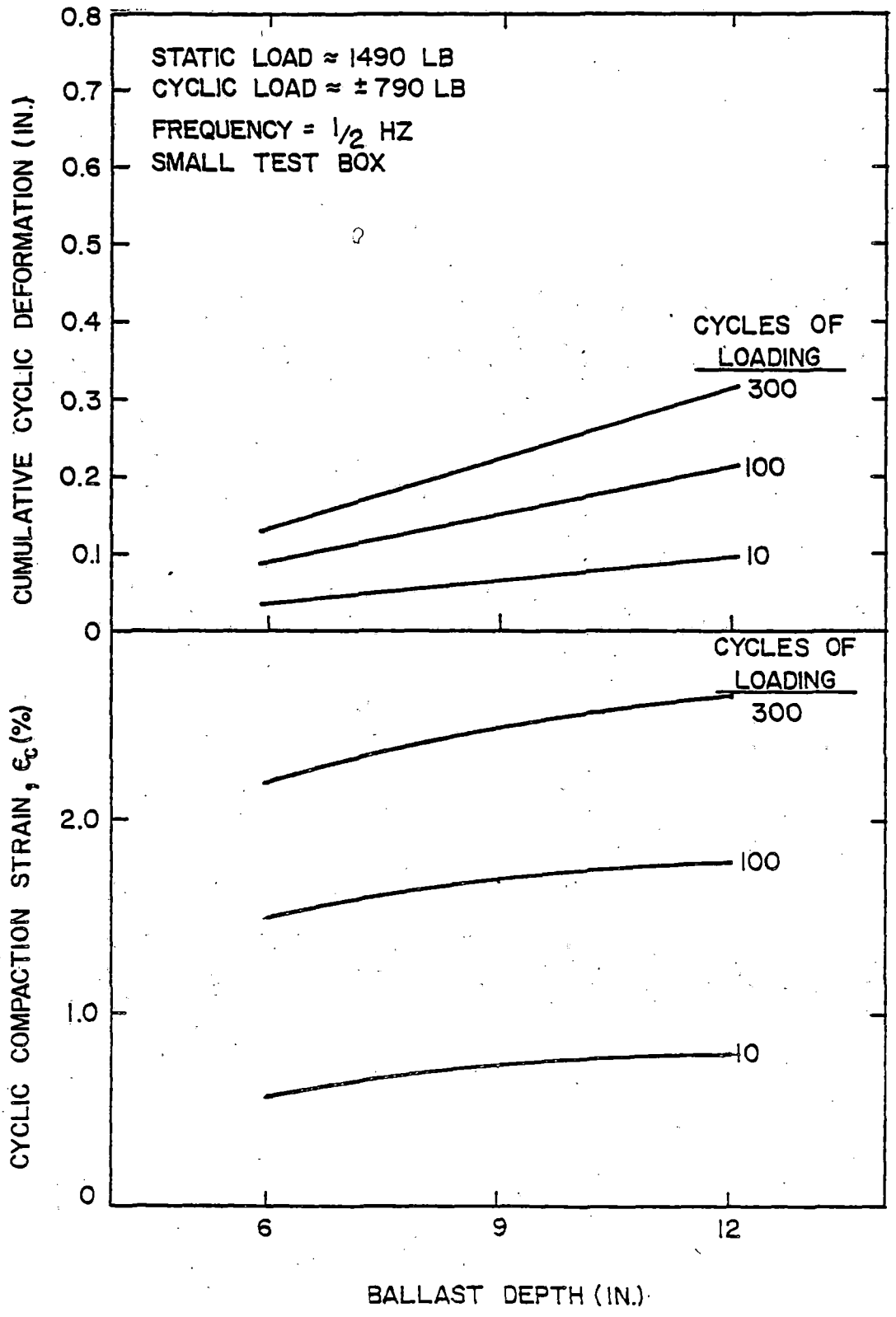

Figure 5.12. The Relationships Between the Cyclic Component of Deformation and Ballast Depth

To represent in terms of a percentage, the quantity is multiplied by 100. The values of cyclic compaction strain for the 9 in. (229 mm) and the 12 in. (305 mm) layer tests are approximately equal, but the values drop off slightly as the depth decreases to 6 in. (152 mm), which generally indicates comparable levels of compaction.

The changes in the physical state of the ballast at various depths after 300 cycles of loading are shown in Fig. 5.13. The BBI at all three deformations differs only slightly for the 12 in. (305 mm) and the 9 in. (229 mm) layer depths. However, the BBI's for the 6 in. (152 mm) layer depth increase significantly, as much as twice the BBI values obtained at the 9 in. (229 mm) or 12 in. (305 mm) layer depth tests. The BBI for the 6 in. (152 mm) layer test may be affected significantly by the bottom boundary.

Lateral Boundary Effects. The lateral boundary effects were tested using the large test box, which has dimensions of 36 in. (0.914 m) by 36 in. (0.914 m) with a 12 in. (305 mm) depth. This box represents essentially a free field condition because the ballast particles are unrestrained from lateral movement. The small box, which has dimensions of 20 in. (508 mm) by 20 in. (508 mm) with a 12 in. (305 mm) depth, was used for all of the tests except those that tested for lateral boundary effects. The lateral constraints in the small box tests were closer to the compaction plate than they were in large box tests. The small box tests were an attempt to simulate, not necessarily duplicate, the effect of in-situ ties which are close to the vibrating ballast compactor plates.

The initial box density was not measured for the large box test series.

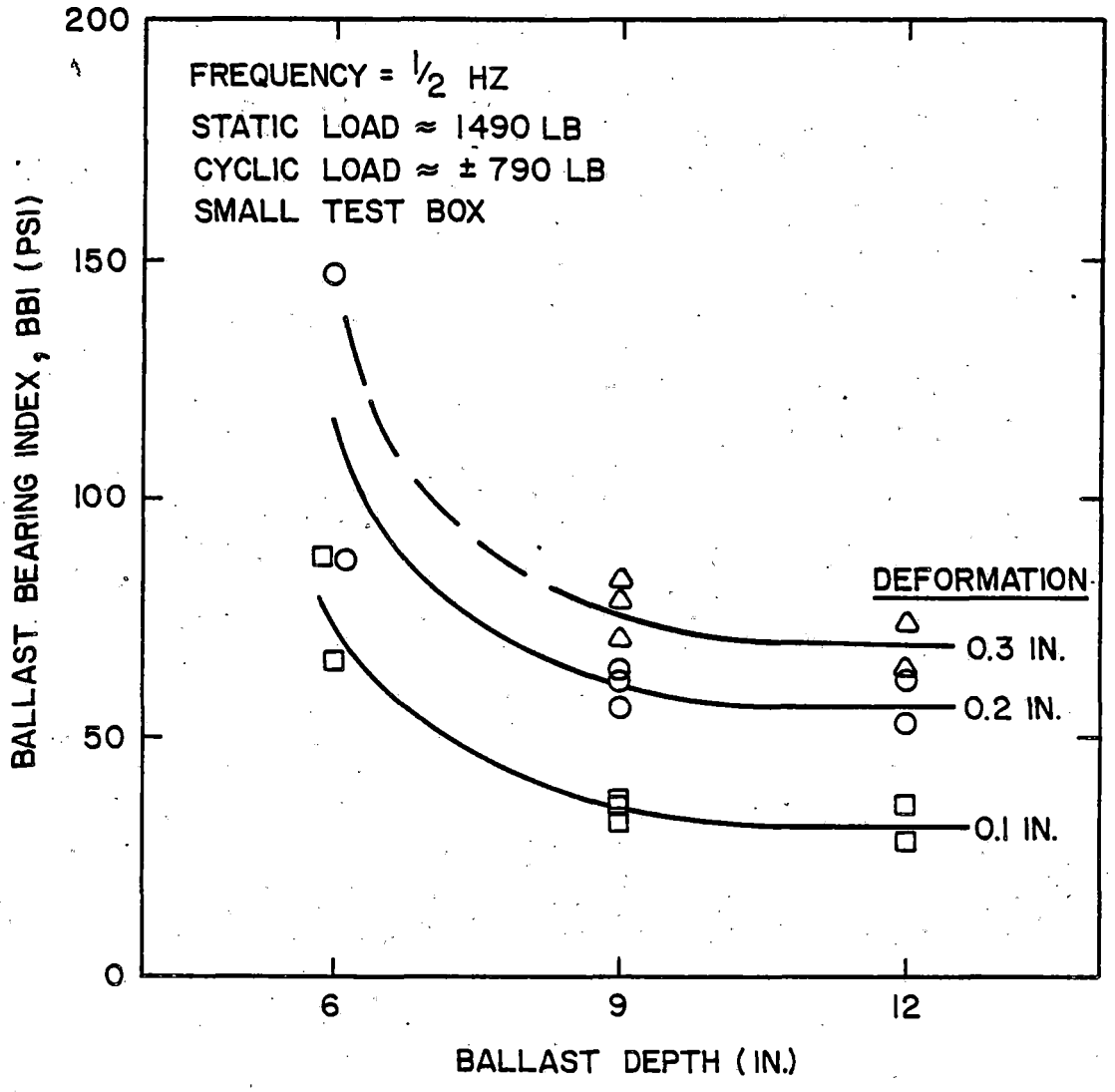

Figure 5.13. The Effect of Ballast Depth on the Ballast Bearing Index After 300 Cycles of Loading

However, the ballast was prepared in exactly the same manner as the small box tests. Therefore, it is reasonable to assume that the loose state ballast density for the large test box was nearly equal to the average density for the small box tests, i.e., 81.9 pcf (1.317 Mg/m^3). Since the initial box densities were nearly equal and the samples were subjected to the same loading conditions, the static deformations can be compared. The average static deformation of the ballast in the small test box, subjected to a 1519 lb (6760 N) load, was 0.275 in. (6.99 mm) (Fig. 5.4) and 0.371 in. (9.42 mm) in the large test box. This represents a 35% increase in deformations for the large box over the small box.

From a regression analysis, the resulting equations for cumulative cyclic deformation as a function of cycles of loading for the large box tests are listed in Table 5.2. Examination of the correlation coefficients indicates that there is a good log-log correlation.

Cumulative cyclic deformation, as a function of load ratio, for 10, 100 and 300 cycles is compared for both the large test box and small test box in Fig. 5.14. Because of the limited number of data points, the large box tests are plotted as only partial lines passing through the origin on the graph. As the lateral boundaries are removed, the cumulative cyclic deformation increases. In other words, the same trend exists for cyclic deformation as exists for static deformation. The average cumulative cyclic deformation increased for the large box test over the small box tests by 76% for 10 cycles, by 35% for 100 cycles and by 27% for 300 cycles. The percentage increases at 100 and 300 cycles appear to be consistent with the percentage increase of the static deformation for the large box tests.

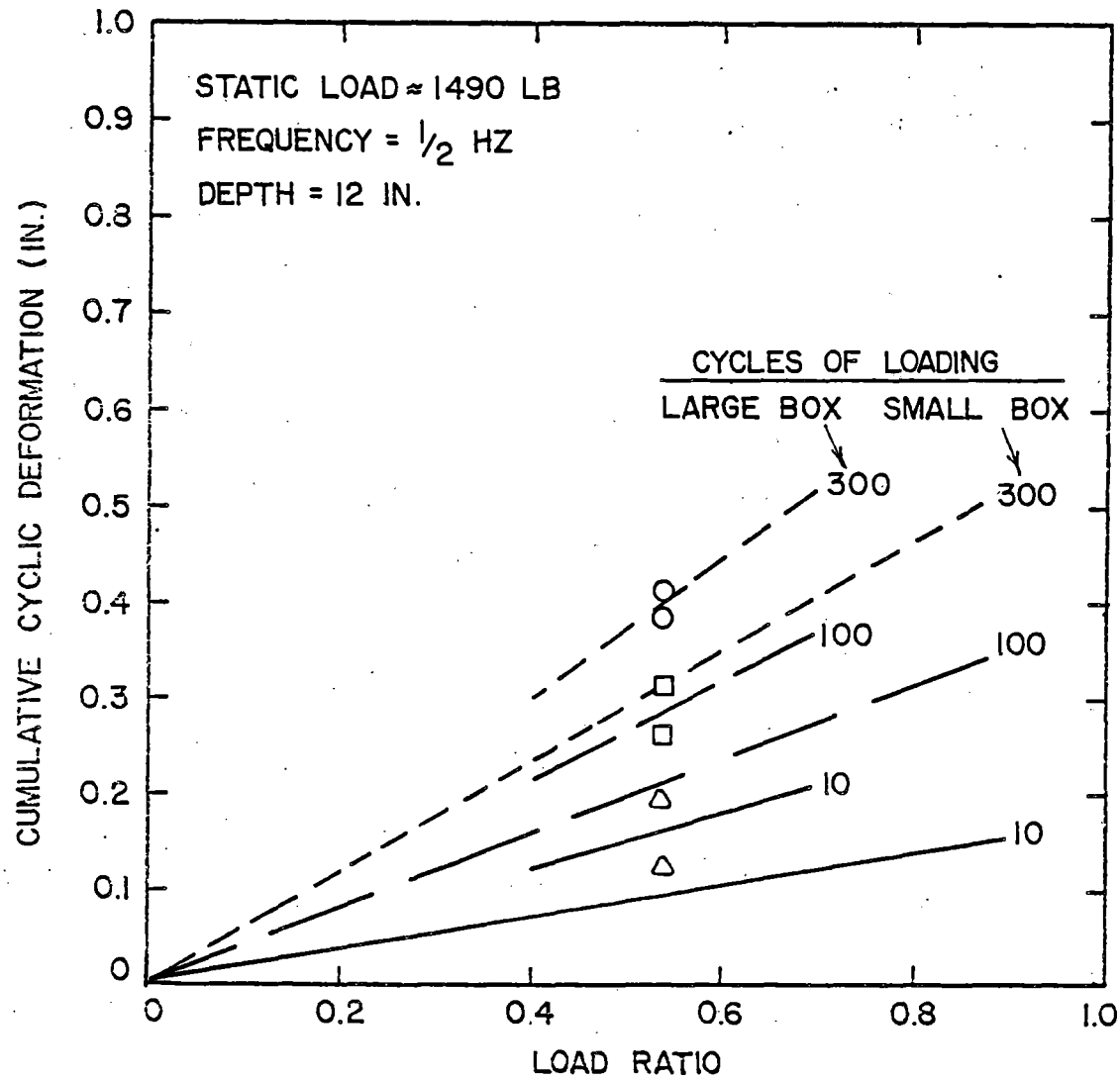

Figure 5.14. The Relationship Between Cumulative Cyclic Deformation and Load Ratio for Different Lateral Boundary Effects

The deformations, both static and cyclic, that occurred in the large test box increases by about 31% over the deformations obtained in the small test box. However, there was very little change in the plate load test results between the two test box sizes, which is evident in Fig. 5.15. Both box sizes yield similar EBI results at all three deformation levels. Also, the lateral dimensions of the test box do not influence these results according to Wayne (Ref. 6). Since the stiffness values for the two test box sizes are similar (Ref. 22), then so is the degree of compaction of the ballast in the zone under the oscillating plate.

The conclusion that can be drawn from this test series is that if no lateral constraints are applied, the tendency is for the ballast particles to move laterally rather than to densify to a greater degree than occurred in the small test box. Thus, the net effect of compaction for the two test box sizes is the same.

Frequency. Most of the tests were conducted at a frequency of 1/2 Hz. However, in order to investigate the effect that frequency has on both the amount of deformation as well as the ballast physical state, three tests were performed in which the frequency was varied but all other parameters remained constant. The different frequencies used for the three tests were 0.1, 2.0 and 4.0 Hz. For all three of these tests, nearly the same mean static load was used; an average of approximately 1490 lb (6631 N). The resulting static deformations were previously included in the discussion of static loads and were of the same order of magnitude as other tests conducted with this mean static load.

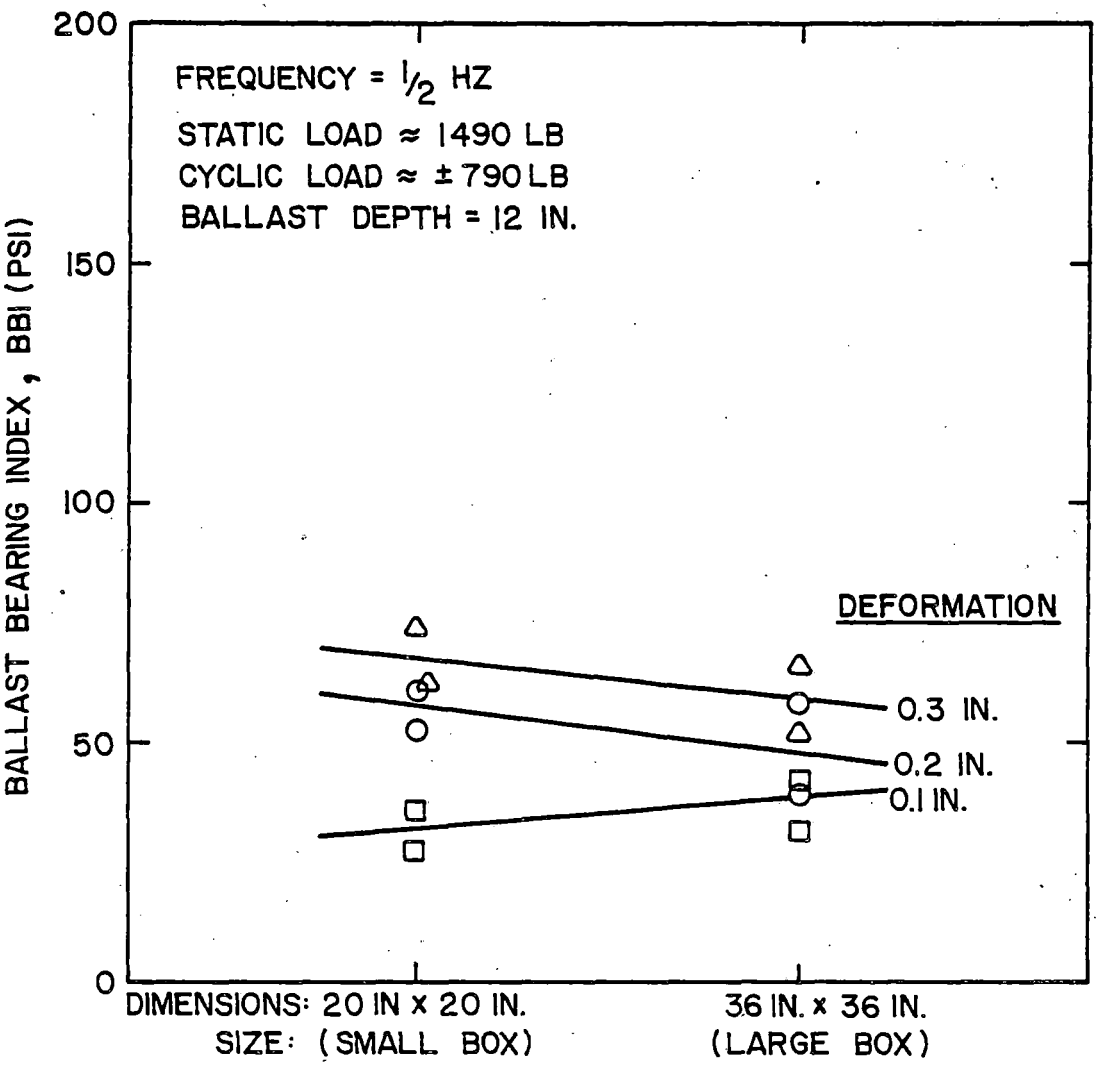

Figure 5.15. The Effect of Test Box Size on the Ballast Bearing Index After 300 Cycles of Loading

The effects of frequency on cumulative cyclic deformation is best represented as a function of load ratio for 10 and 300 cycles in Fig. 5.16. The lines representing the 1/2 Hz test are the same reference lines for an SLR $\simeq$ 1.0 for 10 and 300 cycles illustrated in Figs. 5.11 and 5.14. Examination of Fig. 5.16 reveals that the cumulative cyclic deformations at a given number of cycles for both frequencies of 2.0 Hz and 4.0 Hz is less than that for a frequency of 0.5 Hz, while cumulative cyclic deformations for a frequency of 0.1 Hz was greater than that for a 0.5 Hz. The general trend shows that between the frequencies of 0.1 and 2.0 Hz, the cumulative cyclic deformation decreases as the frequency increases. However, when the frequency was increased from 2.0 Hz to 4.0 Hz, the cumulative cyclic deformation increased, but not to the same order of magnitude that resulted from the 0.5 Hz tests. The limited number of data points makes it difficult to establish conclusive trends concerning the effect of frequency on the amount of cumulative cyclic deformation. The need for further examination of the frequency effect exists to substantiate the results obtained in these tests.

The effect that frequency has on the physical state of the ballast is shown in Fig. 5.17. The loose, uncompacted state is included as a reference point. Test 14A which had a frequency of 0.1 Hz is compared to test 11A which had a frequency of 0.5 Hz because the load ratios for the two tests are nearly equal, i.e. 0.79, and the static load ratios are the same. The overall comparison of the three deformation levels shows that physical states resulting from the two tests is nearly the same. In order to compare test 9A with a frequency of 4.0 Hz to a test at 0.5 Hz, the BBI for a load ratio of 0.239 at a frequency of 0.5 Hz were obtained from curves similar to and

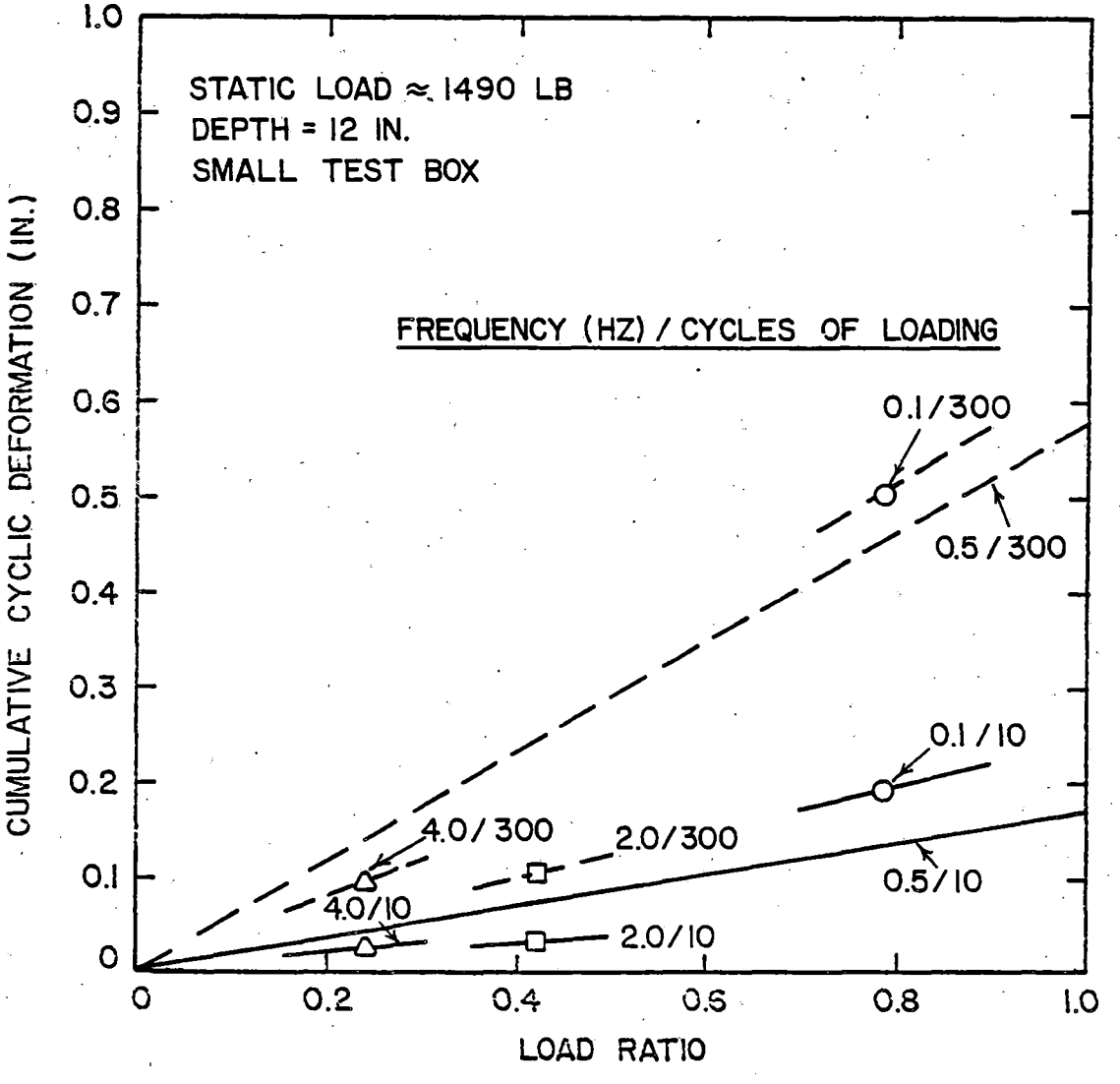

Figure 5.16. The Relationship Between Cumulative Cyclic Deformation and Load Ratio for Various Frequencies

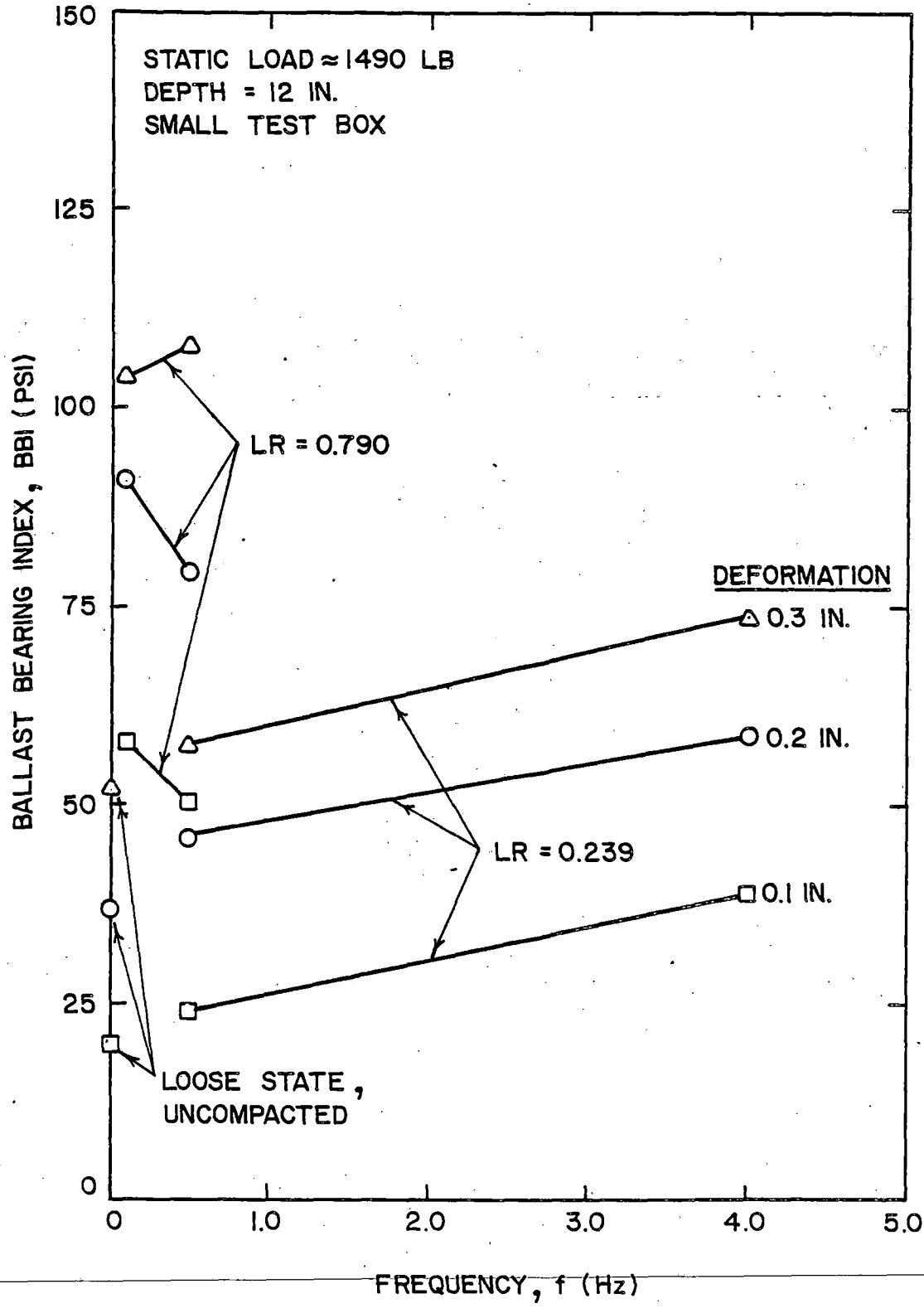

Figure 5.17. The Effect of Frequency on the Ballast Bearing Index After 300 Cycles of Loading

including Fig. 5.10. Fig. 5.17 suggests that there is an increase in plate load resistance (BBI) for all three deformation levels as the frequency is increased.

An in-situ ballast density test was performed on the sample that was compacted at a frequency of 2.0 Hz (Fig. 5.8) which gave a final density of 88.57 pcf (1.419 Mg/m^3). Nearly all of the ballast density tests results, regardless of the loading conditions, yield a result very close to 88.5 pcf (1.418 Mg/m^3) after 300 cycles of loading. Although neither the amount of cumulative cyclic deformation or the ballast density test result indicate that a higher frequency causes a greater amount of compaction to occur, the plate load test suggests, for frequencies greater than 0.5 Hz, that frequency may have an effect. However, it is difficult to make valid conclusions on these trends with the limited amount of data available.

5.3 COMPARISON WITH FIELD DATA

There are two field studies on ballast compaction that are available and are comparable to this study. One is an investigation of ballast properties by SUNYAB at the Illinois Central Gulf Railraod (ICG) [Ref. 23 and 24]. There is a tangent dual main line, of which the Northbound was being subjected to a major maintenance program that included track undercutting, tie tamping and crib and shoulder ballast compaction. The first process was the track undercutting in which all of the ballast material in the cribs, shoulders and beneath the track was removed. All of the fines were removed from this material and were deposited along the side of the track. The clean limestone ballast was then dumped in the center of the track. The track was raised and the ties were tamped. Additional slag ballast was

deposited to fill the cribs and shoulder section before the ballast compactor was used. In-situ ballast density tests and plate load tests were performed at various stages of the above program.

The lowest density state of 84.9 pcf (1.36 Mg/m^3) was found under the tie in the center of the track for the tamped but uncompacted stage. The ballast in the cribs in the center of the track at the same stage was found to have an average density of 91.8 pcf (1.47 Mg/m^3). The lowest density state is comparable to the loose state of 85.5 pcf (1.37 Mg/m^3) obtained in this study. The method of placement of the ballast may account for the difference between the density under the tie and in the crib. The ballast under the tie more or less migrated there from the cribs during the maintenance operations. The energy used in placing the ballast there was very low, thus the density is low. The ballast in the crib, on the other hand, was dumped from a height of a few feet. Thus, the energy associated with that ballast placement was greater and the density measurement yielded a higher value. Incidently, these density values have been modified to represent a 100% limestone sample, since the raw data was for a limestone and slag mixture. The limestone at ICG was approximately the same gradation as the limestone used in this project but it was less angular.

In order to compare the effects of the ballast compaction at ICG and the simulated compactor, the change in crib ballast density must be examined. The compactor used at ICG operated at a frequency of 38 Hz and was applied for approximately 3.5 seconds. Thus, the ballast was subjected to 133 cycles of loading. The average density in the crib after tamping in the area that is to be compacted was 92 pcf (1.474 Mg/m^3). The average density, taken in the same area after tamping and compaction, was 96.4 pcf (1.544 Mg/m^3). This represents an increase in ballast density of 4.4

pcf (0.07 Mg/m^3) due to the use of the ballast compactor. This increase is greater than the increase of 3 pcf (0.048 Mg/m^3) obtained with the simulated compactor. A large part of this difference may depend on the frequency used since it is the parameter with the greatest difference between the two machines. It has been shown in Fig. 5.8 that varying the cyclic and static loads produces only a small change in the resulting ballast density.

The plate load test data was compared by either the BBI, previously defined, or the Modified Ballast Bearing Index (BBI_K). The BBI_K parameter is equal to the BBI at a given deformation level divided by that deformation, i.e. 0.1, 0.2, or 0.3-in. (2.5, 5.1, or 7.6-mm). An average BBI_K is subsequently determined from the three computed values.

Examination of the plate load tests results shows that the lowest average BBI_K occurred in the center of the track beneath the tie. This value was 177 pci (48.1 MN/m^3) which is very close to the 185 pci (50.2 MN/m^3) obtained in this laboratory experiment for the loose state. This value is also consistent with the ballast density test performed in the same area. The average BBI_K in the center of the track in the crib was 236 pci (64.1 MN/m^3) which is consistent with the ballast density measurements in that it is an increase over the below-tie value. As was stated earlier, the ballast in the cribs near the rails, where the compactor plates are placed, was a mixture of slag and limestone ballasts. The percentage of slag increased towards the outside of the track. The average BBI_K outside the rail was 697 pci (189.3 MN/m^3) and the average BBI_K inside the rail was 488 pci (132.5 MN/m^3), but the average value of all tests was 572 pci (155.4 MN/m^3). The large difference between the

inside of the rail and the outside of rail results may not be entirely due to the difference in ballast types. Wayne (Ref. 6) states that average BBI_K values for loose states of limestone and slag are of the same order of magnitude and the same holds true for the dense state values of the two materials.

Since the BBI_K is a function of the static load ratio, the load ratio and the cycles of loading at a given frequency, the resulting BBI_K of the compactor was estimated if it were operating at a frequency of 0.5 Hz. That estimate is 305 pci (82.8 MN/m^3), which is significantly different from average BBI_K value obtained at ICG of 572 pci (155.4 MN/m^3). This fact further reinforces the notion that the operating frequency is a significant factor in changing the physical state of the ballast. The only test that matches the static and cyclic loads of the ballast compactor is Test IIA whose static load is 1,499 lb (6,671 N) and whose cyclic load is 1,258 lbs (2,541 N). The resulting average BBI_K after 300 cycles is 420 pci (114.1 MN/m^3) which is close to the inside of rail value of 488 pci (132.5 MN/m^3), but is much lower than the average value of 572 pci (155.4 MN/m^3).

The second field study which is comparable to this laboratory project was conducted by the Canadian National Railroad (CNR) [Ref. 17]. This study was concerned with plate load test results taken on the track shoulder, under the tie, on the crib surface, and in the crib at a depth equal to the depth of the tie. The plate load test procedure was essentially the same as the SUNYAB procedure with one major exception. Rather than using a load cell to record loads and a DCDT to record deformations on an X-Y recorder, CNR recorded dial gauge readings for deformations and hydraulic jack pressure for loads at various points in the test. These recordings were plotted to obtain a load-deformation curve. They also used pea gravel rather than

plaster as a seating material. The CNR report provides BBI values at 0.3 in. (7.6 mm) deformation. These field plate load test data from the crib near the rail were selected as most appropriate for comparison with the lab results. The CNR ballast was crushed stone.

The BBI at 0.3 in. (7.6 mm) deformation on the undisturbed track was 264 psi (1,819 kN/m^2). Exactly how many million gross tons of traffic had passed over this track since its last track surfacing program is not known. After surfacing and lining only, the BBI at 0.3 in. (7.6 mm) deformation was 63 psi (434 kN/m^2). This is nearly the same as the laboratory loose state condition which is 52 psi (358 kN/m^2). The BBI at 0.3 in. (7.6 mm) deformation after crib and shoulder compaction was 306 psi (2,108 kN/m^2). The BBI at 0.3 in. (7.6 mm) deformation after undercutting and crib compaction was 412 psi (2,839 kN/m^2); and after undercutting and crib and shoulder compaction was 333 psi (2,294 kN/m^2). After undercutting, the track bed was filled with either slag or new crushed rock. The above results are average values that represent many tests. The study does not differentiate the test results for the different ballast types. All of the above values are significantly greater than any of the values obtained in the laboratory tests. The greatest value of BBI at 0.3 in. (7.6 mm) deformation obtained in the laboratory was 140 psi (965 kN/m^2). The static load for this test was 6,197 lb (27,577 N) and the cyclic load was 3,728 lb (16,590 N). All of the CNR values are also greater than the results obtained from ICG.

Exactly why the BBI values in the CNR study are so much greater is difficult to ascertain, but there appear to be factors that are different in the two studies which influence the plate load test results. A more detailed study on plate load test comparisons is discussed by Panuccio and Dorwart (Ref. 4).

6. SUMMARY AND CONCLUSIONS

A summary of the three field compaction mechanisms simulated in the laboratory for a crushed limestone ballast are presented.

6.1 SIMULATED TRACK BED

An old railroad track bed, i.e., one that has not been recently subjected to maintenance operations, was simulated in the laboratory by filling a large test box with 12 in. (0.305 m) of limestone ballast and compacting it with a vibratory plate compactor. The change in the physical state of the ballast during the compaction phase was monitored by plate load tests and in-situ ballast density tests which were performed at certain intervals during the compaction process. The main conclusions from this investigation are:

1. The in-situ ballast density tests that were performed during the compaction of the track bed yielded an average maximum dry density of approximately 110 pcf (1.76 Mg/m^3) after only 25 to 50 passes with the vibratory compactor. This was an increase of about 12 pcf from the loose state.

2. The Ballast Bearing Index (BBI) values obtained from the plate load tests on the compacted track bed leveled off after approximately 500 passes with the vibratory plate compactor. The average maximum BBI value at 0.2 in. (5.1 mm) deformation was approximately 279 psi (1922 kN/m^2).

3. The laboratory ballast density and stiffness values after 1000 compactor passes compared favorably well with field test results for an old track bed condition.

6.2 MANUAL TIE TAMPING

Several lateral tie push tests were performed when a standard railroad tie was placed on the compacted bed with no crib or shoulder, and the effects of various weights placed on the tie were evaluated. Tests were also performed for a semi-filled crib, a full crib, and a full crib with a surcharge load. The ballast shoulder section was subsequently formed and lateral tie push tests were performed on a compacted base, as well as a loose base resulting from various amounts of tamping raises. These ballast physical state test results were also compared with previous reported data.

The following summarizes the important test results obtained from these tests:

1. The lateral tie resistance of an individual tie after manual tie tamping does not appear to be affected by the height of the tamping raise nor the type of raising operation, i.e., full or in lifts. This is for a full loose ballast crib and shoulder condition.

2. The lateral tie resistance increases nearly linearly as the amount of ballast in the cribs increases. Even when the cribs are overfilled, the tie resistance continues to increase in a similar fashion. The crib component of resistance is a significant contributor to the total lateral resistance of an unloaded tie.

3. For ties of various equivalent weights placed on a compacted base with no crib or shoulder ballast, the lateral tie resistance is approximately equal to one-half of the tie weight.

4. The in-situ ballast density test and the plate load test data for both in the crib and under the tie locations produced fairly consistent

results with respect to manual tie tamping. In general, both the ballast density and ballast stiffness under the rails, i.e., the zones of tamping, were reduced after tamping was performed and each of these physical state test values were comparable for different heights of the raises.

The field LTPT results from ICG and FAST were generally greater than the laboratory tests for the after-tamping condition by 50 to 150 lb (223 to 668 N). This difference cannot presently be explained; however, the range of lateral tie resistance values at 0.157 in. (4 mm) displacement were comparable for the two conditions. The laboratory PLT and BDT results, however, compared very favorably to the field test results for the tamped-only condition. Thus, this track condition appears to be reproducible in the laboratory.

6.3 CRIB COMPACTION PLATE

This part of the study was conducted in order to examine the effect that various parameters have on ballast compaction. The ballast compaction was performed in the laboratory on a limestone ballast with a simulated ballast compactor that consisted of a single plate oscillating at a low frequency. The compaction effort included both static and cyclic loading. Apparatus and experimental design considerations for this project were a result of a review of manufacturer's literature on ballast compactors which provided the specifications for the plate shape and size as well as the range of static and cyclic loads to be used. The frequency and application time of ballast compactors was considered in determining the equivalent number of cycles of loading. A test box with a volume of 2.78 cubic feet (0.0787 m^3) was used for most of the tests, but a 9 cubic foot (0.25 m^3) test box was

used to test for lateral boundary effects. The effects of ballast depth and loading frequency were also examined. The amount of compaction for each test was evaluated by one of the physical state tests developed at SUNYAB, i.e., plate load tests or ballast density tests.

The following list is a summary of the results from the tests:

1. As the static load was increased, the static deformation also increased. However, the overall relationship was not linear. The bottom boundary is believed to have influenced the tests with large static loads.
2. When the initial box density increased, the resulting static deformation, for a given static load, decreased.
3. The cumulative cyclic deformation increased as the load ratio was increased for a given static load ratio. The cumulative cyclic deformation increased as the static load ratio increased for a constant load ratio.
4. The ballast density increased only a small amount from the loose state of about 85.5 pcf (1.37 Mg/m^3) to about 88.5 pcf (1.418 Mg/m^3) for the dense state after 300 cycles. The final density state appeared to be independent of the loading conditions.
5. The BBI value at a given deformation increased as the static load ratio was increased for a given load ratio. Similarly, as the load ratio was increased for a given static load ratio, the BBI value increased.
6. When the sample ballast depth was decreased, both the static deformation and the cumulative cyclic deformation decreased when comparing similar loading conditions.
7. The BBI's differed only slightly for the 12 in. (305 mm) and 9 in. (229 mm)

layer depths, but they increased dramatically for the 6 in. (152 mm) layer depths.

8. When the lateral boundary constraints were removed, both the static deformation and the cyclic deformation increased for a given set of loading conditions, but the BBI values were nearly the same. This shows that the amount of compaction was essentially the same for the two test box sizes.

9. When the effects of different frequencies were tested, it was found that the density was no different after compacting at 2.0 Hz than it was after compacting at 0.5 Hz after the same number of cycles and similar loading conditions.

10. For equivalent load ratios, the BBI's resulting from the 0.1 Hz test was essentially the same as the 0.5 Hz test. The test performed at a frequency of 4.0 Hz resulted in greater BBI's than the 0.5 Hz test at an equivalent load ratio.

The test results were also compared to results that were obtained from physical state tests performed in the field. Of the tests performed on the Illinois Central Gulf Railroad, the only results for the loose state that agreed with this experiment were located under the tie in the center of the track. Both the ballast density test and plate load test results compare favorably to the loose state tests for this project. The BBI values in the area that was under direct contact with the vibrating plate increased much more than any BBI values in the lab tests. The CNR conducted a study in which plate load tests were performed on the track in different maintenance stages. The loosest state that occurred in that study was after surfacing

and lining in the crib near the rail where tamping occurred. The plate load resistance at that stage in the field was nearly equal to the loose ballast results in the lab tests before compaction with the oscillating plate. However, the field BBI values after crib compaction were significantly greater than any values obtained in the lab tests after compaction with the plate. The conclusion based on both the ICG and CNR comparisons is that the higher frequencies in the field operation significantly affect the amount of ballast compaction.

...ell and Dorman, N.C., "Construction Studies for the ...
...cal Tie Pull Test and the Plate Load Test," Technical Vapor...
...Corporation Study, Dept. of Civil Engineering, SUNYAB, Aug.

...d M., "A Study of Ballast Density Measurements," M.S. Proje...
... to Dept. of Civil Engineering, SUNYAB, February, 1972.

..., N.C., "The Plate Load Test for Ballast Evaluation," M.S. P...
...mitted to Dept. of Civil Engineering, SUNYAB, February, 1971.

...S., "Field Measurement of Lateral Ballast Density," Inter...
..., Dept. of Civil Engineering, SUNYAB, October, 1974.

...ers, N.C., "Railroad Ballast Data at Track Test," M.S. T...
...ided by Civil Engineering Department, University of Illinois...
...-Champaign, Urbana, 1975.

...1. "Technical Report ...
...ice ...

REFERENCES

1. Selig, E.T., Yoo, T.S. and Panuccio, C.M., "Mechanics of Ballast Compaction: Vol. 2. Field Methods for Ballast Physical State Measurement," Final Report, State University of New York at Buffalo, Contract No. DOT/TSC/1115, Submitted to Transportation Systems Center, U.S. DOT, Cambridge, Massachusetts, September, 1980.

2. Selig, E.T., Yoo, T.S. and Panuccio, C.M., "Mechanics of Ballast Compaction: Vol. 1. Technical Review of Ballast Compaction and Related Topics," Final Report, SUNYAB, Contract No. DOT/TSC/1115, Submitted to Transportation Systems Center, U.S. DOT, Cambridge, Mass., September, 1980.

3. Ciolko, A.T., "The Lateral Tie Push Test for Ballast Evaluation," M.S. Project, Submitted to Department of Civil Engineering, SUNYAB, April, 1977.

4. Panuccio, C.M. and Dorwart, B.C., "Correlation Studies for the Single Lateral Tie Push Test and the Plate Load Test," Internal Report, Ballast Compaction Study, Dept. of Civil Engineering, SUNYAB, August, 1978.

5. Chen, H.M., "A Study of Ballast Density Measurement," M.S. Project Submitted to Dept. of Civil Engineering, SUNYAB, February, 1977.

6. Wayne, R.C., "The Plate Load Test for Ballast Evaluation," M.S. Project Submitted to Dept. of Civil Engineering, SUNYAB, February, 1977.

7. Yoo, T.S., "Field Measurements of In-Situ Ballast Density," Internal Report, Dept. of Civil Engineering, SUNYAB, October, 1978.

8. Petersen, H.C., "Railroad Ballast Lateral Stability Test," M.S. Thesis Submitted to Civil Engineering Department, University of Illinois at Urbana-Champaign, September, 1975.

9. Plasser, "Technical Description of the Consolidating Machine VDM 800 U," Manufacturer's Literature.

10. Plasser Information, "Consolidating Machines," Manufacturer's Literature.

11. Panuccio, C.M., "Trip to Canadian National Railway Site," Internal Report, SUNYAB, June-July, 1976.

12. Office for Research and Experiments of the International Union of Railways, "Optimum Adaptation of the Conventional Track to Future Traffic: Study of the Change in the Track Level as a Function of the Traffic and of the Track Components," ORE Question D117, Report No. 2, UTRECHT, April, 1973.

13. Plasser and Theurer, Manufacturer's Literature on Track Maintenance Equipment Specifications.

Mechanics of Ballast Compaction: Volume 4, Laboratory Investigation of the Effects of Field Compaction Mechanisms, 1982
US DOT, FRA, CM Panuccio, Dr McMahon, ET Selig

U.S. Department
of Transportation

**Research and
Special Programs
Administration**

Kendall Square
Cambridge, Massachusetts 02142

Official Business
Penalty for Private Use $300

Postage and Fees Paid
Research and Special
Programs Administration
DOT 513